NPL Report DES 125

March 1993

RF and Microwave dielectric measurements upon layered materials using a reflectometric coaxial sensor

A P Gregory, R N Clarke, T E Hodgetts and G T Symm
Division of Electrical Science
National Physical Laboratory
Teddington
Middlesex
United Kingdom
TW11 0LW

ABSTRACT

This report describes progress at the National Physical Laboratory on the application of coaxial reflectometric sensors to the measurement of RF and Microwave dielectric properties of laminated materials. Measurements were performed in the range 300 MHz to 3 GHz, but our findings can be applied over the whole of the RF and Microwave range. As a result of the work described both high and low loss materials can be measured by coaxial sensors. Suitable specimens of one, two and three dielectric layers can be characterised. A cell attachment has been constructed for a 14-mm diameter sensor which allows circular specimens to be measured more accurately. The cell also allows liquid immersion measurements to be performed, which affords greatly improved uncertainties. Three independent computer programs have been written to analyse multilayer laminar specimens. The programs have been intercompared and have been shown to agree numerically to well within expected measurement uncertainties. Measurements upon liquid and solid materials of known permittivity have been compared with the program predictions and shown to agree sufficiently well to allow the system to be used for traceable measurements within the National Measurement System.

© Crown copyright 1993

ISSN 01437305

National Physical Laboratory
Teddington, Middlesex, United Kingdom, TW11 0LW

Extracts from this report may be reproduced
provided that the source is acknowledged

Approved on behalf of Chief Executive, NPL,
by Dr T G Blaney, Head, Division of Electrical Science

CONTENTS

Page

1 INTRODUCTION 1

1.1 BACKGROUND 1

1.1.1 The aim of the work . . . . . .
1.1.2 Applications of the work 1
1.1.3 Complex permittivity 2

1.2 REFLECTOMETRIC COAXIAL SENSORS 3

1.3 PREVIOUS WORK AT NPL 7

1.4 A SURVEY OF THE RECENT LITERATURE. 9

1.4.1 'Infinite half-space' geometries, including sensor calibration and uncertainty analysis 9
1.4.2 Coaxial lines and cylindrical cavities 9
1.4.3 Single layer laminas 10
1.4.4 Laminas, airgaps and multilayer geometries 10
1.4.5 Other structures and geometries 10
1.4.6 Summary Discussion - How the NPL work relates to the literature . . . 11

1.5 SUMMARY OF WORK AT NPL ON MULTILAYER LAMINAS 11

2 NEW PROGRAMS FOR LAYERED DIELECTRIC GEOMETRIES. 12

2.1 SUMMARY OF NEW WORK ON COMPUTER PROGRAMS 12

2.2 QUADRATIC EXTRAPOLATION 12

2.3 INTERCOMPARISON GEOMETRIES 13

2.4 THE COMPUTER PROGRAMS 14

2.4.1 Programs previously developed for earlier work . . . 14
2.4.2 The new multilayer programs 15

2.5 NUMERICAL INTERCOMPARISONS OF PROGRAMS . 17

2.5.1 14-mm coaxial sensor with 'infinite half-space' - the high loss case . . . 18
2.5.2 14-mm coaxial sensor in air 22
2.5.3 14mm coaxial sensor with a single layer lamina 24
2.5.4 Tests with physical dielectrics - single layer laminar geometry 25
2.5.5 Relevance to open probe-type sensors 33
2.5.6 Modelling specimens of two and three layers. 34

3 COAXIAL SENSORS AND CELLS - HARDWARE 36

3.1 INTRODUCTION 36

3.2 CYLINDRICAL CELL DESIGN 37

3.2. Annular gaps around the specimen . . 37

3.2.2 Lack of co-planarity of the sensor face 38
3.2.3 Metal loss 38

3.3 TYPE C SENSOR AND CELL CONSTRUCTION AND USE 39

3.4 SENSOR CALIBRATION AND MEASUREMENT 41

3.4.1 Background 41
3.4.2 Experimental evaluation of calibration methods 42

4 INTERCOMPARISON OF MEASUREMENTS WITH THEORY 44

4.1 TRIAL SPECIMENS AND REFERENCE MATERIALS 44

MEASUREMENTS UPON REFERENCE FLUIDS 46

4.3 MEASUREMENTS UPON LIQUID/SOLID COMPOSITES 51

4.4 CHOICE OF MEASUREMENT METHOD FOR SOLIDS . . 54

4.4.1 Liquid immersion 54
4.4.2 Choice of method for porous or soluble specimens 58
4.4.3 Liquid substitution 58
4.4.4 Choice of spacing between sensor flange and specimen 60
4.4.5 Miscellaneous techniques 62

4.5 MEASUREMENTS UPON LAYERED SOLIDS 62

5 UNCERTAINTIES 69

5.1 UNCERTAINTY BUDGET 69

UNCERTAINTIES FOR MEASURING THE NTH LAYER, WHERE $N \geq 3$. 72

6 DISCUSSION AND CONCLUSIONS . 73

SUMMARY OF WHAT HAS BEEN ACHIEVED IN THIS PROJECT 74

6.1.1 Immediate aims 74
6.1.2 How this work contributes to coaxial sensor metrology 74

6.2 POTENTIAL APPLICATIONS OF THE WORK 75

PROBLEMS AND SUGGESTIONS FOR FURTHER WORK . . 76

6.3.1 Reliability of measurements 76
6.3.2 Cavity resonances 76
6.3.3 Suitability of specimens 77
6.3.4 Knowledge of the properties of the reference liquids 78
6.3.5 Metal and contact loss in cells 78

7 ACKNOWLEDGEMENTS 78

8 REFERENCES 80

1 INTRODUCTION

1.1 BACKGROUND

1.1.1 The aim of the work

The work described in this report has been carried out over a period of one year as part of the NPL RF and Microwave standards programme as required by the National Measurement System Policy Unit (NMPSU) of the Department of Trade and Industry (DTI). The requirement was to produce a method for measuring the dielectric properties of parallel-layered composite materials at RF and microwave frequencies up to 3 GHz. It was required to achieve this capability with specimens of small cross-section, which excluded free-field solutions to the problem. Reflectometric coaxial sensor technology is capable of dealing with specimens of limited cross-section and it is a technique in which NPL already has much practical expertise. It was this technique which was adopted for this project. The work was split into four parts:

1. Commissioning, debugging and cross-checking computer programs which can model measurements upon laminated materials with coaxial sensors.
2. Constructing coaxial sensors and specimen cells which allow suitable measurements to be performed.
3. Comparing measurements upon laminates with computer predictions.
4. Demonstrating that these facilities can be set up as a calibration service, as part of the National Measurement System.

These tasks have been completed and are described in this report. The computer programs allow uncertainty estimates to be derived for any candidate material and also allow one to predict whether the coaxial sensor technique is suitable for any given specimen.

1.1.2 Applications of the work

A major requirement for measurements upon laminated materials arises from their widespread use in microwave environments. Examples are **substrate materials** for microwave integrated circuits and **radome materials**. In many cases lamination is carried out so as to meet microwave design requirements such as the minimisation of reflections. However, laminates are often encountered which are not primarily designed for optimised microwave performance. For example, laminated glasses are usually designed with optical and protectional properties in mind: eg. for strengthening or shatter-proofing. Where these materials are used in a microwave environment the microwave engineer requires to know dielectric properties to predict the effects of the lamina upon electromagnetic fields. **Multifrequency** (eg. radar) environments present the engineer with other problems. Laminates optimised for one frequency range will behave completely differently in another and materials have to be well-characterised if their influence upon microwave fields is to be predictable at all frequencies.

Another growing area of application is to characterisation of what might be called 'natural' laminates. Here we refer to applications in the **food-processing** [6] and medical fields [8,9,11,17].

These are important because dielectric measurements, particularly with coaxial sensors, are increasingly being used for diagnostic or control purposes. Biological tissues, like skin for example, are often layered in structure and the efficacy of diagnostic techniques is much enhanced by treating tissues as such rather than as homogeneous materials, as previous coaxial sensor theories have tended to do.

The work reported here has further important consequences for improving coaxial sensor measurements upon *single*-layer homogeneous materials. Coaxial sensors are most successful in measuring malleable solids and liquids - that is with those materials where there is little likelihood of a gap forming between the specimen and the face of the sensor. With hard solids it is unlikely that one can avoid a gap between sensor face and specimen. Even a small gap of the order 10 μm in thickness can produce large errors in permittivity measurement by sensors (10% or more) because it lies in the region where the fringing fields are most intense. The multilayer theory allows **'liquid-immersion' techniques** to be used to overcome this problem. The hard solid specimen is immersed in a well-characterised liquid with permittivity similar to its own and a small gap of known thickness is opened up between it and the face of the sensor. Two- or three-layer theory is then used to measure the properties of the second layer, ie. the specimen in a calculable geometry.

The computer programs written for this project also improve practical sensor measurements for other reasons. Three of the new programs deal explicitly with finite-diameter specimens. Most coaxial sensor analyses previously in use ignore the effects of reflections from the edges of specimens. This can give rise to large errors of measurement - 100% or larger in permittivity - for quite common measurement geometries. The programs allow a comprehensive uncertainty analysis to be performed for any circularly symmetrical coaxial sensor geometry - not just those at NPL. This enables us to advise other metrologists about the likely effectiveness of their measurements.

This work not only allows us to act in an advisory role on coaxial sensor and multilayer dielectric metrology, the new software and hardware is intended to play a role in the National Measurement System by offering an NPL facility for measuring dielectrics. We have already used this system for looking at specimens supplied by potential customers.

1.1.3 Complex permittivity

The object of this work was to determine the dielectric properties of specimens, or of individual layers of multilayered specimens, in terms of their **relative complex permittivity**: $\varepsilon^* = \varepsilon' - j\varepsilon''$. The usual conventions are followed here: $j = \sqrt{-1}$, ε' gives the reactive part of the permittivity and ε'' quantifies the loss or power absorption in the dielectric. Where appropriate, the latter is also expressed in terms of the *loss tangent*, $\tan\delta = \varepsilon''/\varepsilon'$, though the sensor technique more naturally measures ε' and ε'' directly. For typical materials, both ε' and ε'' vary slowly with frequency over the RF and Microwave frequency range as a result of dielectric relaxation processes: ε' always falls with frequency, the more so if ε'' is large [24], whereas ε'' can rise or fall with frequency. Where appropriate, this relaxation behaviour can be described by a theoretical model [18,19] (as in equation 4, Section 4.1, for example), but this is not the major concern of the present project. During this program of work we have used liquids with ε' in the range 2 - 77 and $\tan\delta$ in the range 0.0 - 0.7. Solid laminar specimens possessed ε' in the range 2 - 34, but generally had $\tan\delta < 0.1$. Biological tissues, and tissue-equivalent materials, are ideally suited to the sensor technique, as described elsewhere [8–11,16–19]. Their complex permittivities lie in a similar range to that of the liquids.

1.2 REFLECTOMETRIC COAXIAL SENSORS

If a coaxial line is connected to an electromagnetic signal source at one end but is open-circuited into air at the other, fringing electromagnetic fields emerge from the open end of the line. At low frequencies, these are largely evanescent, which (in this context) is to say that no power is transferred from these fields to the free space around the end of the line. The electromagnetic power is therefore all reflected back again down the coaxial line to the source. In these circumstances microwave engineers say that the admittance *presented to* the line by the fringing fields is purely reactive. This has the consequence that, if Γ is the complex reflection coefficient of the signals from the end of the line, we have $|\Gamma| = 1.0$. As the frequency increases through the microwave band, however, a significant proportion of the signal comes to be radiated into free-space, and so we have $|\Gamma| < 1.0$. Furthermore, if the end of the line is surrounded by a dielectric of permittivity ε^*, the phase of Γ, θ, is significantly affected by the value of ε^* and, even at low RF frequencies where no significant radiation occurs, a lossy dielectric ($\varepsilon'' > 0.0$) will absorb power, thus giving $|\Gamma| < 1.0$. Since the reflection coefficient from any termination of a coaxial line is intimately related to the admittance it presents, we can see that the admittance presented by the fringing fields to the line depends critically upon the dielectric properties of the materials through which the fields pass. This principle provides the basis of a convenient and popular technique for measuring dielectric properties [3,5,10,20] - the open-ended coaxial dielectric sensor. Non-invasive dielectric sensors based upon this principle are used at RF and microwave frequencies in conjunction with reflectometers, such as Automatic Network Analysers (ANAs), to determine complex permittivities of a wide range of dielectric materials.

The geometry of the original NPL coaxial sensors is shown in Figure 1. These sensors are referred to here as 'Type A' and were constructed with the following properties [8,10]:

Sensor Type A:

a, inner conductor radius, = 2.333 mm

b, outer conductor radius, = 7.549 mm

ε_b', bead permittivity, = 2.15

These Type A sensors were referred to as 14-mm sensors because they were constructed from General Radio stock precision 14-mm airline. This diameter was originally chosen because it produces a fringing capacitance of about 0.1 pF into air, which was found to be optimum for measuring biological tissues at about 1 GHz [8–10]. The circular flange at the end of the line was added to aid calculability. The dielectric bead was required both to support the inner-conductor and to present a well-defined interface plane into liquid and air dielectrics. The design of the bead preserves a characteristic impedance of 50 Ω in the line *ibid.*.

In subsequent work it was established that Type A PTFE-beaded sensors could not be adequately sterilised. As this was essential for *in vivo* measurements upon biological tissues [16,17], a new design, 'Type B', was produced with a glued-in thermoplastic bead made from 'Lucentine' for such measurements. The only significant differences between the Type A and B sensors for computational purposes are the permittivities of their respective beads, ε'_b, and the corresponding radii of the inner conductor, a, required to preserve a characteristic impedance of 50Ω through each bead. Type A and B sensors are otherwise identical and both may be represented by Figure 1(a).

Two sensors were used in the present project. One was a conventional NPL Type B 50-mm diameter sensor which was used for high loss work. It offered the convenience of a simple probe-type measurement-geometry and had the advantage that it was more robust and stable than the earlier Type A design. The second sensor was a new 'Type C' 100-mm flange-diameter version, designed to be coupled to a cylindrical dielectric cell for low-loss, liquid-immersion and 'finite specimen diameter' work (see Section 3, below). For computational purposes the important parameters of these two sensors are, however, identical:

Sensors of Types B and C:

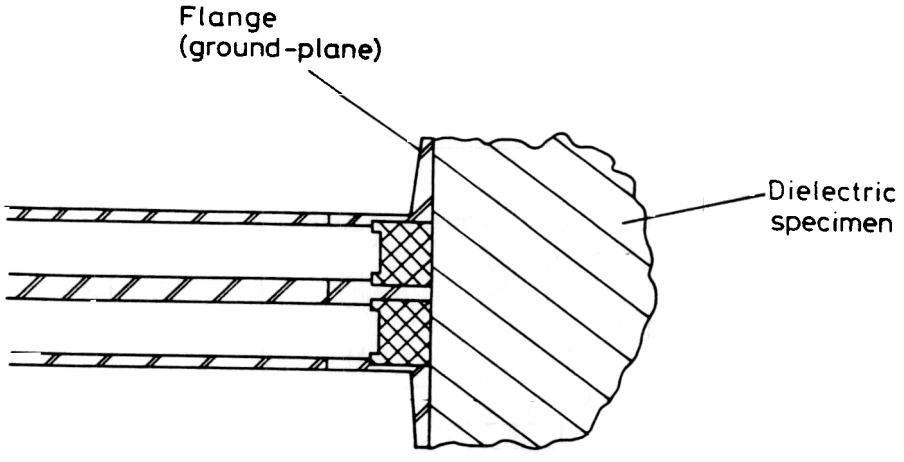
a, inner conductor radius, = 1.994 mm

b, outer conductor radius, = 7.545 mm

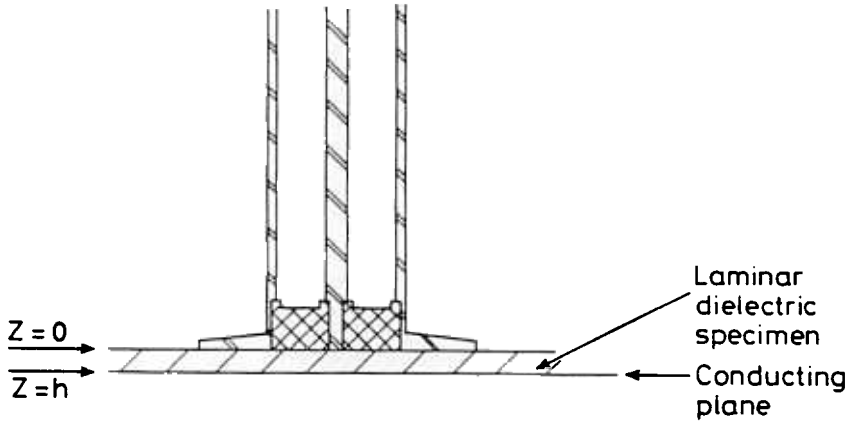
ε_b', bead permittivity, = 2.538

Figure 2 demonstrates the uses of a Type C sensor. Only Type A and Type B sensors can be strictly referred to as 'probes', as is common usage elsewhere. In this report, the general term 'sensor' is used for all three of our reflectometric open-ended coaxial designs.

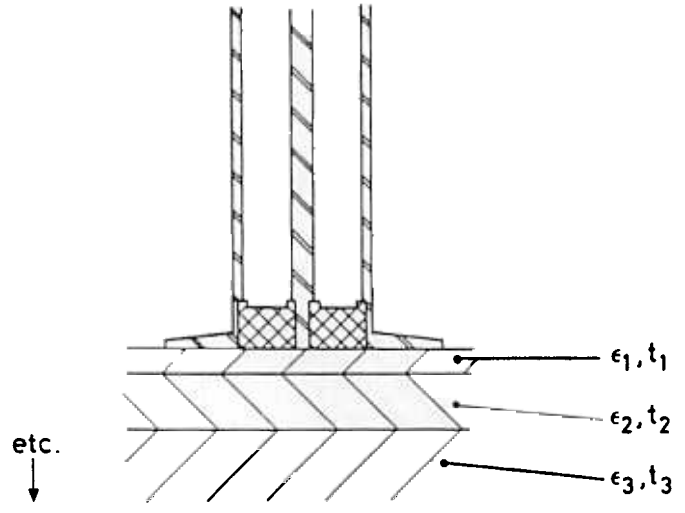
For other types of work, smaller sensor diameters are desirable. Running in parallel with this project has been a project for development of a 7-mm diameter sensor at NPL [12]. Perhaps the most commonly used sensors are those developed by Hewlett-Packard [3,5]. These have a 3.5-mm diameter and operate up to 18 GHz (though with much increased uncertainty compared with NPL sensors). Generally speaking, the larger the diameter of the sensor, the lower the frequency for which it will be optimised. Also, for a given frequency, the lower the permittivity, the larger the sensor diameter should be. These relationships follow from the fact that the fringing admittance is roughly proportional to the diameter multiplied by the frequency. Whichever diameter is used, the relationship between the measured reflection coefficient, Γ, and the complex permittivity, ε^*, is best obtained by the use of electromagnetic field modelling on computers. Use of simple equivalent circuits instead is still common practice but is inadequate for our purposes [10,20,21]. At NPL we have been able to use a number of independent numerical techniques to predict Γ for a given geometry and these have been shown to agree with each other very well [20] - in fact discrepancies were much smaller than the expected measurement uncertainty. Prior to the present work, these solutions have been obtained only for dielectrics which obey the following two conditions: (a) they should fill the *whole* infinite space into which the fringing fields emerge - this may be an 'infinite half-space' or an 'infinite laminar space' - see Figure 1 - and (b) they must be homogeneous. In practice, condition (a) is never attainable, but if the dielectric is sufficiently lossy, it is possible to assume that the 'infinite space' condition holds if reflected signals from the remote specimen faces are largely absorbed in the dielectric, thereby being prevented from returning to the sensor with sufficient magnitude to render the computation invalid. That this is not always the case even with supposed lossy materials was demonstrated some years ago [8,10]: in a beaker of water at around 1 GHz resonances occur which render the 'infinite space' approximation invalid. Work performed in the present programme now allows us to predict and quantify these effects, see Section 2.5.4 below. Condition (b) arose under the older theories because any inhomogeneity in the dielectric gives rise to reflections which can change the quantity of signal power returning to the sensor, and hence to erroneous permittivity measurements. Here again, the present work allows us to go beyond former computational limitations to cover the specific case of a (lossy) stratified medium.



(a) Sensor geometry for measuring an 'infinite half-space'

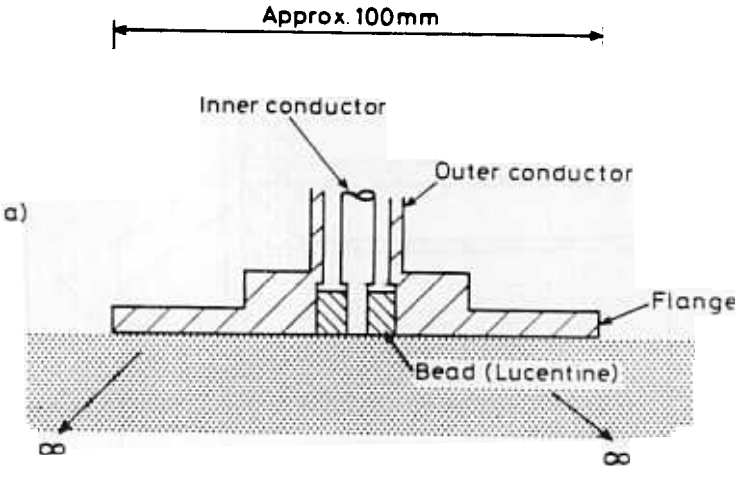


(b) Sensor geometry for measuring a single layer lamina

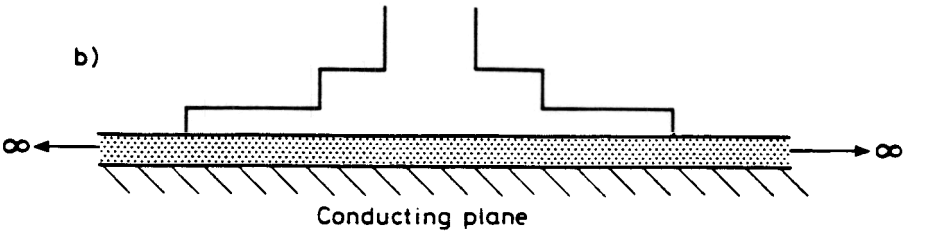


(c) Sensor geometry for measuring a multilayer lamina

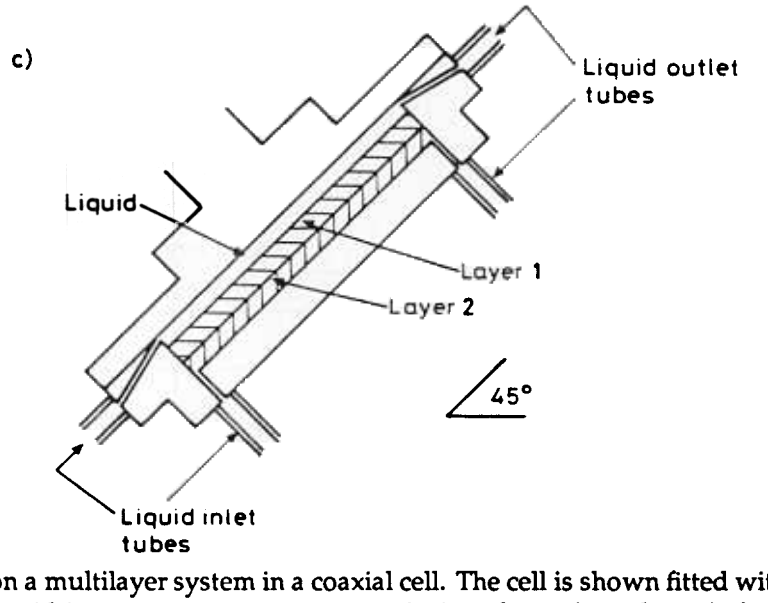
Figure 1 Modes of use of the 14-mm open ended coaxial sensor. The sensor is of NPL Type A or Type B (see text, page 4), with dielectric support beads of PTFE and lucentine, respectively. In both cases the inner-conductor diameter is reduced and the bead is undercut inside the line to preserve a good match to 50Ω characteristic impedance. The flange diameter is 50 mm.



(a) Measurement upon 'infinite half-space' specimens.



(b) Measurement upon a single-layer lamina



(c) Typical measurement upon a multilayer system in a coaxial cell. The cell is shown fitted with inlets and outlets for liquid and liquid-immersion measurements. A ring clamp (not shown) clamps the sensor to the cell.

Figure 2 Modes of application of the NPL Type C 14-mm coaxial sensor

1.3 PREVIOUS WORK AT NPL

The coaxial sensor was first used at NPL in 1984 as a means of measuring biological tissues *in vivo* in a collaborative research programme on cancer screening with The University of Surrey [8–11]. Such sensors had already had a long prior history of use in other laboratories. As already mentioned above, the diameter of the 14-mm NPL sensors was chosen so as to maximise sensitivity for tissue measurements at frequencies up to 1 GHz. Sensors of this diameter are, however, usable at least up to 3 GHz, the upper frequency limit for practical use being dependent on the specimen permittivity. This frequency range is probably the best also for more general diagnostic measurements upon tissues, whether in the medical or food technology fields. Although coaxial sensors were undoubtedly convenient to use, most of the then (1984) current measurement practices and theory prevented them from realising their full metrological potential [8,10]. Further work enabled an improved calibration scheme to be developed and a quantitative comparison study of conventional coaxial sensor practice against the NPL techniques was produced [10]. The Type A sensor design was adopted to allow calibration by means of conventional network analyser artefact standards (eg. short, open and load). Numerical analysis programs relating permittivity, ε^*, to reflection coefficient, Γ, were written, derived from a computer program kindly supplied by Prof. F. E. Gardiol and J Mosig of the École Polytechnique de Lausanne, Switzerland [28]. It was shown that the conventional techniques relying on simple equivalent circuits and reference liquid calibrations could give rise to significant measurement error but that this could be avoided by more comprehensive software and calibration methods.

This first collaborative project was followed by a second, this time with The Oncology Centre (then the Radiotherapy Centre), Bristol. It was instigated by their need to characterise the dielectric properties of tissue to improve hyperthermia treatment of tumours at frequencies up to 900 MHz. This work entailed the construction of new types of sensor, including (as mentioned above) a sterilizable sensor (Type B) and a resonant sensor [16,22]. Three separate computer programs were used and shown to agree for all practical purposes [15,20,39] in their predictions of the relationship between permittivity and complex reflection coefficient. The relationship is perhaps best presented at a given frequency by a mapping from the complex-permittivity ε^*–plane onto the Γ-plane (or Smith Chart). Two examples of this are given in Figure 3. The work further entailed a programme of reference liquid calibrations [18,19] for the following reason. One of our original reasons for rejecting conventional coaxial sensor practice was that reference liquids (such as methanol, ethanol, saline solutions, etc.) were used to calibrate them when the dielectric properties of these liquids were not well-enough known for our purposes [10,19]. At the same time the real advantages and conveniences of being able to use reference liquids for sensor calibration were recognised . The reference liquid calibration programme was therefore conceived in the light of the need for better complex permittivity figures for the liquids. The measurements were performed in specially constructed cells and the permittivity figures obtained for reference liquids show a great improvement upon figures obtained from the literature (this work is not yet published).

The final sub-project in the collaboration with Bristol was the application of coaxial sensors to the measurement of single-layer laminas, see Figure 2 (b). The computer program for the single layer laminas was proposed at NPL by Warham [39], the final version, 'AGPW' (cf. Table 1), being written by one of the present authors (G. T. Symm of the Division of Information Technology and Computing - DITC). Warham's approach to the open-ended sensor (referred to as an 'annular slot antenna') is in turn based upon that of Nevels *et al.* [29]. It was extended beyond their treatment of the semi-infinite half-space dielectric to cover the case of a dielectric lamina backed by a conducting plane parallel to the sensor flange. Comparisons between the

predictions of this program with the results of ANA measurements on reference liquids using a 14 mm sensor up to 3 GHz showed good agreement provided the liquid was lossy [21]. Typical mappings produced by 'AGPW' for the 'infinite half-space' case and for a 1-mm lamina are shown in Figure 3. The successful outcome of this work led to the proposal that the sensor technique could be used for characterising multilayer laminas, which was the starting point for the present project.

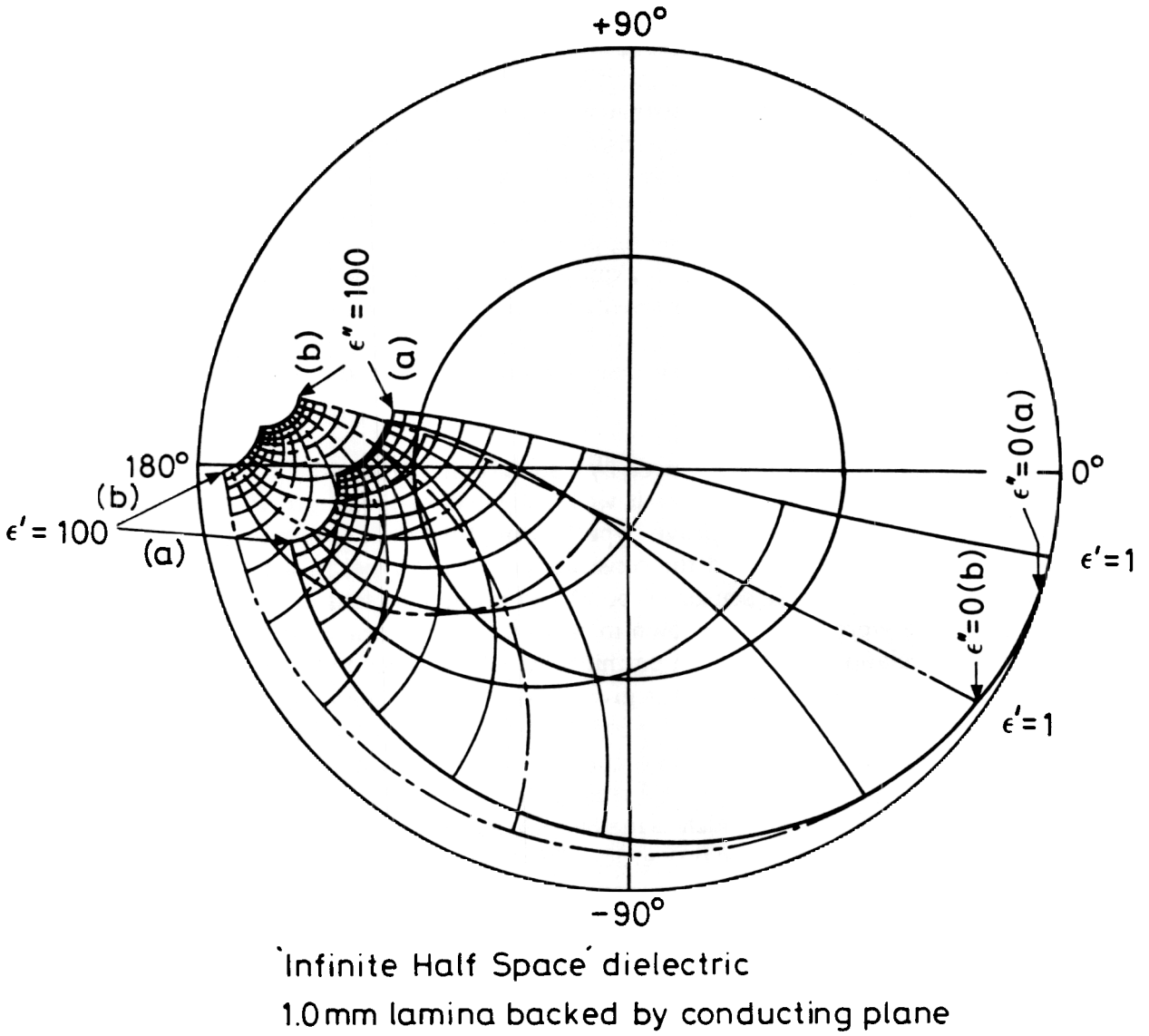


Figure 3 Mappings of the ε^*–plane onto the Γ-plane for a Type A 14-mm coaxial sensor at 2 GHz. The mapping for a 1-mm lamina, (b), is shifted closer to the 'short-circuit' position on the chart ($\Gamma = -1.0$) because fringing capacitances are higher for that geometry (Figure 2(b)) than for an 'infinite half-space' (Figure 2(a)). The computations were performed by program 'AGPW' (cf. Table 1).

A SURVEY OF THE RECENT LITERATURE

There has been widespread use of coaxial sensors over recent decades. Some of the work described above has been mirrored in other laboratories and other work originating elsewhere was adopted into the NPL programmes. That of Mosig *et al.* [28] and Nevels *et al.* [29] has already been cited as having contributed. In the present project, we are indebted to S M Tun [38] for the contribution that his program 'COAX' has made. Also, the method of Saed, Riad and Davis [37] formed the basis of the computer program 'RCAV', described below in Section 2.4.2.

We include here a short survey of recent work on coaxial sensors carried out elsewhere. The survey is not intended to be complete, and in fact concentrates upon laminar, multilayer and related geometries and matters relating to calibration and uncertainties. Nevertheless, it should, among other things, serve to indicate the level of interest that this very convenient sensor technique has aroused. The survey is limited to papers written since 1987, our previous papers [10,20,21] contained surveys of the earlier literature.

'Infinite half-space' geometries, including sensor calibration and uncertainty analysis

Nyshadham, Sibbald and Stuchly [33] have recently published a comprehensive paper dealing with the uncertainties associated with coaxial sensor measurements which arise from the method of calibration. Their calibration standards comprise short, open, water, methanol and 0.5N and 1.0N saline. The relationship between the measurement uncertainties for ε^* and the uncertainties in the relaxation parameters of the reference liquids is worked through in detail and formulae for computing those parameters are provided. Their concern over the uncertainties in ε^* of the reference liquids is one which has been shared at NPL [18,19].

Misra *et al.* [26] are also concerned with sensor calibration errors and have analysed the effects of approximate models of sensors, coming to similar conclusions as ourselves [10] regarding the compensatory effects of reference liquid calibration. Otto and Chew [34] used a shorted waveguide cavity at the end of a large diameter (32.5 mm), flanged coaxial sensor to *calibrate* the latter for probe-type measurements. However, their computational technique would, of course, be relevant to measurements of (single layer) dielectrics in such cavities. Integral equations for coaxial sensor admittance are also considered by Xu, Bosisio and Bose [42].

Coaxial lines and cylindrical cavities

Besides Saed, Riad and Davis [37] and Otto and Chew [34], as mentioned in the last two sections, Saed [36] has also considered the case of a larger-diameter circular waveguide cavity, containing a specimen, situated on-axis between *two* standard coaxial sections. This geometry has the advantage that transmission as well as reflection measurements can be performed on the specimen. Belhadj-Tahar *et al.* [1] have analysed similar one-port and two-port cavities which are however the *same* diameter as the coaxial outer conductor. They have also recently extended these analyses to uniaxial materials [2].

Single layer laminas

The case of the infinite diameter single-layer lamina backed by a conducting plane has also been considered by Nishikata and Shimizu [31] and Fan and Misra [7]. The former workers expound their approach in some detail and also present measurements.

Laminas, airgaps and multilayer geometries

We are aware, at present, of three other papers that deal with the genuinely multilayer case (The term 'multilayer' is used here to refer to specimens with 3 or more layers). The first is by Moschuring and Wolff [27]. They consider stratified media such as might be used for microwave integrated circuit substrates and are specifically concerned with inhomogeneities in the latter. Li *et al* [23] have an interest in measuring the moisturisation of human skin, which has led them to study the infinite-flange multilayer geometry for very similar reasons to those we have described in Section 1.1.2. They present measurements on skin through a saline layer and are concerned with the uncertainties of such measurements. More recently, a paper has come to our notice by Xu and Bosisio [43], which was published since our own work on multilayer systems was started. Their analysis is for geometries similar to figures 1(a) and (b) and their experimental work has included measurement of surface resistivity of thin-films. In addition to these three papers, Nishikata and Shimizu [32] have analysed the 'sandwich' case of a solid laminar specimen backed by a conducting plane, similar to Figure 1 (b), but with a gap on either side of the dielectric.

1.4.5 Other structures and geometries

The advantage of all of the above analyses from the dielectric metrologist's point of view is that they all deal with flat specimens, which tend to be 'standard' in this field. Analyses of other specimen geometries are of course possible but, except (a) in cases where specimens are manufactured in a 'special' geometry, and are required to be measured in that geometry, and (b) in the case of liquids (or malleable solids like powders), any other geometries can be somewhat less than convenient for measurement purposes. Analyses of non-planar geometries still need to be carried out for cases (a) and (b), however, and are also relevant to the production of calibration standards.

Macphie, Opie and Ries [25] analyse a single layer structure similar to the NPL Type C sensor connected to a larger diameter cylindrical waveguide, Figure 2 (c). Here, however, the inner conductor is extended some distance, as a 'probe', into the circular waveguide section. Daywitt [5] has analysed the so-called *'discontinuous-inner'* geometry. This is a standard computational problem which deals with a geometry similar to that just mentioned, but with a circular waveguide section having the *same* diameter as the outer conductor of the coaxial section. This geometry is otherwise known as a *'shielded open-circuit'*. Daywitt's analysis differs from that of the standard problem by analysing a geometry in which a cylindrical hole is bored concentrically into the centre-conductor ('hollow centre conductor').

Wheeler and Nevels [40] have analysed an 'infinite half-space' geometry in which the coaxial ('open-circuit') aperture is covered by a dielectric hemisphere. Xu and Bosisio [41] consider the case where the inner conductor itself is extended in the form of a hemisphere to increase the

sensitivity of the sensor and Nevels and Wheeler again [30] go on to consider a combination of these two geometries.

Summary Discussion - How the NPL work relates to the literature

It is clear that other workers share many of the interests which originally instigated the NPL coaxial sensor programme. The requirement to demonstrate traceability in the present project, however, gives rise to a different emphasis in our investigations. Theoretical papers in this area of research have typically reported only a single new computational technique and measurements are often not on materials whose permittivity is traceable. There are exceptions to both of these statements, eg. References 42 and 33 respectively, but, to the best of our knowledge, the present programme is the first to produce comprehensive *multiple* intercomparisons between computer programs and measurements upon *traceable* dielectric reference materials in single, double and multilayer laminar form. The main aim of our approach has been to provide confidence in techniques that greatly extend the range of application of coaxial sensors and at the same time guarantee traceability.

SUMMARY OF WORK AT NPL ON MULTILAYER LAMINAS

A brief summary of the work carried out in the present project follows:

Three different computer routines were developed for computations on dielectrics with two or more layers. The routines were intercompared and shown to give consistent results as did a computer program which was purchased to help provide confidence in the intercomparisons and to assist in the process of deriving an uncertainty budget.

A new Type C coaxial sensor was developed together with a cylindrical 'cavity' or waveguide cell to enable calculable measurements to be performed upon low loss materials and to allow improved measurements to be performed upon solid laminas by means of a liquid-immersion technique. Techniques of calibration and measurement were developed both for this sensor and the 'high-loss' Type B sensor to enable them to perform multilayer lamina measurements.

A number of dielectric specimens were machined, and standard dielectric specimens were used, for stacking into multilayer arrays to test the techniques and programs. All of these specimens had previously been characterised by means of other techniques. In addition the multilayer programs were tested against two-layer and multi-layer systems in which at least one layer was a reference liquid. This had the advantage that the thickness of that layer could be changed and it also provided a ready means of testing the system with well-characterised lossy materials. One of the programs has been 'inverted' so as to allow complex permittivity of a single layer to be computed from the measured reflection coefficient (rather than vice versa). This 'inverted' form is the most convenient for use during measurements.

The measurement/program intercomparisons show that single and multiple layer dielectrics can be characterised in conformance with the requirements of NMSPU. In summary: measurements upon specimens less than 50-mm in diameter are possible. 95%-confidence level uncertainties of better than 3% are possible for one layer and better than 10% for the second layer of a multilayer system, where the thicknesses of the layers are known. Uncertainties for any layer in a multilayer system can be computed.

2 NEW PROGRAMS FOR LAYERED DIELECTRIC GEOMETRIES.

2.1 SUMMARY OF NEW WORK ON COMPUTER PROGRAMS

Three types of program have been commissioned and one has been purchased to analyse reflection coefficients from open-ended coaxial sensors when they are placed up against multilayer dielectrics. This aspect of the project required comprehensive checking of programs to ensure that they were operating correctly. This was one of the reasons for commissioning more than one program: when two or more programs working on different computational principles are intercompared and are found to agree, confidence in all of them is enhanced in a way that would not be possible with only one program. The second reason for requiring more than one program is that each program is optimised for different loss and specimen geometry conditions: the diversity of specimen type has to be mirrored in a diversity of program types. Nevertheless, all programs were written so as to be applied to certain common, 'standard', geometries which allowed us not only to intercompare them with each other but also with long-standing tried-and-tested NPL programs for 'infinite-half-space' and 'infinite' single-layer laminas.

The intercomparison proved to be very successful in showing up program bugs. They were identified and corrected with much greater efficiency through the ongoing intercomparison programme than would otherwise have been possible. Any discrepancies that came to light were immediately brought to the attention of the programmers and in all cases it was possible to identify and correct errors. It is not, of course, possible to say that all errors and bugs have been removed, but we can say that residual mutual discrepancies are significantly smaller than expected measurement errors. The new and existing programs are described below in Section 2.4, following a preliminary discussion of an important computational technique which improves computer predictions (Section 2.2), and a description of the intercomparison geometries used (Section 2.3).

2.2 QUADRATIC EXTRAPOLATION

In our previous work on coaxial sensors (see Section 1.3) the field modelling programs were themselves subjected to intercomparison and were tested so as to establish their optimum method of use. It was discovered through this process that every program was improved by using it with a **quadratic extrapolation technique** [20] and this feature was also implemented in two of the new programs. All of our programs work on the basis of some kind of *discretisation*. That is to say that, in modelling the electromagnetic fields, one has to analyse them as superpositions of discrete normal modes [10,39], or else one slices space into a number of rings (circular symmetry) [39]. In the case of the lamina [21,39], one additionally has to compute total fields as sums of multiple-reflected signals between sensor flange and back-short. In each case the number of modes, rings or reflections has to be limited in practice to a small finite number, whereas the correct numerical solution requires that an *infinite* number of modes etc. is used. The limitations are of computer memory and time. Quadratic extrapolation allows one to estimate an approximate solution for an infinite number of modes whilst only needing to compute solutions for small finite numbers. Henceforth in this section discussion of 'modes' should be understood to apply equally well to 'rings' and 'reflections'.

Assume one wishes to estimate the reflection coefficient, Γ_∞, that one would obtain were the program able to handle an infinite number of modes. Let Γ_n be the approximate reflection

coefficient delivered by the program in a computation using only a finite number, n, of modes. Quadratic extrapolation assumes that Γ_n is related to the desired result Γ_∞ by the following series, which is terminated after the quadratic term:

$$\Gamma_n = \Gamma_\infty + a/n + b/n^2 + \qquad (1)$$

Here a and b are constants that characterise the approximation process. By applying (1) three times, for the program results Γ_m, Γ_{2m}, and Γ_{4m}, where m is some integer, we can derive:

$$\Gamma_\infty = (8\Gamma_{4m} - 6\Gamma_{2m} + \Gamma_m)/3 \qquad (2)$$

This extrapolation will only work well if Γ_m, Γ_{2m}, and Γ_{4m} are *in fact* tending towards an asymptotic value; it may give spurious results otherwise.

After testing on the earlier NPL programs [20], it was found in general that $m = 4$ was perfectly adequate for our practical purposes.

As already mentioned, the object of using such extrapolations is to save computing time:- a result obtained by quadratically extrapolating from, say, Γ_4, Γ_8, and Γ_{16} to Γ_∞, is much quicker to obtain than, say, Γ_{64} but the evidence shows it is typically just as good an approximation to Γ_∞. In all cases the importance of quadratic extrapolation in this work is shown by the following discovery. If quadratic extrapolation is not used and n lies in the range 4 to 8, residual computational errors will be comparable, if not larger than, expected measurement errors; where quadratic extrapolation is used, computational errors become much smaller, and are often insignificant in comparison with measurement errors.

2.3 INTERCOMPARISON GEOMETRIES

As described in the next section, each of our programs is optimised for a different type of geometry. However, in the limit, each can be made to deal with at least one geometry which can be treated by the others. This makes the intercomparisons possible. The following geometries can be used for comparing the new programs with the previously existing ones, summarised in Reference 20:

G1: The 'infinite half-space' open-ended coaxial sensor geometry. See Figure 1 (a). Here a coaxial line emerges perpendicularly through an 'infinite' perfectly conducting plane, having an open end in that plane. The half-space beyond the plane is completely filled with a dielectric having a complex permittivity ε^*. The programs written for NPL coaxial sensor work prior to the present project [10,15,20,21,39] can compute the reflection coefficient, Γ, of this geometry when supplied with a value for ε^*. The new multilayer programs can handle this geometry as a limiting case.

G2: The open-ended coaxial sensor with an 'infinite' lamina. See Figure 1 (b). The dielectric specimen is in the form of an 'infinite' parallel-sided lamina sandwiched between the sensor flange and an infinite conducting plane. The new programs can be compared here with 'AGPW' [20,39] in the limit of large specimen diameter.

Geometries which can be handled only by the new programs include:

G3: The open-ended coaxial sensor with a finite-radius lamina. The geometry is similar to G2 but with a circular specimen filling a 'short-circuited', perfectly conducting cylinder or circular waveguide. In the case of specimens having significant loss, it is possible to simulate a cylinder of *'infinite'* length by using a long but finite length.

G4: Multilayer specimens The main aim of this research programme is to be able to deal with multilayer specimens made from a number of face-contiguous parallel-sided laminas, each having a different, but uniform and isotropic, complex permittivity. The geometries are otherwise the same as G2 or G3.

In Section 2.4, following, each program is characterised in terms of which of these geometries it can model.

2.4 THE COMPUTER PROGRAMS

2.4.1 Programs previously developed for earlier work

The importance of the three programs 'TEH', 'GTS' and 'AGPW' for the present project is not to be underestimated, even though they cannot handle multilayer geometries. They have already been well tested, both through intercomparison with each other and by comparing with measurements on 'known' materials [10,21]. They therefore form a 'standard' against which each of the new programs can be compared, for suitable simple specimen geometries. They are summarised in Table 1. Each one of them employs a TEM/TM modal field decomposition in the coaxial section and each deals with the 'infinite-half-space' geometry [10,20]. The third program 'AGPW' also handles the 'infinite' diameter *single*-layer lamina [39]. The column labelled 'Geometry' summarises the geometries the programs can handle, as listed in the previous section.

Table 1 Programs in use prior to the present project

Method	Programmer	Abbrev.	Computer, etc.	Geometry	Reference
Variational	T E Hodgetts	TEH	HP Series 300, Pascal	G1	[15]
Point matching	G T Symm	GTS	ICL 2972, Fortran	G1	[10,28]
Nevels *et al.*	A G P Warham	AGPW	VAX, Fortran	G1 G2	[39,29]

The Tables 2 (a), (b) & (c) show the results of intercomparing these three programs for 'typical' hypothetical complex permittivities in an 'infinite half-space' geometry. These comparisons were carried out by S Jenkins (1989) [16,20]. The computations use the optimised versions of the quadratically extrapolated programs (as elsewhere in this report).

The computational discrepancies are to be compared with best possible anticipated measurement uncertainties of 0.003 for $|\Gamma|$ and 0.1° for θ.

Table 2 Comparison of 'infinite half-space' programs

(a) Frequency 100 MHz, $\varepsilon^* = 100 - 1000j$

Program	$\|\Gamma\|$	phase, θ
TEH Variational	0.4851	-176.4760
GTS Point-matching	0.4847	-176.4747
AGPW Nevels *et al.*	0.4850	-176.4779

(b) Frequency 1 GHz, $\varepsilon^* = 100 - 100j$

Program	$\|\Gamma\|$	phase, θ
TEH Variational	0.6716	-165.5363
GTS Point-matching	0.6716	-165.5391
AGPW Nevels *et al.*	0.6715	-165.5499

(c) Frequency 2 GHz, $\varepsilon^* = 50 - 50j$

Program	$\|\Gamma\|$	phase, θ
TEH Variational	0.6345	-169.6633
GTS Point-matching	0.6341	-169.6766
AGPW Nevels *et al.*	0.6343	-169.6859

2.4.2 The new multilayer programs

One program was purchased, but the other three were commissioned by the RF and Microwave Group from other members of NPL staff. They are summarised in Table 3. It should be pointed out that although this work was exclusively concerned with dielectric measurements, these programs can readily be modified to handle isotropic, linear magnetic materials.

Table 3 New multilayer programs

Method	Programmer	Abbrev.	Computer, etc.	Geometry	Reference
Variational	T E Hodgetts	TEH2 TEH3	HP Series 300, Pascal	G3 G4 2-, 3-layer	[14]*
Integral Equation	G T Symm	MIC2	VAX Fortran	G1 G2 G4 multilayer	[39]*
Saed *et al.*	G T Symm	RCAV RCAV3	VAX Fortran	G1 G2 G3 G4 1-, 2-, 3-layer	[37]*
S M Tun	S M Tun	COAX	386 SX PC	G3 G4 multilayer	[38]

*Some or all aspects of 'TEH2', 'TEH3', 'MIC2', 'RCAV' and 'RCAV3' are being applied for the first time in this project and are presented for the first time in this report

Short descriptions of each of these programs follow.

Program 'COAX'

This is a commercially available program. It was purchased from Dr Soe Min Tun of SMT Consultants Ltd. via Antenna Software Ltd. 'COAX' enables scattering coefficients to be computed for arbitrary coaxial geometries. These include longitudinal sections in which no inner conductor is present and sections which may be filled with homogeneous dielectric. Multilayer geometries are readily modelled [38]. Version 1.01 of the program was specially commissioned to allow the permittivity of each dielectric to be a complex quantity, ie. *lossy* dielectrics are allowed. The program has been purchased as object code only and it operates on a 386SX PC. During the evaluation phases of this project, this program has proved invaluable: through the intercomparisons it contibuted to providing confidence in *all* of the programs. Its main advantage was its geometric flexibility which allowed it to be used, for example, for checking errors caused by air gaps and estimating uncertainties. However, its major *dis*advantages from our point-of-view are two-fold and they come into play when one is actually performing measurements: (1) The program does not perform quadratic extrapolation. It has to be run three times with different mode numbers and the results has to be extrapolated by a special auxiliary program. This proves to be very time consuming. (2) Its availability only in object code format makes it very difficult to include it in computer loops for long runs of measurements. For these reasons, the purpose-written programs are far more efficient and convenient to use in the long run for coaxial sensor measurements.

Program 'MIC2'

This program was written by one of the authors, Dr George Symm of DITC, NPL. It is designed to deal with *lossy* layered dielectrics which fill an 'infinite half space' beyond the end of the sensor. The program is an extension of 'AGPW' written by A G P Warham and is based upon a suggestion of his [39]. It can deal with parallel multilayer dielectrics provided they are lossy. It can effectively handle 'zero' loss, however, by attributing to the dielectric a very small loss whose influence upon $|\Gamma|$ is insignificant compared to the sensitivity of measurements. This has been done for air, for example in Table 4 below. The program is implemented on the NPL VAX and is written in Fortran 77.

Programs 'TEH2' and 'TEH3'

These two programs are based on routines supplied by T E Hodgetts, Division of Electrical Science, NPL, Branch C, Malvern. They are designed to deal with lossy and non-lossy dielectrics of finite cross-section. 'TEH2' is restricted to two layers, 'TEH3' is extended to three layers, and similar 'TEHn' ($n > 3$) versions of the program can readily be written, as required. In respect of their being finite cross-section programs, 'TEH2' and 'TEH3' deal with geometries similar to 'COAX', 'RCAV' and 'RCAV3', including the Type C coaxial sensor geometry when it is connected to the cylindrical cell, as shown in Figure 2 (c). The mathematical routines at the heart of TEH2/3 is an implementation of the theory described in Reference 14. Much of the earlier testing and numerical intercomparison of this numerical technique was performed with 'TEH2', as can be seen from the tables in this section. However, where it is not necessary to distinguish between the two programs, the form 'TEH2/3' will be used in this report to signifiy either. This program is written in Hewlett-Packard (HP) Pascal and runs on HP Series 300 workstations.

Programs 'RCAV' and 'RCAV3'

These programs were again written in Fortran 77 for the NPL VAX computer by by Dr G T Symm. The former is concerned with a single-layer case and the latter with a stratified specimen of up to three layers. The geometry they handle is otherwise the same as for 'TEH2/3' and so is appropriate for the cylindrical coaxial cell. They offer a completely independent means of computing reflection coefficients for this case. The two programs are developed from the work of Saed *et al.* [37].

At present, for convenience, all programs have been limited to three-layered structures, which in all but special cases discussed in Section 5.2, below, is probably the practical limit for the technique. However, the extension of the programs to cover a larger number of layers is essentially trivial, should it be required.

All of these programs compute reflection coefficients from known complex permittivities and geometries. At the time of writing, only 'TEH2' and 'TEH3' in Table 3 have been *inverted* into a form suitable for normal *measurements* of permittivity. This entails the writing of a version of each program which, by means of iteration, computes complex permittivity of a single layer of dielectric, given (i) the measured reflection coefficient, (ii) the overall geometry (ie. layer thicknesses, etc.) and (iii) the permittivity of all other layers. This inversion can also be applied to 'MIC2', 'RCAV' and 'RCAV3' without difficulty. All programs in Table 1, for example, have already been inverted in this way. In view of the large number of degrees of freedom in multilayer measurements, however, it is probably best to 'invert' and optimise programs whenever required for a specific measurement problem.

'TEH2/3' and 'MIC2' were written to use quadratic extrapolation, as explained in Section 2.2. This was not found to be necessary with 'RCAV' and 'RCAV3' where 20 modes are normally used in the coaxial line (but 40 modes in Tables 8 and 9). Quadratic extrapolation has to be performed *externally* to the program in the case of 'COAX', as described above. Where extrapolation is applied, considerable effort went into testing the correct value for m to be used in each case, but as before, $m = 4$ (ie. with quadratic extrapolation from Γ_4, Γ_8 and Γ_{16}) was found to be adequate. Note that these subscripts refer to the number of modes used *in the coaxial line.* Programs 'TEH2/3', 'RCAV' and 'COAX' also use discrete modes in the cylindrical cell section which has a considerably larger radius than the coaxial line. In general the number of modes used in the cell section was scaled approximately in the ratio of radii of cell to coaxial line outer: $(r : b)$. For example, corresponding to $n = 4, 8, 16$ modes in the coaxial line, 'COAX' was used with 20, 40 and 80 modes respectively for a 26-mm radius cell. In 'RCAV', the number of modes in the cell is $r/(b-a)$ times the number in the coaxial line.

2.5 NUMERICAL INTERCOMPARISONS OF PROGRAMS

Please note that, except where otherwise stated, the computations presented in this section (Section 2.5) are for an NPL Type A sensor. This allows continuity with previous intercomparisons which were performed prior to the time that sensors of Types B and C were available.

The new programs of Table 3 deal with complicated geometries and their computations are performed using a significant number of normal modes, rings, reflections, etc. They can therefore require considerable central processor time to run on our computers. It is typically necessary to leave a computation on, say, measurements at 30 frequencies to run overnight. During

development, when programs have to be run intensively for testing purposes, it was therefore required to work efficiently to save effort. Fortunately, it was not necessary to test all programs for all possible initial conditions: 'typical' and 'limiting' cases were often sufficient to demonstrate agreement. Where there are blank entries in the comparison tables that follow (Tables 4 - 10), therefore, it may be assumed that this is done without any compromise to the quality of the work, but for reasons of economy of time or finance.

Likewise, comparisons presented for the 'finite radius' programs do not always present data for the same value of radius, r. The radii chosen for a given program often depend upon particular circumstances which occurred during the development of each individual program. While a rationale for them could be given, it would be inappropriate (and longwinded) to present this background in the present report. Again, it may be assumed that the data presented is sufficiently representative of the agreement of the programs. Where radii-values, r, differ, this is either because they all lie in a range where sensitivity to r is insignificant or else because a particular point about the effects of changing r is being made.

The program intercomparisons are presented here in some depth because it is important that we demonstrate that they can provide a route to *traceable* measurements. Where the only route from measurement (of Γ) to result (ε^*) is via complex numerical analysis routines, as here, we believe that confidence in the computations can only be obtained by intercomparisons of a number of different techniques. This is directly analogous to the normal tried-and-tested metrological practice of performing *measurements* on a given device, specimen, etc. by a number of techniques in order to gain confidence in results. Satisfactory agreement is taken as corroboration and so validates *all* of the techniques. Indeed, it is difficult to imagine any other form of procedure which could do this.

2.5.1 14-mm coaxial sensor with 'infinite half-space' - the high loss case

'COAX', 'RCAV' and 'MIC2' were run in order to try to reproduce the results of Table 2. After a considerable amount of initial testing, to establish the optimum value for m in equation (2) for quadratic extrapolation, satisfactory agreement was obtained in all cases. Figures 4 - 6 illustrate this for 'COAX'. The results from 'COAX' are compared with the infinite-half space programs (Table 1) the extrapolated results from which are in Table 2. These Figures illustrate the effectiveness of the extrapolation procedure. The 'COAX' values are computed for $m = 4$, a waveguide (cavity) radius, $r = 26$ mm and length, $h = 60$ mm. The values of Γ_n for $n = m$, $2m$ and $4m$, are shown together with the corresponding extrapolations. It will be noted that the extrapolations agree very well, especially in Figure 4. The small discrepancies in extrapolations in Figures 5 and 6 are caused partly by the residual effects of using different geometries in the calculations. However, the main cause of disagreement is believed to lie with the limited accuracy of the version of 'COAX' used due to computer memory limitations. The residual discrepancies are smaller than the anticipated measurement uncertainties by a factor of at least three. Similar results have been obtained with 'RCAV' and 'MIC2'. They agree more closely with the values in Table 2 than does 'COAX'.

These results provide extra confidence that the infinite half-space computations are valid. Some of the results from 'GTS', 'TEH' and 'AGPW' were published previously [20]. Their Γ_n values all approach Γ_∞ from the same direction, so that, despite the excellent agreement of the extrapolated values, it was still possible that they could all share a common systematic error. The results from 'COAX' home-in onto the extrapolated value from the *other side* of the complex plane, supporting the conjecture that there is no bias of the results.

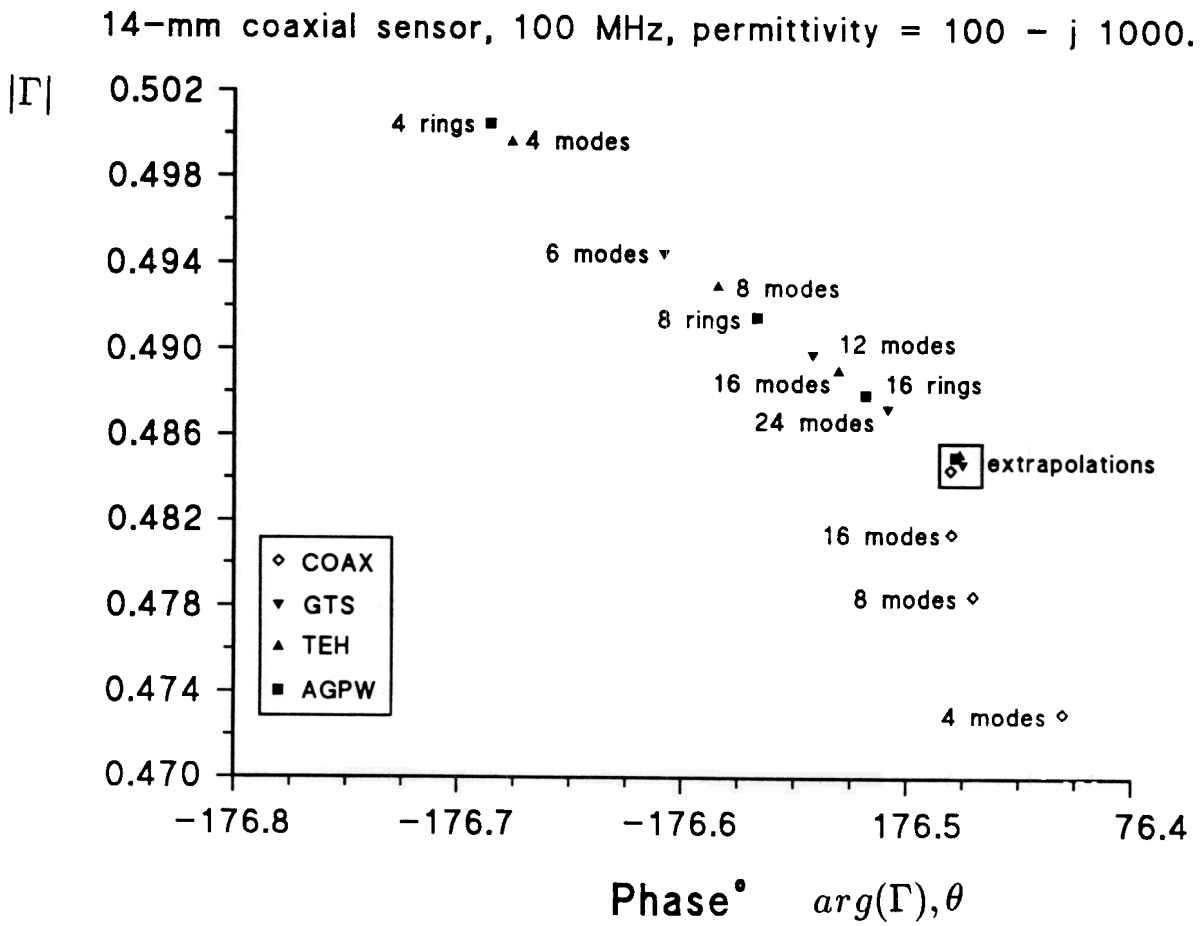


Figure 4 'Infinite half-space' program comparison, 100 MHz. Showing how various values of Γ_n (Equation (1)), computed by programs 'COAX', 'GTS', 'TEH' and 'AGPW', approximate to Γ_∞.

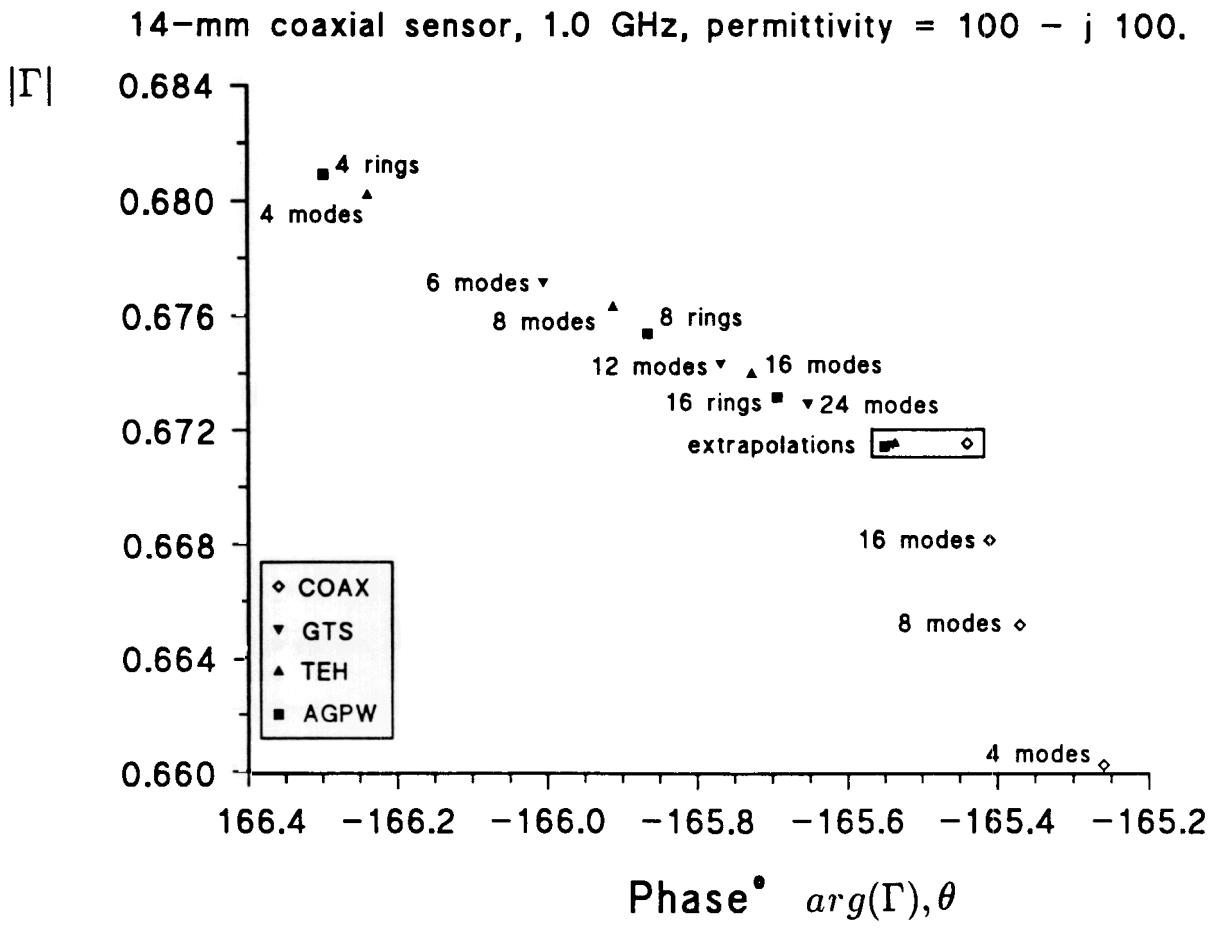


Figure 5 'Infinite half-space' program comparison, 1 GHz.

(see caption to Figure 4)

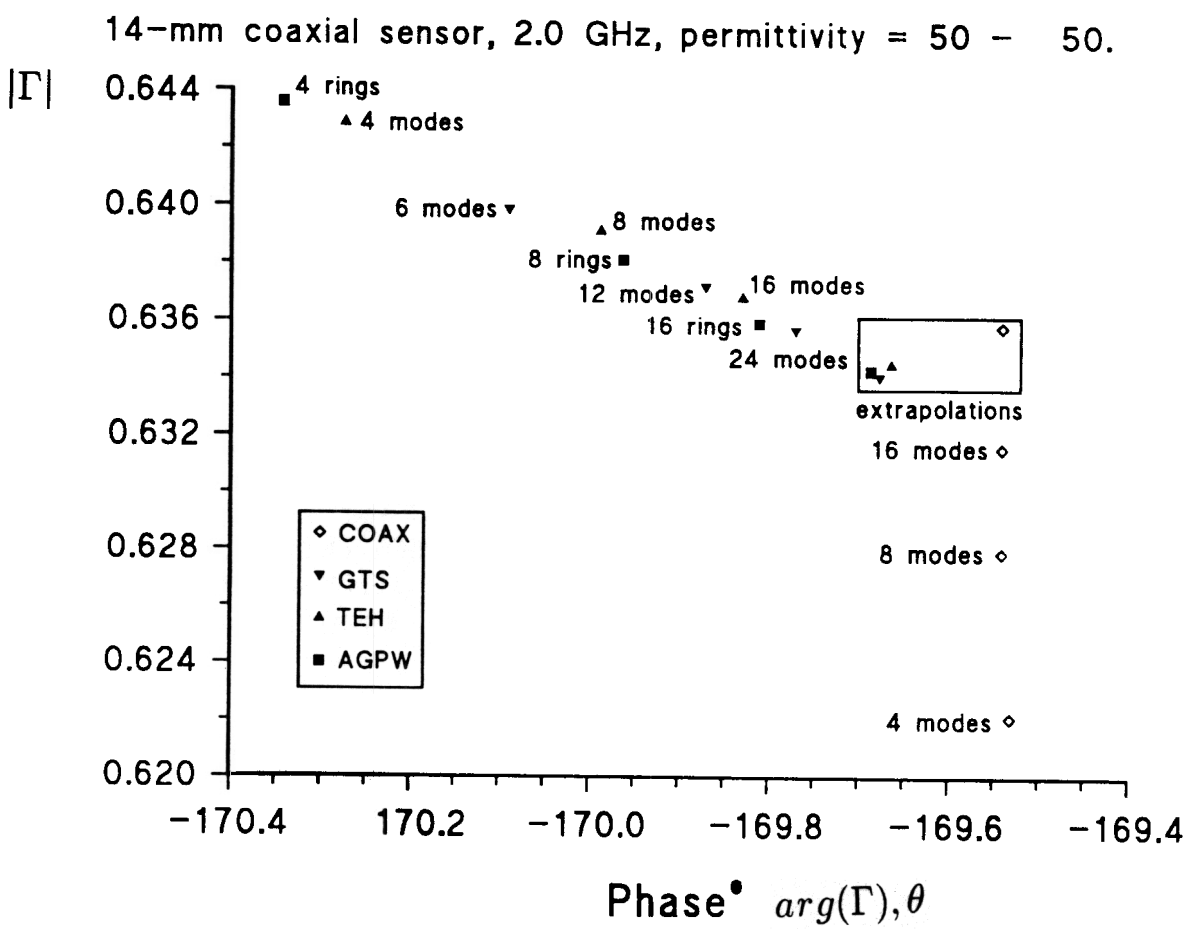


Figure 6 'Infinite half-space' program comparison, 2 GHz.

(see caption to Figure 4)

2.5.2 14-mm coaxial sensor in air

At the opposite extreme of permittivity and loss to the examples described in the last section is air dielectric (for which ε' is as low as possible, at 1.0, and ε'' is effectively zero). It is important to model such limiting cases to show that programs work well for them, as this gives confidence that the numerical models will also work well for the intermediate values of permittivity found in practical measurements.

Here we are comparing computations for an 'infinite half-space' of air. This means that the 'finite-radius' programs ('TEH2/3', 'COAX', 'RCAV') should ideally be supplied with values of the cell (circular waveguide) radius, r, and length, h, which are sufficiently large as to approximate to ∞, so far as the fringing admittances of the sensor are concerned.

When the coaxial sensor is open-circuited into a half-space of air dielectric at frequencies up to 3 GHz one obtains a value for Γ such that $|\Gamma| \approx 1.0$ and a value for its phase, θ whose magnitude increases smoothly with frequency. θ is actually negative because the fringing fields largely present a capacitive admittance to the line. $|\Gamma|$ actually has a value which is very slightly less than 1.0 (more so with increasing frequency) because the sensor is radiating small amounts of power [10,19,20]. However in the specific case of air (as opposed to higher permittivity) dielectric, the power loss is insignificant compared with measurement uncertainties and so $|\Gamma|$ can practically be taken as 1.0 and only the computed phase, θ, need be tabulated and intercompared between programs.

Table 4 shows such an intercomparison between the programs listed in Table 3. Computations with 'COAX' are for a circular waveguide section radius, r, of 26 mm and 48 mm and for an assumed cell length, h, of 60 mm. The larger radius of 48 mm was investigated because, unlike the hypothetical dielectrics used in Sections 2.4.1 and 2.5.1, air is a low loss dielectric and electromagnetic fields of significant magnitude *will* reach the outer walls of the waveguide section, thereby altering Γ. The computations with 'TEH2' and 'RCAV' are for h = 60 mm and r = 35 mm, which corresponds to the radius of a cell actually used for many of our measurements.

Table 4 14-mm coaxial sensor comparison for air dielectric.

The comparison is between all basic programs in Table 3. The table entries are the computed phase, θ, of the reflection coefficient, Γ. ($|\Gamma| \approx 1.0$).

Freq. (GHz) r =	'COAX' 26 mm	'COAX' 48 mm	'TEH2' 35 mm	'RCAV' 35 mm	'MIC2' ∞	'AGPW' ∞
0.100	-0.38	-0.38	-0.38	-0.38	-0.38	
0.200	-0.77	-0.77	-0.77	-0.77		
0.300	-1.15	-1.15	-1.15	-1.15		-1.15
0.400	-1.56	-1.53	-1.53	-1.54		-1.53
0.500	-1.92	-1.92	-1.92	-1.92		-1.91
0.600	-2.32	-2.30	-2.30	-2.31		-2.30
0.700	-2.68	-2.69	-2.69	-2.69		-2.68
0.800	-3.09	-3.07	-3.08	-3.08		-3.07
0.900	-3.45	-3.46	-3.46	-3.46		-3.45
1.000	-3.86	-3.85	-3.85	-3.85	-3.83	-3.84
1.100	-4.25	-4.23	-4.24	-4.24		-4.23
1.200	-4.64	-4.62	-4.62	-4.63		-4.61
1.300	-5.03	-5.01	-5.01	-5.02		-5.00
1.400	-5.42	-5.40	-5.40	-5.41		-5.39
1.500	-5.81	-5.80	-5.80	-5.80		-5.78
1.600	-6.20	-6.19	-6.20	-6.19		-6.17
1.700	-6.59	-6.59	-6.58	-6.59		-6.56
1.800	-6.98	-6.99	-6.98	-6.98		-6.96
1.900	-7.35	-7.39	-7.38	-7.38		-7.36
2.000	-7.77	-7.80	-7.78	-7.78	-7.73	-7.75
2.100	-8.17	-8.21	-8.18	-8.19		-8.15
2.200	-8.60	-8.64	-8.59	-8.59		-8.54
2.300	-8.98	-9.13	-9.00	-9.00		-8.94
2.400	-9.41	-9.28	-9.41	-9.41		-9.35
2.500	-9.79	-9.66	-9.83	-9.83		-9.75
2.600	-10.23	-10.06	-10.25	-10.26		-10.16
2.700	-10.62	-10.46	-10.69	-10.69		-10.56
2.800	-11.04	-10.86	-11.14	-11.14		-10.97
2.900	-11.46	-11.27	-11.60	-11.62		-11.38
3.000	-11.88	-11.68	-12.12	-12.13	-11.76	-11.79

Table 4 in general shows excellent agreement between the programs but with some interesting features which should be mentioned. We can conveniently take the results from the 'infinite half-space' program 'AGPW' (ie. the final column) as a norm against which the others can be compared. The phase magnitude computed by 'COAX' for r = 26 mm is generally slightly higher, diverging linearly with frequency from that of 'AGPW'. This is caused by the presence of the 26-mm-radius waveguide wall in the 'COAX' computation which gives rise to a higher fringing capacitance. One would expect that this capacitive effect would be smaller with a larger waveguide radius. Following the 'COAX' column for r = 48 mm, this is indeed the case up to about 1.6 GHz, but between 1.8 and 2.3 GHz the 'COAX' phase magnitudes are larger, and on passing from 2.3 to 2.4 GHz they abruptly become smaller again. This feature is readily associated with the onset of wave propagation in the circular waveguide section. Below 2.4 GHz all electromagnetic fields in the 48-mm radius waveguide are evanescent, but on passing above that frequency the TM_{01} mode begins to propagate. The same phenomenon can be seen in the 'TEH2' and 'RCAV' columns where the onset of propagation in the narrower 35-mm waveguide does not commence until just above 3 GHz, but the effects on Γ can be seen at lower frequencies in the form of a sharp rise in phase magnitude.

It can be seen that the attempt to make r take a sufficiently large value as to approximate to $r = \infty$ has shown up a problem. In the discussion of practical measurements, Section 6, below, it will be seen that this same phenomenon - onset of propagating modes - gives rise to resonant behaviour in actual dielectric specimens. This phenomenon has not always been taken into account in coaxial-sensor metrology. Wherever the 'infinite' half-space model is explicitly or tacitly assumed, such resonances cannot be allowed for. In the present context of modelling air dielectric, however, and considering the magnitude of anticipated *measurement* uncertainties for θ, (typically of the order $\pm 0.2°$ or more), one may conclude that *all* of the programs agree for virtually all practical purposes for the case of the coaxial sensor feeding into air. This observation even applies to the 48-mm radius case. This is an important finding for practical measurements because 'sensor-into-air' is a natural ANA calibration standard in coaxial sensor metrology. It has been shown here to be theoretically viable.

2.5.3 14 mm coaxial sensor with a single layer lamina

The new programs listed in Table 3 are intended to be used with more complex geometries than the 'infinite half-space'. The simplest geometry of interest is the single layer lamina [21]. 'MIC2', like 'AGPW', assumes 'infinite' radius specimens, so comparisons with programs which deal with finite-diameter specimens must again be performed for large r. In the limit of large radius, for a sufficiently lossy dielectric, all three such programs should deliver the same value for Γ.

The intercomparison was again performed for the three 'test' permittivities of section 2.4.1: $\varepsilon^* = 100 - 1000j$, $\varepsilon^* = 100 - 100j$, $\varepsilon^* = 50 - 50j$, as shown in Table 5. In all cases the lamina thickness $h = 1.0$ mm. The radius, r, is either 26 mm ('COAX'), 35 mm ('RCAV', 'TEH2') or ∞ ('AGPW', 'MIC2').

Again in Table 5, the discrepancies are well within expected measurement uncertainties. The loss of these 'hypothetical' dielectrics is believed to be sufficiently high to ensure that the effects of the wall of the cavity/waveguide section are barely 'seen' by the sensor. That this is not always the case with actual dielectric specimens is demonstrated in the next section.

Table 5 Comparison of Γ-values computed for 1-mm thick laminar dielectrics.

(a) Lamina 1 mm thick, $\varepsilon^* = 100 - 1000j$.

Freq. (GHz)	'COAX' $r = 26$ mm	'TEH2' $r = 35$ mm	'RCAV' $r = 35$ mm	'MIC2' $r = \infty$	'AGPW' $r = \infty$
0.100	0.7298 −178.84°	0.7322 −178.88°	0.7320 −178.89°	0.7315 −178.85°	0.7305 −178.78°
1.000	0.9532 +176.55°	0.9533 +176.51°	0.9535 +176.52°	0.9534 +176.51°	0.9534 +176.51°
2.000	0.9301 +175.12°	0.9296 +175.08°	0.9298 +175.08°	0.9296 +175.07°	0.9297 +175.08°
3.000	0.9173 +176.00°	0.9166 +175.97°	0.9168 +175.96°	0.9166 +175.96°	0.9166 +175.96°

(b) Lamina 1 mm thick, $\varepsilon^* = 100 - 100j$.

Freq. (GHz)	'COAX' $r = 26$ mm	'TEH2' $r = 35$ mm	'RCAV' $r = 35$ mm	'MIC2' $r = \infty$	'AGPW' $r = \infty$
	0.4186 −82.51°	0.4176 −83.34°	0.4170 −83.63°	0.4159 −83.39°	0.4177 −82.69°
	0.8380 −175.22°	0.8382 −175.39°	0.8390 −175.33°	0.8385 −175.33°	0.8391 −175.36°
2.000	0.8945 +176.68°	0.8941 +176.60°	0.8945 −176.59°	0.8942 +176.59°	0.8942 +176.58°
	0.8911 +171.19°	0.8908 +171.09°	0.8911 +171.09°	0.8909 +171.08°	0.8908 +171.09°

(c) Lamina 1 mm thick, $\varepsilon^* = 50 - 50j$.

Freq. (GHz)	'COAX' $r = 26$ mm	'TEH2' $r = 35$ mm	'RCAV' $r = 35$ mm	'MIC2' $r = \infty$	'AGPW' $r = \infty$
0.100	0.5549 −39.68°	0.5520 −40.07°	0.5509 −40.21°	0.5508 −40.09°	0.5539 −39.72°
1.000	0.7247 −166.09°	0.7215 −166.33°	0.7197 −166.67°	0.7197 −166.57°	0.7211 −166.53°
2.000	0.8268 −179.10°	0.8268 −179.14°	0.8271 −179.18°	0.8267 −179.17°	0.8263 −179.21°
3.000	0.8573 +174.15°	0.8569 +174.15°	0.8574 +174.14°	0.8571 +174.13°	0.8572 +174.16°

2.5.4 Tests with physical dielectrics - single layer laminar geometry

The following tables and diagrams, take the permittivity of a real dielectric reference liquid and compare computed values for Γ as a function of thickness, h, or radius, r, at a fixed frequency. A comparison has already been published [21] between an earlier version of 'AGPW' (called 'ALT') and actual measurements with a coaxial sensor. The measurements were on methanol at 20°C and deionised water at 22°C. They were performed by S Jenkins (now Dr S Etzel) and they achieved very good agreement with the computations. Nevertheless, there *were* small discrepancies in the published figures and it is now possible to say much more about what the sources of these discrepancies probably were. Tables 6 and 7 reproduce the measured figures of Reference 21, but with updated values from the amended version of 'AGPW', and with entries also included for 'COAX' and 'MIC2'.

Table 6 Comparison of measured and computed reflection coefficients for methanol. The measurements were at 20°C with a Type A 14 mm coaxial sensor and show the effect of changing liquid specimen thickness, h (mm).

$\varepsilon^* =$		30.84 - 8.39j		25.03 - 12.90j		19.66 - 13.97j	
		1 GHz		2 GHz		3 GHz	
h (mm)		$\lvert\Gamma\rvert$	$\theta°$	$\lvert\Gamma\rvert$	$\theta°$	$\lvert\Gamma\rvert$	$\theta°$
0.07	Measured	0.990	-177.3	0.986	-178.6	0.985	-179.1
	COAX r = 39 mm					0.9729	-179.06
	MIC2					0.9729	-179.08
	AGPW	0.9750	-175.42	0.9749	-178.11	0.9754	-179.21
0.27	Measured	0.941	-167.7	0.929	-174.4	0.930	-177.2
	COAX r = 39 mm					0.9075	-176.82
	MIC2					0.9075	-176.94
	AGPW	0.9079	-163.42	0.9072	-172.94	0.9084	-176.80
0.47	Measured	0.896	-158.5	0.874	-170.2	0.874	-175.4
	COAX r = 39 mm					0.8541	-175.15
	MIC2					0.8536	-175.30
	AGPW	0.8652	-153.55	0.8563	-169.08	0.8538	-175.33
0.97	Measured	0.818	-140.8	0.772	-162.2	0.763	-172.6
	COAX r = 39 mm					0.7480	-172.42
	MIC2					0.7488	-172.65
	AGPW	0.7880	-135.73	0.7573	-161.44	0.7488	-172.64
2.97	Measured	0.709	-112.2	0.587	-146.1	0.520	-164.5
	COAX r = 39 mm					0.5117	-164.37
	MIC2					0.5086	-164.65
	AGPW	0.6970	-105.36	0.5667	-144.90	0.5086	-164.68
4.97	Measured	0.683	-101.5	0.539	-136.9	0.462	-153.0
	COAX r = 39 mm					0.4587	-152.96
	MIC2					0.4553	-153.02
	AGPW	0.6905	-95.68	0.5250	-134.87	0.4553	-153.04
9.97	Measured	0.702	-93.5	0.560	-130.0	0.508	-147.5
	COAX r = 39 mm					0.5056	-148.09
	MIC2					0.5035	-148.13
	AGPW	0.7124	-89.83	0.5566	-128.29	0.5036	-148.16

Table 7 Comparison of measured and computed reflection coefficients for deionised water. The measurements were at 22°C and with a Type A 14 mm coaxial sensor. Computations with 'COAX' were again for r = 26 mm but also included, marked 'COAX*' are values computed by Dr Soe Min Tun of SMT Consultants Ltd. on an enhanced version of the program 'COAX' for r = 52 mm.

ε^* =		79.27 - 4.19j		78.57 - 8.29j		77.43 - 12.24j	
		1 GHz		2 GHz		3 GHz	
h (mm)		$\lvert\Gamma\rvert$	θ°	$\lvert\Gamma\rvert$	θ°	$\lvert\Gamma\rvert$	θ°
0.1	Measured	0.980	-177.3	0.992	-179.0	0.993	179.8
	COAX r = 26 mm					*0.9948*	*179.65*
	COAX* r = 52 mm					*0.9937*	
	MIC2					0.9936	179.69
	AGPW	0.9944	-177.53	0.9939	-179.64	0.9827	179.60
0.3	Measured	0.954	-172.7	0.981	-177.9	0.982	179.2
	COAX r = 26 mm					*0.9821*	*178.78*
	COAX* r = 52 mm					*0.9814*	
	MIC2					0.9811	178.97
	AGPW	0.9828	-172.89	0.9854	-178.44	0.9806	179.00
0.5	Measured	0.940	-168.4	0.972	-176.9	0.970	178.6
	COAX r = 26 mm					*0.9698*	*177.78*
	COAX* r = 52 mm					*0.9693*	
	MIC2					0.9687	178.14
	AGPW	0.9734	-169.34	0.9704	-177.68	0.9710	178.14
1.0	Measured	0.920	-160.5	0.951	-175.6	0.940	176.2
	COAX r = 26 mm					*0.9326*	*174.78*
	COAX* r = 52 mm					*0.9362*	
	MIC2					0.9347	175.65
	AGPW	0.9258	-162.24	0.9407	-176.53	0.9344	175.68
3.0	Measured	0.871	-147.6	0.861	-173.9	0.633	170.9
	COAX r = 26 mm					*0.5493*	*176.82*
	COAX* r = 52 mm					*0.6172*	
	MIC2					0.6133	171.55
	AGPW	0.8766	-148.76	0.8118	-174.10	0.6135	171.58
5.0	Measured	0.859	-143.5	0.771	-167.3	0.778	-164.7
	COAX r = 26 mm					*0.8036*	*-165.08*
	COAX* r = 52 mm					*0.7766*	
	MIC2					0.7786	-164.86
	AGPW	0.8556	-142.83	0.7493	-166.32	0.7786	-164.87
10.0	Measured	0.891	-140.9	0.854	-164.6	0.746	-174.2
	COAX r = 26 mm					*0.7648*	*-174.51*
	COAX* r = 52 mm					*0.7380*	
	MIC2					0.7371	-174.34
	AGPW	0.8825	-138.16	0.8558	-165.21	0.7372	-174.33

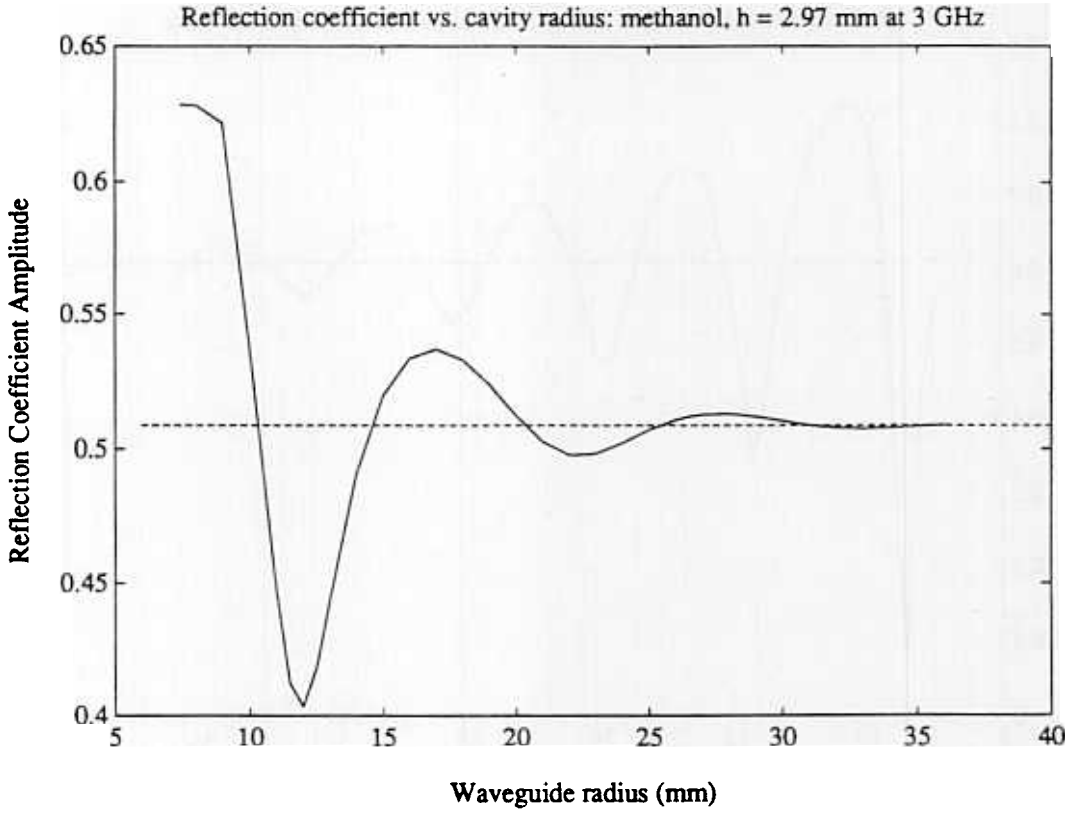
In Tables 6 and 7 it may be noted that the tabulated figures from 'AGPW' differ slightly from the published ones [21]. This is because an improved version of 'AGPW' is being used. These differences are invariably not significant in measurement terms.

Note that program/measurement discrepancies are generally smaller in Table 6 (methanol) than in Table 7 (water). The reason is that methanol is lossier than water and that *both in theory*

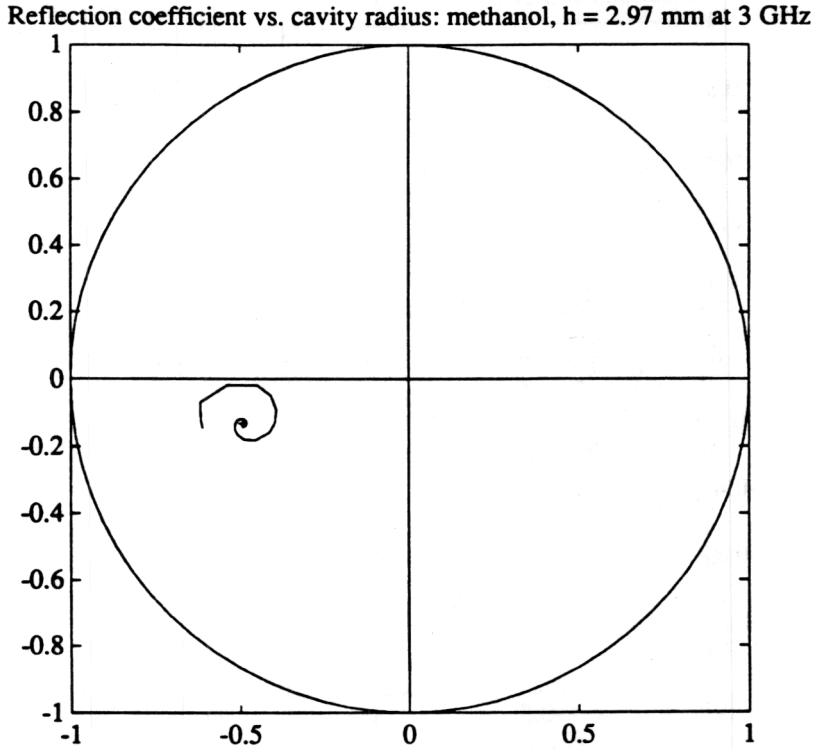
and in practical measurement the effects of reflection from the edge of the specimen will be more significant for the latter. The 'COAX' values for 3 GHz, r = 26 mm in Table 7 are particularly telling in this respect. The figures for h = 3.0 mm, and to a lesser extent h = 5.0 mm, disagree particularly seriously, yet the figure for 'COAX*' for which r = 52 mm agrees well with the computed figures for 'infinite' radius from 'AGPW' and 'MIC2'. What is happening here is that the water-filled cavity at the end of the coaxial line is resonating for this particular combination of r and h, giving rise to a much greater absorption in the water for h = 26mm. The cavity is not resonating for h = 52mm. The basic resonance mode is that of the TM_{01} for a cylindrical cavity, though it will be distorted by the coupling to the coaxial line.

In the corresponding measurements [21], the radius of the flange of the 14-mm sensor was only 25 mm, but the conducting plane behind the specimen was much larger. At the time of this work (1990) only the 'infinite' radius program 'AGPW' was available to us and it was necessary to try to reproduce as closely as possible the experimental conditions assumed by the program - that there were no reflections from the edge of the specimen. It was found that a large ground plane behind the liquid 'lamina' specimen actually minimised these reflections, the mismatch between the parallel transmission line formed by sensor flange and backplane and the liquid being reduced by the more gradual transition. One might expect, therefore, in Table 7, that the measurements should agree better with 'AGPW' than with 'COAX', since the latter effectively *maximises* reflections from the edge of the specimen by placing a conducting reflector there. In the actual measurements, it is estimated that these edge reflections were reduced in magnitude by a factor of 2 at least, and probably by a factor closer to 4. Some evidence for this interpretation comes from the worst-fit case for water noted above: Table 7 for h = 3.0 mm at 3 GHz. Here the discrepancies (Measurement – 'AGPW'-value) have the opposite sign to the discrepancies ('COAX'-value – 'AGPW'-value) for both $|\Gamma|$ and for θ. This is exactly what one would expect from the fact that the outer rim of the sensor is presented with an 'open' circuit into water rather than a 'short' circuit as computed by 'COAX'. However, it would be right to treat this interpretation with some circumspection because there are other significant errors which add to discrepancies in the measurements. Thus, ANA measurement errors and lack of precise knowledge of the permittivity of the liquid were estimated to contribute uncertainties of similar magnitude to edge-reflection to the overall measurement uncertainty, as noted in Reference 21.

As noted above, it was discovered from Table 7, in comparing 'AGPW' figures for Γ of a water lamina ($r = \infty$) with those computed by 'COAX' (r finite), that disagreement was reasonably low for small gaps, but reached a maximum for h = 3 mm. Further computations were therefore performed for a full range of r values, starting from the radius of the outer conductor of the coaxial line, 7.549 mm, and ending with r = 36 mm, which is about as large as is practicable. In these computations, which are illustrated in Figures 7 and 8 and Tables 8 and 9, h was set (nominally) to 3 mm so as to stand a good chance of maximising these edge effects in order to study them more fully.

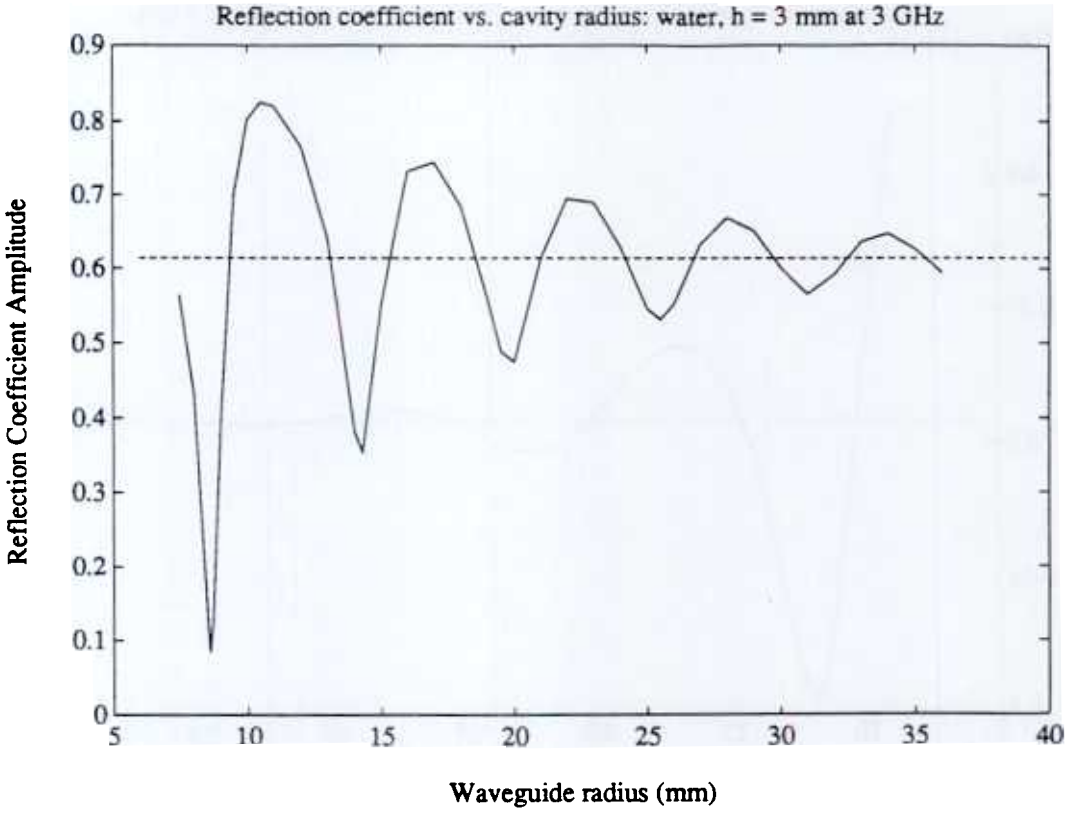


(a) $|\Gamma|$ for a 2.97-mm lamina of methanol at 3 GHz, see Table 8. 'COAX' with 8 modes only in the coaxial section.

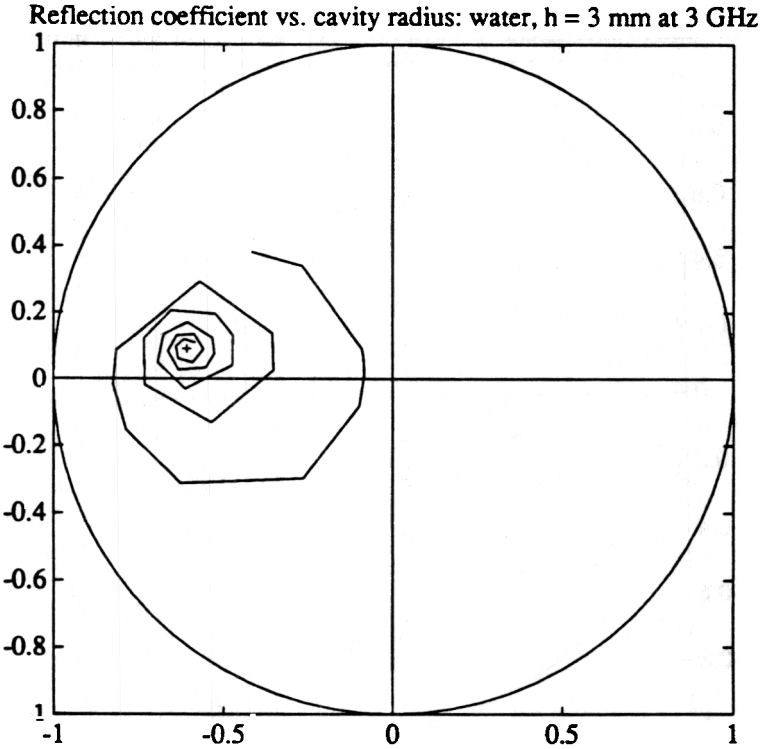


(b) Polar plot of Γ for a 2.97-mm lamina of methanol at 3 GHz, see Table 8. 'COAX' with 8 modes only in the coaxial section.

Figure 7 Γ from a cavity filled with methanol as a function of cavity radius, r.



(a) $|\Gamma|$ for a 3.0-mm lamina of water at 3 GHz, see Table 9. 'COAX' with 8 modes only in the coaxial section.



(b) Polar plot of Γ for a 3.0-mm lamina of water at 3 GHz, see Table 9. 'COAX' with 8 modes only in the coaxial section.

Figure 8 Γ from a cavity filled with deionised water as a function of cavity radius, r.

Table 8 Values of Γ for a 'lamina' of methanol as a function of its radius, r. Computations are for a 2.97-mm thickness of methanol at 3 GHz and 20°C. In the 'COAX' computations 8 modes only were employed (see text). 'TEH2' uses normal quadratic extrapolation. At 3 GHz, $\varepsilon^* = 19.66 - 13.97j$.

Radius, r	'COAX'		'TEH2'		'RCAV'	
(mm)	$\lvert\Gamma\rvert$	θ	$\lvert\Gamma\rvert$	θ	$\lvert\Gamma\rvert$	θ
7.459	0.6284	−166.74			0.6283	−166.65
8.00	0.6166	−166.74			0.6216	−168.73
9.00	0.5940	−173.84	0.5944	−173.50	0.5946	−173.56
10.00	0.5301	−178.57	0.5377	−178.07	0.5377	−178.14
11.00	0.4432	−178.57	0.4477	−177.79	0.4476	−177.81
11.50	0.4081	−173.90			0.4124	−173.24
12.00	0.3865	−166.82	0.4029	−166.89	0.4032	−166.89
12.50	0.4046	−161.50			0.4182	−161.71
13.00	0.4343	−158.72	0.4432	−158.89	0.4438	−158.93
14.00	0.4787	−157.10	0.4904	−158.11	0.4909	−158.17
15.00	0.5126	−159.42	0.5192	−159.72	0.5196	−159.78
16.00	0.5299	−161.78	0.5331	−161.75	0.5334	−161.81
17.00	0.5304	−163.51	0.5366	−163.66	0.5369	−163.72
18.00	0.5289	−165.35	0.5326	−165.24	0.5329	−165.29
19.00	0.5164	−166.23	0.5235	−166.28	0.5237	−166.34
20.00	0.5072	−166.77	0.5121	−166.61	0.5123	−166.66
21.00	0.4939	−166.14	0.5023	−166.21	0.5026	−166.26
22.00	0.4913	−165.44	0.4973	−165.36	0.4977	−165.40
23.00	0.4888	−164.28	0.4978	−164.50	0.4982	−164.54
24.00	0.4952	−163.94	0.5017	−163.97	0.5021	−164.02
25.00	0.4975	−163.51	0.5064	−163.82	0.5069	−163.88
26.00	0.5036	−163.89	0.5103	−163.97	0.5106	−164.02
26.50	0.5058	−164.10			0.5119	−164.15
27.00	0.5034	−163.93	0.5123	−164.25	0.5126	−164.31
28.00	0.5056	−164.47	0.5125	−164.55	0.5129	−164.60
29.00	0.5025	−164.46	0.5115	−164.77	0.5119	−164.82
30.00	0.5026	−164.78	0.5099	−164.87	0.5103	−164.93
31.00	0.5026	−164.70	0.5084	−164.86	0.5087	−164.91
32.00	0.4996	−164.90	0.5073	-164.77	0.5077	−164.82
33.00	0.5008	−164.66	0.5070	−164.66	0.5074	−164.71
34.00	0.4992	−164.39	0.5072	−164.56	0.5076	−164.61
35.00	0.5013	−164.48	0.5078	−164.50	0.5082	−164.56
36.00	0.5002	−164.30	0.5084	−164.50	0.5088	−164.55

Table 9 Values of Γ for a 'lamina' of water as a function of its radius, r. Computations are for a 3.00-mm thickness of water at 3 GHz and 22°C. In the 'COAX' computations 8 modes only were employed (see text). 'TEH2' uses normal quadratic extrapolation. At 3 GHz $\varepsilon^* = 77.4349 - 12.2458j$.

Radius, r (mm)	'COAX'		'TEH2'		'RCAV'	
	$\lvert\Gamma\rvert$	θ	$\lvert\Gamma\rvert$	θ	$\lvert\Gamma\rvert$	θ
7.549	0.5653	+137.37			0.5635	+137.35
8.00	0.4640	+127.26	0.4335	+128.23	0.4323	+128.18
8.50	0.1697	−15.41	0.1307	+134.34	0.1291	+134.91
8.52	0.1569	−16.09			0.1161	+139.61
8.55	0.1369	−17.27			0.0987	+150.00
8.57	0.1231	+125.44			0.0907	+158.98
8.60	0.1019	+129.99			0.0851	+175.07
8.70	0.0601	−24.42			0.1281	−140.54
9.00	0.3669	−129.64	0.3949	−131.39	0.3976	−131.54
9.50	0.6946	−153.02	0.6985	−153.32	0.6997	−153.47
10.00	0.7861	−166.99	0.8011	−168.84	0.8015	−168.95
10.50	0.8186	−178.14			0.8250	-178.90
11.00	0.8172	+174.12	0.8194	+174.00	0.8197	+173.92
12.00	0.7643	+162.75	0.7673	+162.86	0.7669	+162.80
13.00	0.6442	+152.42	0.6415	+152.85	0.6405	+152.79
14.00	0.3818	+154.81	0.3824	+158.51	0.3813	+158.72
14.30	0.3414	+172.25			0.3530	+175.70
15.00	0.5271	−165.81	0.5498	−166.17	0.5514	−166.22
16.00	0.7261	−178.42	0.7311	−178.56	0.7315	-178.65
17.00	0.7396	+170.59	0.7445	+170.60	0.7443	+170.53
18.00	0.6846	+162.29	0.6856	+162.55	0.6850	+162.50
19.00	0.5582	+158.42	0.5593	+159.42	0.5583	+159.43
19.50	0.4867	+162.89			0.4895	+164.39
20.00	0.4658	+173.69	0.4746	+174.84	0.4750	+174.97
21.00	0.5959	−177.09	0.6121	−177.15	0.6131	−177.20
22.00	0.6882	+175.92	0.6950	+175.92	0.6952	+175.84
23.00	0.6882	+168.60	0.6900	+168.80	0.6898	+168.74
24.00	0.6266	+163.82	0.6296	+164.30	0.6289	+164.27
25.00	0.5397	+165.71	0.5467	+166.78	0.5462	+166.84
25.50	0.5219	+170.71			0.5317	+171.80
26.00	0.5407	+175.75	0.5518	+176.39	0.5524	+176.43
27.00	0.6191	+177.40	0.6322	+177.50	0.6328	+177.45
28.00	0.6610	+172.70	0.6684	+172.85	0.6685	+172.80
29.00	0.6443	+168.06	0.6514	+168.42	0.6510	+168.38
30.00	0.5965	+166.39	0.6019	+167.00	0.6014	+167.01
31.00	0.5591	+170.18	0.5655	+170.83	0.5655	+170.88
32.00	0.5804	+174.82	0.5914	+175.26	0.5920	+175.26
33.00	0.6277	+174.27	0.6354	+174.51	0.6358	+174.47
34.00	0.6397	+171.05	0.6475	+171.35	0.6474	+171.30
35.00	0.6217	+168.54	0.6271	+168.96	0.6268	+168.93
36.00	0.5873	+168.70	0.5950	+169.33	0.5947	+169.35

In Figures 7 and 8 the dashed line or cross corresponds to the value from 'AGPW' for the infinite radius case: $r = \infty$. The computations that have been plotted are those from 'RCAV' given in the final two columns of Tables 8 and 9. It can be seen that the value for Γ computed by 'RCAV' gradually approximates to the 'AGPW' value as r is increased, but that, in the case of water, the difference between $r = 36$ mm and $r = \infty$ is still significant compared with measurement uncertainties. The precise behaviour of the curve can be described in terms of continuous phase change in a lossy 'short-circuited' radial transmission line, which produces more loss and phase offset as r (the 'length' of the line) is increased. Alternatively, the response can be interpreted as resulting from relatively low Q-factor resonances in a TM_{0n}-mode cavity. The points on the curve furthest from the edge of the Smith chart mark the resonance conditions. In this latter view the coaxial line acts as a coupling aperture into the cavity which will itself damp the resonances. In Tables 8 and 9, the 'COAX' computations were performed with only 8 modes in the coaxial section to save time. The figures from 'TEH2' use full ($n = 4, 8, 16$)-mode quadratic extrapolation, while 'RCAV' uses 40 modes, which are more than sufficient to give figures with uncertainties much better than those encountered in practical measurements. However, 8 modes are not usually sufficient and so it is to be expected that there will be significant discrepancies between the 'COAX' and the other figures. Nevertheless, the 'COAX' figures do preserve the physics of the situation.

Residual discrepancies in Tables 8 and 9 between 'TEH2' and 'RCAV', which should both agree in their solutions for this geometry, are, on inspection, found to be largest for the largest resonances - ie. in cases where $|\Gamma|$ falls to a minimum; $r \approx 8.6$ mm in Table 9 being the most significant. This is not surprising. The $r = 8.6$ mm case for water, exhibits quite a high Q-factor of approximately 9. (It should be remembered that in a resonance more power is absorbed, so that $|\Gamma|$ falls - in this case almost to zero). In these resonances the sensitivity of the programs to small differences in computational assumptions is enhanced by a similar factor. Thus 'TEH2' and 'RCAV' use totally different computational techniques and we must expect that their predicted values for Γ will disagree most near the peak of the resonance. This is further demonstrated by the bad agreement of the 'COAX' computations for $r = 8.6$. Here the lack of quadratic extrapolation in the computation amounts to the assumption that there are only 8 modes present in the coaxial section (and 10 in the water). This changes completely the reactive conditions of the resonance ($|\Gamma|$-minimum), shifting the radius, r, required to peak the resonance from approximately $r = 8.6$ mm closer to 8.7 mm. It will be seen later (eg. Section 4.2) that the peaks of resonances are also the points at which *measurements* disagree most with theory - in this case because of small non-compliances of the actual measurement geometry with the 'perfect' geometry assumed by the programs.

2.5.5 Relevance to open probe-type sensors

In the case of probe sensors, of the type shown in Figure 1, two kinds of geometry-related errors can arise. Firstly, reflections from remote perimeters of the specimen (or from the walls of its containing vessel) are not accounted for in some computations. These reflections are especially significant at higher frequencies in high permittivity materials of low loss. Secondly, errors arise because of the finite diameter of the flange, which is assumed infinite in the computations. Recent work (to be covered in a forthcoming publication) has shown that this latter effect can have significant consequences when the frequency is such that the flange itself acts as a resonant element. (See item 11 in the uncertainty budget, Section 5.1).

We can conclude from Tables 8 and 9 and Figures 7 and 8 that, at least at 3 GHz, methanol is sufficiently lossy to allow 'COAX' to approximate to the infinite lamina case when the

radius used in the computation is 26 mm or greater. This is convenient because the smaller the value of r, the faster is the program to run because fewer modes are used. This is clearly not the case for water at 3 GHz for any 'reasonable' assumed radius (ie. $r < 50$ mm). This to some extent vindicates the claims made in the early (1984-89) NPL work on 'probe' sensors [10], that a 25-mm flange was adequate for lossy materials like biological tissue and methanol but that significant resonances occur within the body of a less-lossy material such as water. Nevertheless, 25 mm is seen here only to have been barely adequate. It should be borne in mind that at lower frequencies, tissues and polar liquids such as methanol are less lossy, and it might be thought that errors from these two geometric effects would increase with falling frequency. In fact, computational tests have shown that the magnitude of these effects falls with frequency to become negligible at the lowest frequencies at which the sensors are used (300 MHz and below).

2.5.6 Modelling specimens of two and three layers.

As we have seen, much of the checking of the new programs listed in Table 3 has been performed upon certain 'standard' geometries which contain only one (possibly hypothetical) dielectric material. All of the known bugs in the programs were detected and removed by analysing such single-layer geometries. On applying the multilayer programs 'MIC2', 'TEH2/3' and 'RCAV3' to systems with two or more layers, the same high level of agreement was retained. Table 10 will serve here to demonstrate this. The Table lists the predicted Γ figures from a two layer structure of ethanol ($t_1 = 0.514$ mm, see Figure 1 (c)) and a polymer (notionally 'Delrin', $t_2 = 1.003$ mm, $\varepsilon^* = 2.960 - 0.0j$). The permittivity of the ethanol changes with frequency, ε'' peaking near 0.8 GHz, as shown in the table. The computations are performed for the Type C sensor and a 70-mm-diameter cell because continuity with earlier computations for the Type A sensor is not relevant for these multilayer results (they were not possible prior to the present project).

Table 10 Values of Γ from 'RCAV3' and 'TEH2' for a two layer structure in a 70-mm-diameter cell attached to a Type C sensor. Layer 1: thickness 0.514 mm, is ethanol, for which ε^* is given in the table. Layer 2: thickness 1.003 mm, is notionally the polymer 'Delrin', $\varepsilon^* = 2.96 - 0.0j$ at all frequencies.

Frequency r	Γ from 'RCAV3'		Γ from 'TEH2'		ε^*-ethanol	
(GHz)	$\lvert\Gamma\rvert$	θ	$\lvert\Gamma\rvert$	θ	ε'	ε''
0.3	0.9707	-12.50	0.9707	-12.48	22.85	6.69
0.5	0.9332	-19.58	0.9332	-19.55	19.69	9.23
0.8	0.8790	-28.50	0.8790	-28.46	15.19	10.41
1.0	0.8493	-33.91	0.8493	-33.85	12.89	10.23
1.5	0.7589	-49.85	0.7590	-49.76	9.29	8.81
2.0	0.7711	-49.69	0.7711	-49.58	7.48	7.35
2.5	0.7628	-63.38	0.7628	-63.27	6.49	6.21
3.0	0.7483	-76.02	0.7482	-75.89	5.91	5.33

The level of agreement in Table 10 is, if anything, better than that encountered in Tables 4 - 9, and this has been achieved in a two-layer system with two very disparate dielectrics. This demonstrates that no additional computational problems have arisen with the introduction of dielectric interfaces into the system. The figures in Table 10 are not plotted here since numerous similar plots of 1-, 2- and 3-layer structures, showing both measured and computed data, are given in Section 4.

The demonstration of this high level of agreement (typically, better than ±0.001 in $|\Gamma|$ and ±0.1° for θ, *away from resonances*) means that the measurement program can proceed on a firm basis of confidence in the computational procedures. It will, in fact, be seen in Section 4 that measurement discrepancies exceed those of the software, typically by an order of magnitude (and by a greater extent near resonances). It is now therefore appropriate to turn to the measurements, starting with a description of the equipment used.

3 COAXIAL SENSORS AND CELLS - HARDWARE

3.1 INTRODUCTION

As in previous work [10,20–22], all measurements were performed using a Hewlett Packard Automatic Network Analyser (ANA) - in this case an HP8753B ANA, which operates up to 6 GHz but has only been used up to 3 GHz for the measurements reported here. Again, as in previous work, the ANA measurement port was connected to the sensor via a precision flexible cable fitted with APC-7 connectors. The adaption to 14-mm line was via GR900 connectors, with the adaptor directly placed between sensor and cable. During measurements the cable was flexed as little as possible. It was not found necessary to make special provisions for temperature stabilisation, but all measurements were performed in a temperature stabilised laboratory.

Development of the NPL 14-mm coaxial sensors was discussed in Sections 1.2 and 1.3. All of the results presented in this section (Section 3) of the report were obtained with the Type C sensor and various different cell attachments, as shown in Figure 2 (c), for example. However, a significant amount of the development work that led to these measurements was performed using a Type B 'probe'-type sensor (see Section 1.2 and Figure 1 for details). There is no loss of generality in our reporting here only results from the Type C sensor and cell. They were used because, in combination, they are more calculable than an open 'probe' sensor. Our findings are, in any case, of relevance to both open and cell geometries, but the advantages of the latter are as follows:

In low-loss materials significant electromagnetic power is reflected from the sides and rear face of specimens so that it is necessary to place those faces in a geometry which is calculable. A metallic 'short-circuit' immediately adjacent to the face is the most predictable and calculable condition.

- The combination of a finite-diameter flange with the computational assumption that it is actually 'infinite' in diameter produces measurement errors (as discussed in Section 2.5.5). The presence of the cavity wall, as assumed by 'RCAV', 'TEH2/3' and 'COAX', overcomes this problem.
- A cell is in any case required to contain reference liquids, both for testing the programs and for calibration measurements.
- A cell of this type allows liquid-immersion techniques to be used for solids - a procedure which has long been recognised as good working practice for dielectric measurements on solids and which allows measurements to be performed with reduced uncertainties.
- The cell acts as an electromagnetic screen and also keeps the specimens isolated from the environment, thereby preventing contamination - especially of liquids.

It must be admitted that the need to place specimens in cells to some extent detracts from the convenience of using the sensor as a simple probe, ie. by placing its face in good contact with a flat surface of a specimen. The very popularity of the sensor derives from this convenient practice. However, we have shown during the course of this work (see 2.5.4) that the shape and size of specimens *are* crucially important in coaxial sensor metrology, and, certainly for moderately-sized low-loss specimens, serious measurement errors occur if the 'infinite half-space' assumption is made. In general one would expect to be able to use a 'probe' sensor,

however, whenever specimens are sufficiently lossy and large to allow this 'infinite half-space' assumption to be valid. This would often be the case, say, for tissues, foodstuffs and foam-RAM, but in all other cases it would seem to be essential to use a controlled and properly calculable geometry.

Having recognised that some convenience must be sacrificed in using the cell, it is relevant to point out some mitigating factors:

- There is no additional lack of convenience in measuring liquids - they have to be contained somehow.
- The metrological requirement is for the specimen to be a lamina, with flat, parallel faces, machined in the form of a disc. This is, however, already an 'industry standard' shape for RF and microwave dielectric specimens. Specimens suitable for the Type C cell could therefore also be suitable for other dielectric measurement techniques. The diameter of the disc is not a critical parameter for this work because it is not expensive to machine the relevant section of the cell from brass to fit any chosen diameter up to 80 mm. Machining tolerances are not critical. In fact, two cell diameters have been used in this work: 70 mm and 50 mm - the latter was used to allow measurements to be performed upon standard NPL specimens which have been characterised many times before. The computer programs will of course work with any desired diameter.
- Flexibility of the cell design also allows specimens of any thickness to be measured in a cylindrical cell with a piston backshort (see Section 3.3).
- The new Type C coaxial sensor can also be used without the cell. It has a 'flange' diameter of 100 mm (as opposed to the 50 mm of earlier models) - as shown in Figure 2 (a). As such, it provides a better approximation to the 'infinite radius' condition (Figure 2 (a) and 2 (b)) than previous sensors.

The following section (3.2) considers aspects of the cell design.

3.2 CYLINDRICAL CELL DESIGN

3.2.1 Annular gaps around the specimen

It was made clear above that any gap between a solid specimen and the face of the sensor can give rise to large errors of measurement unless it is taken fully into account by the theory. This can easily be done with the multilayer theory of 'MIC2', 'RCAV' or 'TEH3' etc., whether liquid immersion is used or not. However, in the cylindrical cell one might also be concerned with gaps at the *back of the specimen* and *around its cylindrical sides*. The former can readily be treated in the same way by the multilayer theory as a gap on the front face. In fact, gaps at the back of the specimen would have less effect upon the measured value for Γ because the field-strength is smaller there. *Annular* gaps between the specimen and the circular waveguide wall are, however, another matter, because the available programs assume uniformity of ε^* with r.

Practical considerations require that specimen diameter is smaller than that of the cell, to allow room for it to be inserted into the cell without getting stuck. In past NPL experience with

cylindrical cavities, for example, 49.6-mm-diameter specimens have been used with a 50-mm diameter TE_{01}-mode cavity, since it was found that specimens with diameters larger than this tended to get stuck. Assuming this policy is followed in the present case, the question arises as to what effect the annular gap will have, since it cannot be compensated by any computations presently available to us. Liquid immersion can again, of course, alleviate effects caused by the gap, provided a liquid with a suitable permittivity match is available, and that the specimen is of a type that *can* be so immersed (liquid immersion cannot be used with porous or soluble specimens). However, again, exact calculations on the annular gap cannot be performed in the way that they can for the planar gaps by means of the multilayer theories.

Nevertheless, the following consideration leads us to the conclusion that the effects of a small annular gap, no more than 0.2 mm thick, say, are probably not significant. As already described, the fields emerging from the coaxial aperture fringe out across the specimen to the backshort so as to launch a *di*vergent radial mode into the specimen disc. Towards its edge (provided the specimen is significantly larger in diameter than the coaxial outer) the electric field lines will lie directly through the width of the specimen, emerging perpendicularly from the flange and backshort. The radial mode will therefore encounter the circular wall of the cavity as a short circuit and so a reflected *con*vergent radial wave will be set up so as to make the electric field strength on the wall zero. In the region or gap close to the wall, the field strength will therefore be very low. In these circumstances, experience with other dielectric measurement techniques (eg. The 'Roberts and von Hippel' waveguide technique [19] and open resonator metrology) shows that the fields hardly 'see' the material in the gap. To put this another way, the energy density in the field in this region is very low so that substitution of one dielectric species for another here has little perturbing effect upon the fields. Our measurements inside the cell would seem to support this interpretation, but it remains a speculation which ought to be backed up at some future date by further experiment and/or computations.

Lack of co-planarity of the sensor face

It will be appreciated that if the inner conductor of the sensor were to protrude only slightly into the cell (say by 10μm), significant errors might result. As in the case of a gap between specimen and sensor, the technique is hypercritical to small imperfections in geometry in this region. Fortunately, the effects of such practical imperfections can be computed, in this case by the program 'COAX' [13]. The results of such an analysis are summarised in Section 5.1.

Metal loss

Our earlier coaxial sensor work was predominantly concerned with high loss materials, while the present project required extension of the technique to low losses. In the completely enclosed Type C cell used for this work, one must therefore expect high Q-factor resonances to occur and the possibility arises that loss in the metal walls of the cell may be dominant. All of the programs listed in Table 3 assume perfectly conducting metalwork. The question arises as to whether significant error might arise from this assumption. In fact, as shown in Section 4, measured losses for very low loss materials are significantly in excess of the predicted values, especially when the system is resonating. The losses can be reproduced to some extent by inserting 'lumped' ie. very thin, resistive layers into a model of a multilayer system. This may be adequate for contact impedances but it is an unsatisfactory model for distributed (metal)

losses. These effects have been minimised by coating all surfaces with a gold film, but this will neither remove all metal loss nor eliminate contact or leakage losses. Gold flashing is also desirable to prevent contamination of liquids used for test, liquid-immersion work and sensor calibration by metal corrosion products. This is clearly an area where further work needs to be done, as discussed in Section 6 below.

3.3 TYPE C SENSOR AND CELL - CONSTRUCTION AND USE

Taking into account all of the factors detailed in Section 3.2, the sensor design went ahead along the lines shown in Figure 2. The Type C sensor and its 100-mm diameter flange are clamped onto the cell by an outer ring (not shown). All metalwork is gold-flashed brass (apart from parts of the clamp which are in stainless steel). The mating surface of the cell has an inert silicone rubber o-ring inset into it at a radius of 45 mm to prevent liquid leakage. The surface is carefully machined to have a closer contact near its inner edge than elsewhere. The contact is direct metal to metal (as in precision sexless connector outer conductors, eg. GR900, APC7) and is thought to be adequate because both surfaces are gold coated. Liquid inlets and outlets into the cavity are no more than 1-mm in diameter which is sufficiently small to render their perturbation to the fields in the cavity negligible. The placing of these inlets and outlets is such as to ensure that the cell, in the regions where no solid dielectrics are present, can be completely filled with liquid and that bubbles can be excluded.

The rear conducting plane or 'backshort' of the cell is applied in one of two ways.

- **Geometry 1.** 'Fixed-length' cell attachments can be clamped into place giving cell thicknesses of nominally 5.0 and 10.0 mm. These attachments have liquid inlets/outlets in the back face and the body of the cell also has inlet/outlet combinations very close to the sensor flange face. These two sets of inlets/outlets can be used to 'sandwich' solid specimens between liquid layers. When fixed-length cells are in use the whole assembly of cell/sensor is canted at an angle of 45° to the horizontal, with the sensor pointing downwards. This allows any bubbles in the liquid between the specimen and sensor flange to escape out of the top-front outlet, as shown in figure 2 (c). These cells have only been made for 70-mm (nominal) diameter specimens.
- **Geometry 2.** The alternative arrangement gives rise to a 'variable-thickness' cell. Here an open-ended cylinderical cell of 50 or 70-mm inner diameter 36-mm long is clamped to the Type C sensor flange. The whole assembly is arranged vertically with the open end of the cylinder above and the sensor pointing upwards below it. The specimen can be lowered into the cell so-formed and liquid poured below or above it. Side inlets into the cell allow further liquid to be pumped in if necessary. The backshort is provided by a slide-fit metal piston which can be clamped down upon the specimen.

A third possible design which has been considered is to use a micrometer-driven backshort, but this has so far proved to be an unnecessary extension to the cell.

The narrow liquid inlets/outlets to the cell require that liquid be pumped into the cell from a reservoir system, because the surface tension is otherwise too great for many liquids to flow. The pump system is shown in Figure 9.

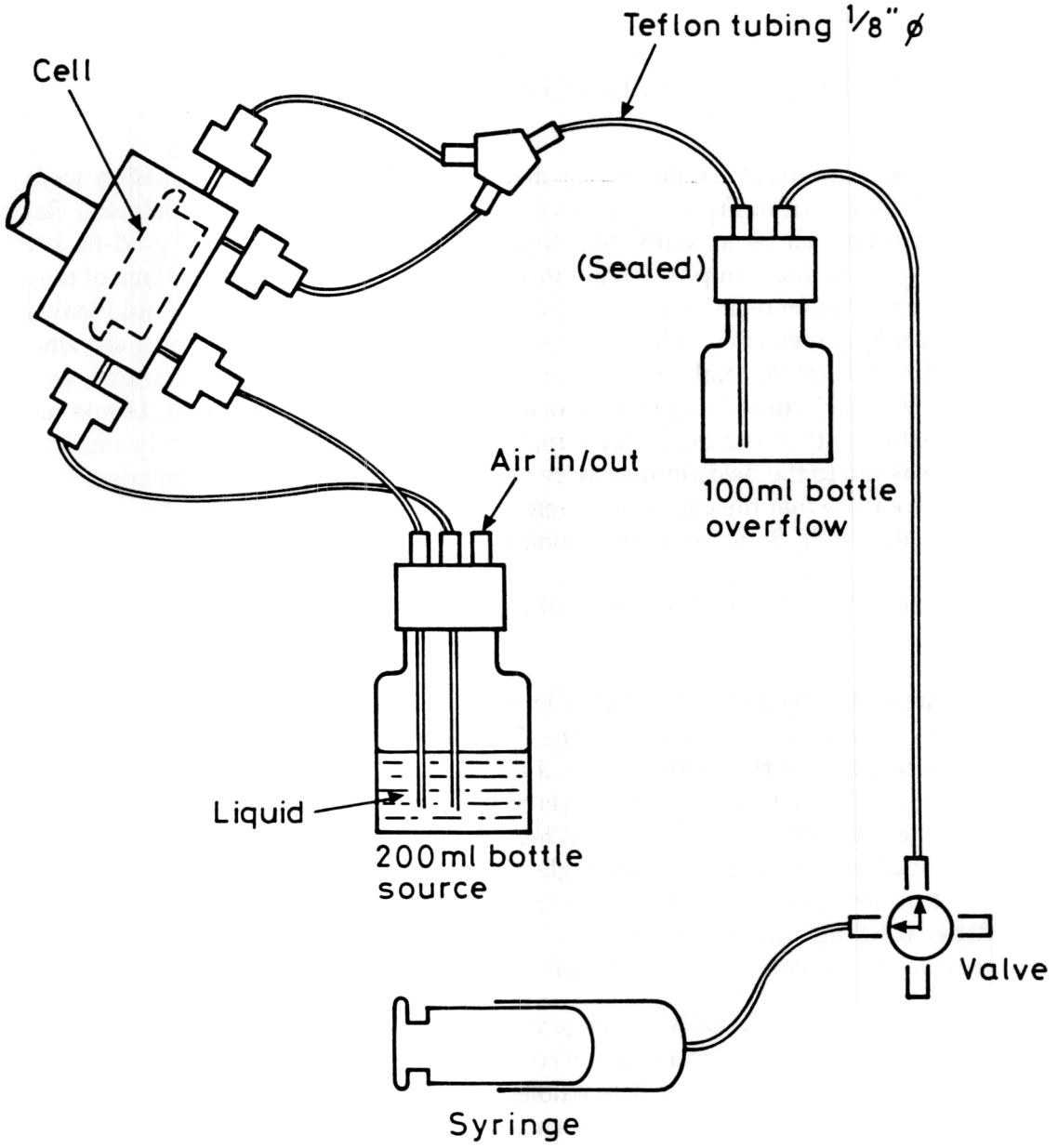


Figure 9 The liquid pump and reservoir system used to introduce reference liquids into the Type C cell.

It has been found perfectly adequate to use a syringe as the pump, acting in a 'suction' mode. The valve in the diagram can be closed once liquid has been seen to flow right through the cell - this allows the syringe to be reset as well. Tubing is of PTFE, which is inert, to prevent

leaching out of plasticisers etc. which are present in other forms of flexible tubing.

The placing of solid specimens in the cell is readily done if the specimen is to contact the coaxial sensor and backshort. However, for reasons detailed in Section 4.4 below, it is sometimes better to support the specimen parallel to, but away from the sensor flange. A convenient way of effecting this has been found to be the use of single-ply nylon wire. The wire is used as a spacer and is placed between the specimen and flange (or backshort) in a circle (which does not have to be complete). It ideally touches the outer circular waveguide (cavity) wall at all points and so is placed as far away from the coaxial aperture as possible. Nylon wire is ideal for this task because it is naturally springy and, if coiled beforehand, it will tend to spring out to the largest possible diameter, ie. fit snugly against the waveguide wall. It has already been argued (Section 3.2.1) that the presence of a small amount of 'the wrong' dielectric in this region has very little perturbing effect upon measurements and this has indeed been found to be the case. Nylon wires of various diameters can be used to provide different spacings. Nylon is a hard polymer and so measurement of its mean diameter with a micrometer prior to insertion into the cavity gives a good indication of the specimen spacing to within 0.003 mm (95% confidence level). Other technique was to use small pieces of porous polymer sponge material near the perimeterof the cavity to press solid specimens against one end of the cavity.

The whole cell assembly forms a considerable mass of metal which would be ideally suited to temperature controlled measurements, were heating/cooling elements to be attached and the whole suitably lagged. The work reported here, however, has all been performed at ambient temperatures.

SENSOR CALIBRATION AND MEASUREMENT

Background

Calibration defines a scale for reflectivity measurements, and corrects for the effects of mismatches. Prior to measurements on dielectric specimens, a coaxial sensor needs to be calibrated at the working face of the flange. In calibrating, we are actually determining the three complex coefficients of a bilinear transform:

$$\Gamma_t = \frac{a\Gamma_r + b}{c\Gamma_r + 1} \tag{3}$$

which relates 'raw' and 'true' reflection coefficients, Γ_r and Γ_t respectively, where a, b and c are the complex coefficients which characterise scaling (a) and mismatch imperfections (b, c) in the measurement apparatus. Γ_r is the apparent reflection coefficient 'seen' by the ANA, while Γ_t is that 'seen' by the sensor; ie. Γ_t is the reflection coefficient computed directly by the programs of Section 2. Provided (i) that the measurement equipment remains stable, and (ii) the instrumentation responds linearly to voltage, and (iii) that there are no mismatches near the face of the sensor which generate higher order, evanescent modes of significant amplitude at the face, then a, b and c are formally adequate to correct for all transmission-line imperfections situated between the ANA and the measurement face of the sensor. They are parameters which must nevertheless be obtained separately for each measurement frequency. To determine these three coefficients uniquely, 'raw' measurements on three standards (which have accurately known or defined reflection coefficients) are required.

The factors influencing the choice of calibration technique include accuracy, convenience and reliability (in a reliable method, the chances of something going amiss without the operator being aware of it are small). Two basic approaches to calibration have been used, one using a *substitute connector* (see eg. [10]) and the other using *reference liquids* (eg. [18,19]).

With our sensors two calibration standards can easily be attained - the 'short' and 'open' conditions. When the inner and outer conductors are shorted together (with metal foil) the Γ_t should be -1.0, assuming perfect contact. When the sensor is 'open-circuited' to air, Γ_t can be computed, as illustrated above in Table 4 and Section 2.5.2. Although the use of metal foil has been found to be much the best method of shorting the coaxial sensor, poor contact is sometimes unknowingly obtained. We therefore made it our practice to measure this 'short' condition a number of times during calibration. The use of a least-squares specially written program for determining the calibration coefficients made it possible to identify and exclude poor measurements by a check of residual calibration errors.

In the reference-liquid calibration method, a third standard is obtained by immersing the sensor in a liquid of measured dielectric properties. A number of these have been characterised recently at NPL [4,18,19] and Debye-liquids, like the lower n-alcohols, are now in common use here for such calibrations.

In the substitute-connector method, the flange of the coaxial sensor is replaced with a connector, which has nominally identical electrical design and ideally possesses no extra mismatches [10]. The substitute connector has the correct fittings to allow coaxial standards to be attached (in this case a GR900 50 Ω match standard). After calibration with coaxial standards, the flange is re-attached, and a *secondary calibration* is performed using raw measurements of the sensor open-circuited, shorted with metal foil, or both. The secondary correction adjusts the bilinear correction coefficients to compensate for ill-matching of the sensor and substitute connector.

For a coaxial sensor with a cell, the 'open-circuit' and reference-liquid immersion conditions were always obtained with the cell attached, since this is nearest to the condition of usage. The Γ_t values were in this case computed, using 'TEH2', 'TEH3' or 'RCAV3', from the exact dimensions of the cell. Ethanol was generally used as the reference liquid for calibration. When fixed-length cells were in use, the calibration liquid filled the whole cavity. With the variable length cell, sufficient liquid was used for the effects of reflection from the liquid surface to be negligible.

In general, the internal ANA calibration procedures are unsuited to the requirements of this work. A flexible and interactive program was written to provide a more convenient means of calibration. This program, the design of substitute connectors and the secondary calibration procedures are discussed in greater detail in a companion paper [13], which is being prepared.

3.4.2 Experimental evaluation of calibration methods

Before measurements on multilayer specimens were undertaken, the calibration methods were tested in measurements on various reference liquids. Some of these are described in detail in Section 4.2. Ethanol was generally used as the reference liquid for calibration, agreement with published dielectric data for methanol, propan-1-ol and butan-1-ol was sought. It was found that up to a frequency of 3 GHz good agreement with other NPL data could be obtained for methanol [18], but not for propan-1-ol or butan-1-ol above 1.5 GHz. Some of the discrepancy is believed to be caused by finite-flange effects, as discussed in Section 2.5.5, but

disagreements persisted even when using other designs of coaxial sensor, so some suspicion may fall on the data in Reference 18 for these two liquids. This highlights the need for more work on reference liquids, which is a policy we continue to advocate at NPL. The agreement between the substitute-connector and reference-liquid methods was generally good. Early work used a 14 mm coaxial sensor of Type A (PTFE bead), but leakage of reference liquids into the sensor, and actual movement of the bead, proved troublesome. Since PTFE cannot be secured with glue, this is not easily rectified. For the remainder of the work, Type B and C sensors with Lucentine beads (which were glued in to give a seal) were used, as described in Section 3.1.

The results of this evaluation are being presented in the forthcoming paper [13].

4 INTERCOMPARISON OF MEASUREMENTS WITH THEORY

4.1 TRIAL SPECIMENS AND REFERENCE MATERIALS

Specimens of two different diameters were used during this project: (1) new specimens of 70-mm diameter, specially prepared for this work, (2) specimens of 49.6-mm diameter which have been used as microwave standards at NPL for over a decade and are therefore well-known in their microwave properties. All of these specimens have been characterised for comparison purposes at 10 GHz and above. In general, their low loss allows their properties to be extrapolated down to our measurement frequencies (3 GHz and below) with confidence. It was not found necessary to glue any of these specimens together into multilayer composites because simple clamping was found to be adequate and it also had the advantage that the various materials could be reassembled into a variety of different laminates.

The dielectric properties of these specimens at microwave frequencies are given in Tables 11 and 12, below, where $\tan\delta$ ($= \varepsilon''/\varepsilon'$) has been tabulated rather than ε''. The specimens of Table 11 have also been measured at frequencies below 300 MHz as a check. The physics of dielectric relaxation allows one to predict to soem extent the change of ε^* with frequency [24]. When ε'' is low (as with all of these specimens, except the glass, polystyrene and Delrin), ε' barely changes with frequency. Furthermore, since ε'' is well below the sensitivity of the coaxial sensor technique (which is estimated to correspond to a $\tan\delta$ of approximately 0.05 at present) the microwave permittivities of Tables 11 and 12 may reliably be taken as correct for ε' all the way down to 100 MHz for most of the specimens and ε'' may be taken as practically zero. The reason for performing these calibration measurements at 10 GHz and above is that the 10-GHz TE_{01}-mode cavity and 36 and 72-GHz open resonators are by far the most accurate and sensitive permittivity measurement facilities we have at NPL. Conventional measurements upon laminar specimens in the band 1 MHz - 2 GHz (ie. up to a frequency at which microwave cavities can be made with practical linear dimensions) are notoriously difficult and often inaccurate. It is precisely because of these drawbacks that computer-centred metrological techniques are being introduced. Such techniques, of which the coaxial sensor is an example, can be more convenient and accurate, but only on the basis of computer-based numerical analysis.

It is only with the lossier specimens that the extrapolation approach cannot be applied. The 'Black Delrin', polystyrene and plate-glass specimens of Table 11 were therefore also measured from 30 kHz to 10 MHz in a three-terminal capacitance cell, chiefly to determine the magnitude of the loss at those frequencies and we have *interpolated* their permittivities into our frequency range.

Table 11 70-mm diameter solid specimens used to make up multilayer composites. The measurements were performed in the NPL open resonators.

Specimen material	thicknesses mm	ε' 36 GHz	$\tan\delta$ 36 GHz	ε' 72 GHz	$\tan\delta$ 72 GHz
Polystyrene	1.007	2.570	< 0.01	2.573	< 0.01
PTFE	2.903	2.051	< 0.01	2.052	< 0.01
Black Delrin	1.003, 1.984, 4.012	2.90	0.02	2.87	0.01
Plate Glass	2.078	6.76	0.03	6.71	*

* not measured

Table 12 49.6-mm standard solid specimens used to make up multilayer systems. Measurements were in a TE_{01}-mode cavity.

Specimen material	thickness mm	ε' 10 GHz	$\tan\delta$ 10 GHz
High Density Polyethylene (HDPE)*	1.036, 2.038	2.36	0.0002
Cordierite	5.105	5.98	0.0001
Alumina	5.33	9.75	0.0007
Barium Strontium Zirconate	1.415	34.2	0.0009

*HDPE Grade 'Rigidex 2000'

The specimens were specifically chosen to represent a wide range of real permittivity values (ε' from 2.0 to 34) but none of them possess notably high loss. For this reason, and for reasons of convenience and flexibility, liquid specimens were used to make up high-loss and variable-thickness components of laminates. In the RF range with which we are concerned here, uncertainties in dielectric loss for solid specimens are generally much worse than for liquids. It is best during the testing of a new measurement technique to employ materials with well-known properties, and in this respect polar liquids can fulfil our requirements in a way that solid materials cannot. Thus, it is possible to predict ε^* for a well-characterised lossy reference liquid to 1%, but one would be hard pressed to find an *alternative* technique to the present one which gives $\tan\delta$ of a small cross-section lossy lamina to better than 20% in our frequency range.

The three liquids used as lossy specimen material were deionised water, methanol and ethanol, which as the result of recent work at NPL [18,19] and elsewhere (see references in [19]) are thought to be sufficiently well-known to be used as reference liquids. These same liquids, along with cyclohexane, were also used for checking the Type C cell in a single layer configuration, as described in Section 4.2. Their relaxation properties are summarised in Table 13. ε^* can be computed at any frequency, f, from the Debye Relaxation parameters [18,19], thus:

$$\varepsilon^* = \varepsilon' - j\varepsilon'' = \varepsilon_\infty + \frac{(\varepsilon_s - \varepsilon_\infty)}{(1 + jf/f_r)} \tag{4}$$

In equation (4) ε_s is the 'static' permittivity, ie. ε' at low (sub-RF) frequencies, ε_∞ is the value towards which ε' tends as the frequency is increased well above the microwave range and f_r is the relaxation frequency, at which ε'' reaches a maximum.

Table 13 Reference Liquids used in testing the multilayer measurements.

(a) Relaxation parameters at 20°C

Liquid	ε_s	ε_∞	f_r (MHz)
Deionised water	80.21	5.62	17.00
Methanol	33.65	5.76	2.709
Ethanol	25.28	4.44	0.826
Cyclohexane	2.024	*	*

(b) Relaxation parameters at 25°C

Liquid	ε_s	ε_∞	f_r (MHz)
Deionised water	78.36	5.16	19.24
Methanol	32.65	5.60	2.978
Ethanol	24.51	4.38	0.939
Cyclohexane	2.016	*	*

* For the purposes of the present project, cyclohexane may be considered practically lossless; the static permittivity value, ε_s, gives ε' across the complete frequency range of interest, $\varepsilon'' \approx 0.0$.

4.2 MEASUREMENTS UPON REFERENCE FLUIDS

As described in Sections 1.2 and 1.3, liquid measurements in the 'probe', ie. 'infinite half-space', geometry have been performed successfully at NPL [10] and by our collaborators [22] for some years, so it will not be necessary to present them further here. The same may be said of the 'infinite-lamina' geometry [21]. These correspond to geometries G! and G2 of Section 2.3. However, there have been no prior reports of measurements upon specimens in cylindrical cells like that of Figure 2 (c) (Geometry G3). We therefore report here comparisons between measurement and theory for this cell when liquid-filled. These are, in a sense, the easiest possible measurements which could be performed with such a cell and it will be appreciated that if agreement could not be obtained in such a case, it could not be expected in the more complex multilayer case. Starting in this section, then, with this simple geometry, Sections 4.2, 4.3 and 4.5 cover measurements upon ever more complex layered structures. All measurements reported in Section 4 have been obtained with the Type C sensor and cell, and the computations in Section 4 were therefore performed for geometries G3 and G4, rather than for open geometries such as G1.

Figure 10 shows a comparison between theory and measurement for a cell of 5.04-mm depth filled with methanol at 21°C. Bearing in mind the expected measurement uncertainties (see Section 5, below), it is difficult to see how better agreement could be obtained. The Γ-values are tabulated in Table 14.

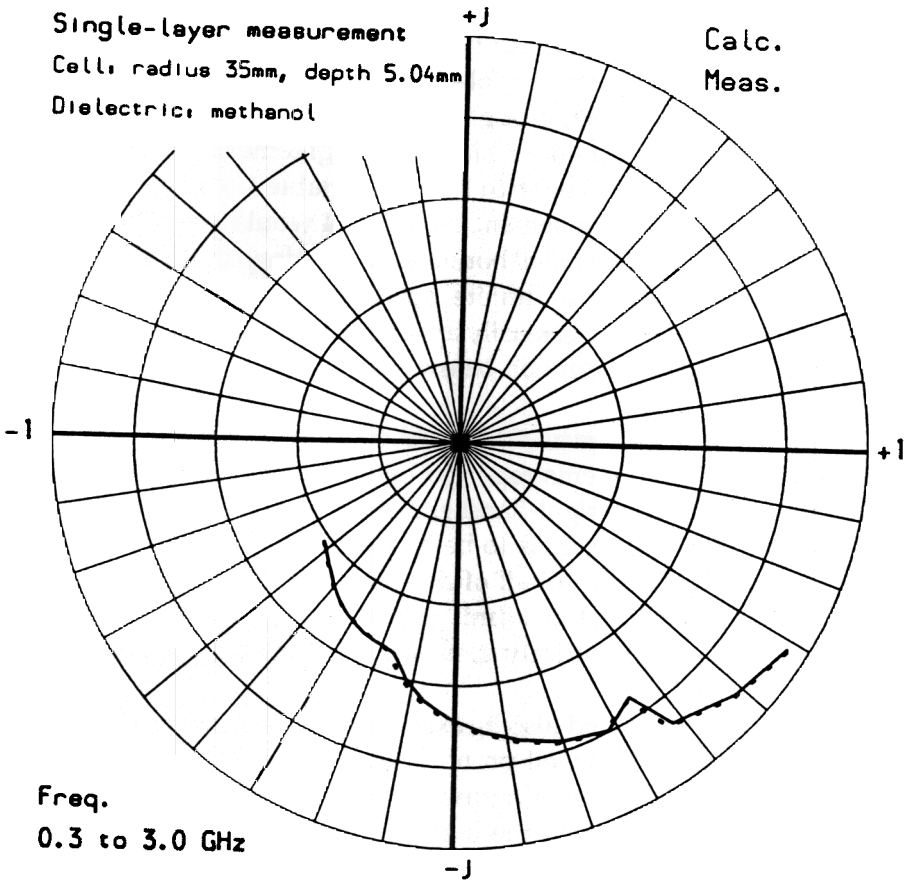


Figure 10 Comparison between 'TEH2' and measurements upon a 5.04-mm thick cavity filled with methanol. Polar plot of Γ

Table 14 Comparison of theory and measurement – methanol in a cylindrical cell; depth h = 5.04 mm, radius r = 35 mm.

Frequency (GHz)	'TEH2'		measured	
	$\lvert\Gamma\rvert$	θ	$\lvert\Gamma\rvert$	θ
0.3	0.9535	-31.68	0.9511	-31.33
0.6	0.7564	-56.07	0.7512	-55.44
1.0	0.7135	-86.02	0.7150	-84.59
1.5	0.5409	-108.54	0.5440	-106.47
2.0	0.4977	-124.50	0.5050	-122.65
3.0	0.4111	-144.21	0.4175	-141.87

It is to be noted that the agreement between theory and measurement in Table 14 is generally better than that shown for methanol in Table 6 for an attempted 'infinite' lamina geometry. In particular, these measured $|\Gamma|$ values agree overall more closely with the 'TEH2' values in Table 14 than do the similar measurements in Table 6 with the corresponding 'AGPW' figures. The same is true of θ-values up to 2 GHz, though there is a tendency for 'TEH2' to underestimate $|\theta|$ by a constant proportion of the angle, which makes agreement in θ slightly worse at 3 GHz. Apart from this effect, which is thought to be a correctable systematic geometric effect (see Section 4.4), the generally better agreement of Table 14 would seem to vindicate our policy of attempting to reproduce reliable *radial* boundary conditions in these measurements, rather than attempting to emulate a difficult 'infinite' specimen case, as in Reference 21 and Tables 6 and 7. (This observation does not necessarily apply to the emulation of a specimen of 'infinite' depth, h, see Figure 11 and the discussion below.)

Certain features of the trace in Figure 10 should be mentioned, because they will recur in many of the multilayer measurements reported below. It follows the variation of Γ with frequency starting at 300 MHz at the right-hand end and finishing at 3 GHz at the left hand end. The clockwise change with frequency is to be expected in all Smith Chart (ie. Γ-plane) presentations. The trace lies in the lower half of the complex plane indicating that the specimen and cavity present a largely capacitive admittance to the sensor. The trace further lies some way inside the edge of the chart, indicating, in this case, that the dielectric is lossy.

The features mentioned so far would also be expected for methanol measured in a non-cavity, open 'probe' geometry, but the two well-pronounced cusps on the trace are to be attributed to resonances inside the cavity. The lower frequency (right-hand) cusp corresponds to a TM_{010}-mode resonance inside the cavity, and the higher frequency cusp to the TM_{020} mode. These resonance features are in fact similar to those exhibited in Table 4, as discussed in Section 2.5.2, and, for methanol, they were presented theoretically (albeit from a different viewpoint) in Table 8, Section 2.5.4. In a 'perfect' cylindrical cavity (ie. one in which the coupling coefficient and loss are infinitesimally small) TM_{0n0} resonances occur at frequencies, f_n, such that $f_n = j_{0n} \times c/(2\pi r\sqrt{\varepsilon'})$, where the j_{0n} are the zeros of the Bessel function J_0 (2.4048, 5.5201, 8.6537 ... etc.), r is the radius of the cavity (35 mm), c is the speed of light and ε' is the real relative permittivity of the material filling the cavity. Our cavity here is far from 'perfect' in this sense, having a very large coupling to the coaxial line and containing, as it does, a lossy liquid. Nevertheless, a similar formula may be taken as a very rough guide to frequencies at which one might expect resonances to occur: $f_n \approx \Re e(j_{0n} \times c/(2\pi r\sqrt{\varepsilon^*}))$.

Cavity resonances measured in reflection always cause the value of Γ to traverse an approximate circle on the Γ-plane (or Smith Chart) towards (or around) the centre of the chart. At resonance, greater currents flow, increasing the energy dissipated in lossy elements, causing $|\Gamma|$ to fall. Large phase changes also occur which can make the trace move rapidly across the chart as frequency changes. However, in Figure 10 the dielectric is very lossy, having $\tan\delta$ values of 0.18 and 0.42 for resonances at 0.58 and 1.45 GHz, respectively. One would therefore expect relatively small resonance circles and Q-factors of $1/\tan\delta$ = 5.5 and 2.4, respectively. These correspond to resonance widths of 0.1 and 0.6 GHz which are to be compared with the frequency step of 0.1 GHz which is used for all of our measurements. The circle at 0.58 GHz does not therefore manifest itself as such on the trace, but is represented by a single point, appearing to be merely a dip in the response. In fact, if the Q-factor of the resonance is sufficiently low, the 'circle' will not appear at all because, as we have seen, there is in any case a tendency for the trace to move clockwise around the chart as the admittance of the fringing capacitance increases with frequency. Small resonances would therefore be spread out and appear as dips or cusps in the response, as is the case with the TM_{020}-mode resonance in

Figure 10.

If the cell is gradually made deeper (ie. h is increased), the Q-factors of the resonances will fall, because more lossy material is present, reducing the magnitude of the cusps of Figure 10. The limit of this process is shown in Figure 11 which is a measured response for an 'infinite' thickness cell of 35-mm radius. This is created by using the Type C sensor and its cell in Geometry 2 of Section 3.3, *without* the piston and simply adding liquid continuously until the meniscus is sufficiently far away from the coaxial sensor face to produce no further change in Γ. It will be seen that the amplitude of TM_{0n}-mode resonances is much reduced in Figure 11. This is compatible with our long-term contention that, in certain geometries, finite quantities of sufficiently lossy material can be treated (mathematically) as if they are 'infinite' in extent. The theoretical limits of this assumption were examined in Section 2.5.4. In the cylindrical cells (Geometry 2, Section 3.3), it seems to be more easy to emulate infinite-thickness (h) than infinite-radius (r), as shown in the discussion on Tables 6 and 11 above.

Similar agreement between measurement and theory was obtained for ethanol and other liquids employed. Figure 12, for example, shows a measurement/theory comparison for cyclohexane. Here the reference liquid is very low loss, so no change in resonance amplitude or $|\Gamma|$ is to be expected. Instead, the resonance should circle the whole Γ-plane very rapidly. It is better to show such behaviour on a phase/frequency chart, as given in the figure, because the phase, θ, contains all of the useful information to be gained from the measurement. The phase excursion at the resonant frequency is, in fact a complete cycle of 360°, but is again represented only by a few points to either side of the actual resonance frequency (near 2.2 GHz). The curves nevertheless again show good agreement between theory and measurement. It will be noted that discrepancies are at a maximum near the resonance. This is to be expected, as explained in Section 2.5.4 in the discussion upon Tables 8 and 9. We again expect that such discrepancies will be magnified in the ratio of the Q-factor of the resonances, as is borne out below.

In Figure 12, in noting the overall agreement of the measurement with the computation, we should not ignore the fact that there is again, as with Figure 10, (and ignoring the perturbations near the resonance) a systematic drift of measured phase away from the computed phase as the frequency increases - it amounts to 0.84° at 3 GHz in -21.86° (3.8%). Such discrepancies were not unexpected, they have been found before at NPL in low permittivity sensor-measurements and are to be attributed to geometric imperfections - see Section 4.4. It is important to note that such discrepancies are *not* symptomatic of a basic limitation for measuring ε^* for solid specimens. If the geometric imperfections are recognised, it is correct metrological procedure to *correct* for them by a liquid substitution or liquid immersion method (see Sections 4.4.1 and 4.4.3). Direct reference to the known permittivity of a reference liquid (see Table 13) could possibly reduce Γ uncertainties to the order of 1%.

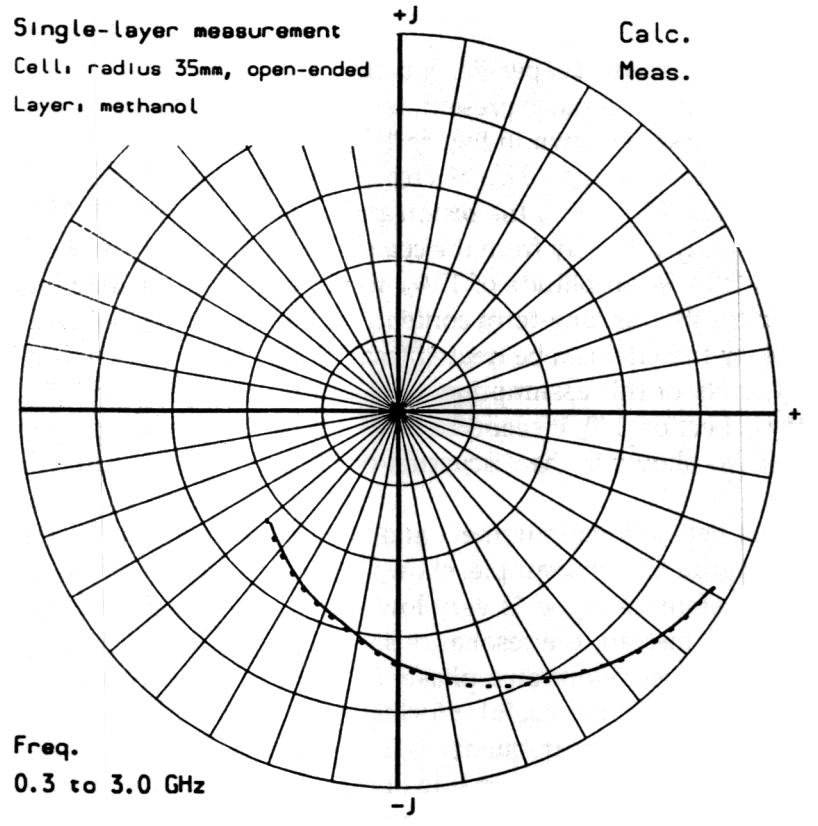


Figure 11 Comparison between 'TEH2' and measurements upon an 'infinitely'-thick cavity filled with methanol. This polar plot of Γ can be compared directly with Figure 10.

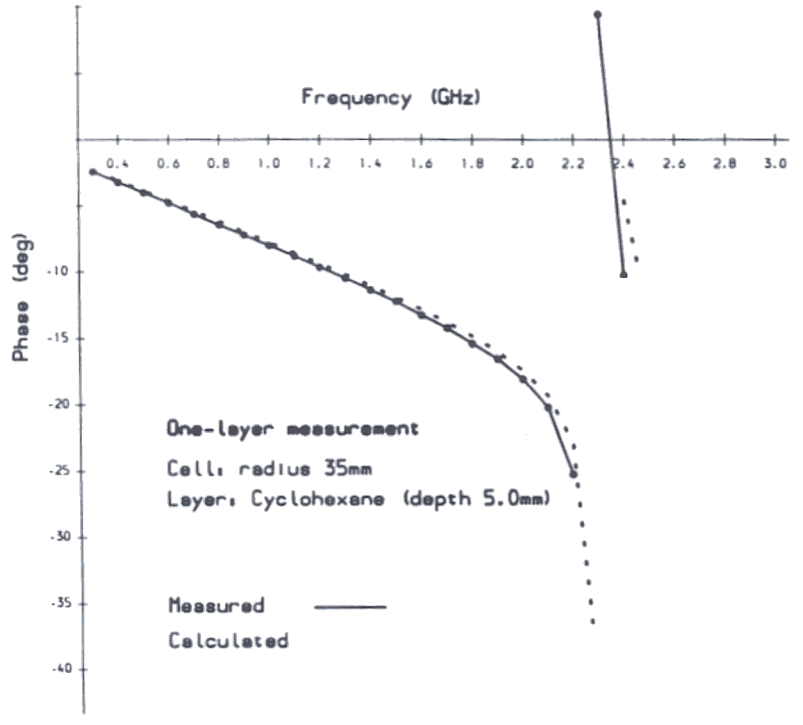


Figure 12 Comparison between 'TEH2' and measurements upon an 'infinitely'-thick cavity filled with cyclohexane. This is a plot of θ, the phase of Γ; $|\Gamma| \approx 1.0$

4.3 MEASUREMENTS UPON LIQUID/SOLID COMPOSITES

Before proceeding to consideration of measurements upon layered solids - the major aim of this project - we present examples of measurement/theory intercomparisons of liquid/solid composites. As mentioned above, these measurements have been performed at the development stage of this measurement technique because it is advisable to use the most flexible methods available during testing. Liquid layers are used as a substitute for solid layers: this has the advantages that the thickness of the liquid layer can be changed and that a *calculable high-loss* layer can be introduced into a composite 'specimen', allowing us to demonstrate that the system works over a large range of losses. This surrogate *test* role of the liquids, in which a liquid layer 'stands in' for a solid layer, is to be contrasted with two long-term measurement techniques in which liquids should continue to be used. These are *liquid immersion* and *liquid substitution*, see Sections 4.4.1 and 4.4.3, which are used in measurements upon multilayered specimens which have wholly solid components.

Figure 13 is a polar plot of a two-layer ethanol/cordierite composite. (See Tables 12 and 13 for the dielectric properties of these two materials.) In this figure, a continuous line is plotted for measurements *away from* the TM_{010} resonance and individual points are plotted *on* the resonance. This has the double advantage of emphasising the good agreement away from the resonance and showing up discrepancies obtained on the resonance. Only 4 points lie on the resonance but important features should be noted about them. Firstly, a resonance circle through the computed points (marked '+') passes closer to the centre of the polar chart than the equivalent circle through the measured points (marked 'o'). Secondly, the measured points are more closely spaced around the circle than the computed points. Both of these features are symptomatic of the measured Q-factor being lower than the computed Q-factor. This is again an indication that a numerical model which lacks contributions from metal loss and leakage will significantly underestimate the loss close to resonances. Nevertheless, both $|\Gamma|$ and θ agree at points well away from the resonance.

The ability to provide information on the third layer in a three layer system is demonstrated by Figure 14. This shows measurements upon two closely similar 50-mm-diameter composite systems: (1) (cyclohexane / high-density-polyethylene / cordierite-ceramic) and (2) (cyclohexane / high-density-polyethylene / barium-strontium-zirconate-ceramic). The first two layers are identical in thickness and material in both cases, while the properties of the third layer are given in Table 12 (permittivities 6.0 and 34.2 respectively). It will be seen from the figure that Γ for the two specimens is not only predicted to be significantly different at all frequencies but is measured to be so. The program 'TEH3' correctly predicts both the rate of change of θ with frequency at points away from the resonance *and* the resonant frequency in both cases. This is achieved in spite of the fact that there is almost 1.6 mm of low permittivity dielectric between the sensor and ceramic in each case.

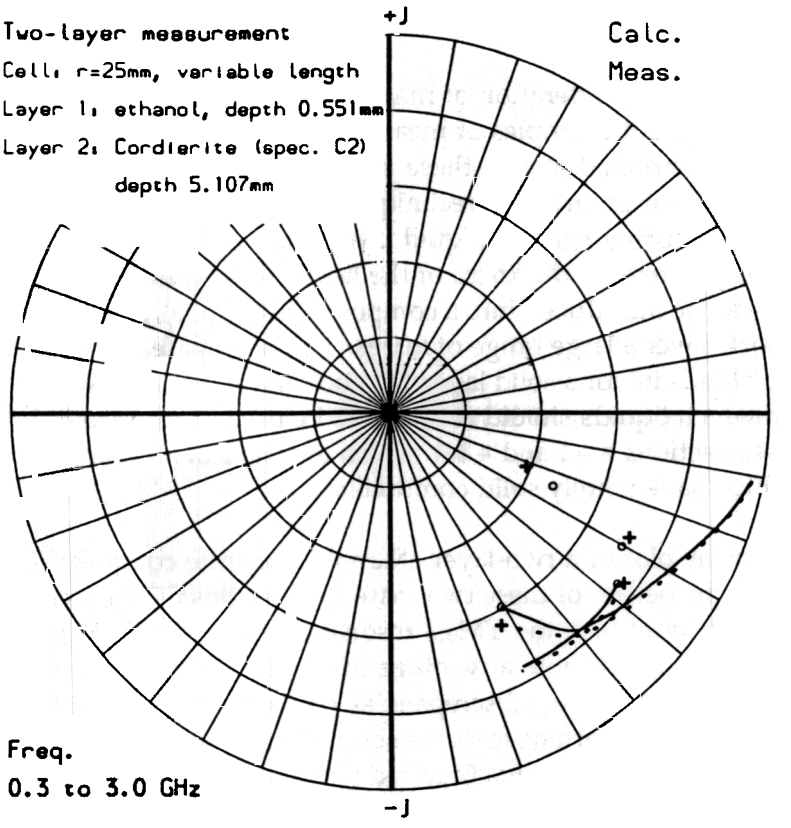


Figure 13 Measurement/program ('TEH2') comparison upon a two-layer liquid/ceramic composite specimen. Layer 1 is ethanol, layer 2 is cordierite. The cell diameter is 50 mm.

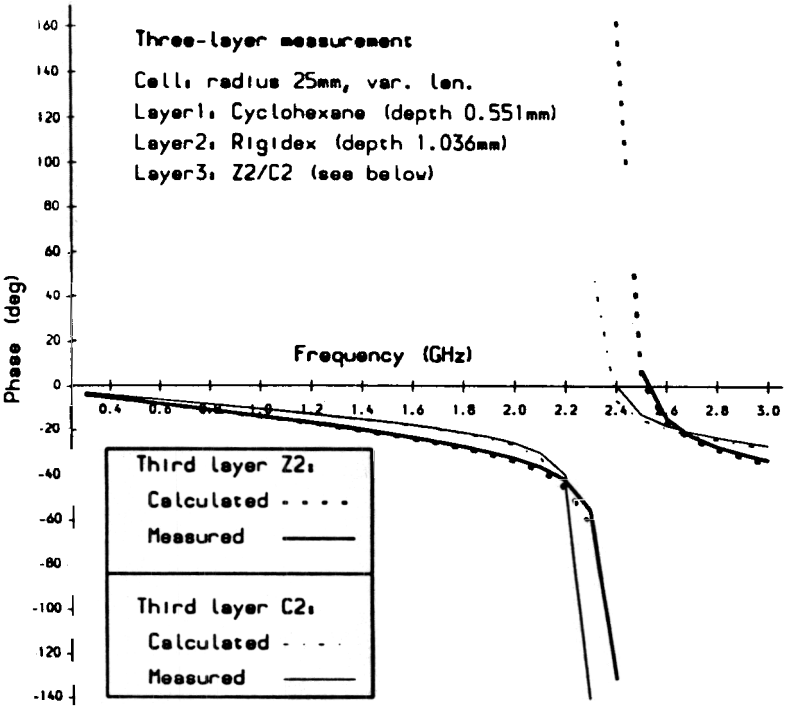


Figure 14 Measurement/Program ('TEH3') comparison upon two composite specimens of three-layers, in the order (liquid / polymer / ceramic). Layers 1 and 2 are cyclohexane and polyethylene. Layer 3 is either cordierite or zirconate (C2 or Z2 , respectively, see Table 12). The cell diameter is 50 mm. A phase plot is used because losses are too low to be measured.

As far as we are aware, this is the first report anywhere in the coaxial-sensor literature of the detection of a significant permittivity change in other than the first and second layers of a genuine multilayer composite. It is, moreover, possible to go further and compute from the measurements quantitative estimates of the ε' (= ε_3) of the third layer, in both cases. Thus we have:

cordierite: θ_m (3 GHz) = -26.42°
θ_t (3 GHz) = -27.47°

where θ_m is the measured angle at 3 GHz, and θ_t is computed by 'TEH3' using the parameters and specimen thicknesses given in Tables 11 – 13. Now, from θ_m we can reverse this process using the 'inverse' version of 'TEH3' (see Section 2.4.2, page 16). On the assumption that we know the properties of the first two layers ($\varepsilon_1, t_1, \varepsilon_2, t_2$) and the thickness, t_3, of the third layer, we can compute ε_3, and so 'measure' the permittivity of the cordierite. We make the further assumption, consistent with the discussion below in Section 4.4, that there are geometric imperfections in the composite cell which contribute an equivalent extra layer of 0.05 mm thickness above the ceramic. We therefore take t_1 = 0.601 mm and obtain:

cordierite: 'measured' ε' (3 GHz) = 5.68
actual ε' (Table 12) = 5.98

This is a discrepancy of less than the 10% we were aiming for in the measurement of the *second* layer of a composite, let alone the third layer, and it is measured in conditions which are far from optimum in terms of uncertainty of ε^* for the third layer. If the additional layer of cyclohexane is ignored, (using t_1 = 0.551) a figure of ε' = 5.49 is obtained which is still within 10%. Note that, though the value for ε' in Table 12 was measured at 10 GHz, rather than 3 GHz, the loss of the specimen is so low that the same value would be valid at 3 GHz.

We can perform similar calculations with the barium strontium zirconate:

zirconate: θ_m (3 GHz) = -32.94°
θ_t (3 GHz) = -34.65°
'measured' ε' (3 GHz) = 34.5
actual ε' (Table 12) = 34.2

with a result that is again well within 10% of the correct figure (although the unreasonably good agreement should be regarded as fortuitous - discrepancies of the order 5% might be expected). In this case however, ignoring the additional cyclohexane gap (ie. taking t_1 = 0.551) gives ε' = 29.4, which is more than 10% away from the correct figure, but in a much more difficult metrological case than cordierite. Bearing in mind, in the case of both ceramics, that the 'measured' ε' figures could have been improved by suitable liquid-substitution techniques, it is possible to see the power of the sensor/cell technique from this example.

In the light of the examples of measurements given in Sections 4.2 and 4.3, and of the relevant theoretical observations of Section 2, it is now appropriate to discuss the procedures which

have been developed for traceable measurements upon layered composites. This topic will be presented in Section 4.4 prior to the discussion of measurements on wholly-solid specimens in Section 4.5. It is appropriate to cover this at this point because the methods resulted from an interactive learning process; they were developed gradually as experience was gained, and the measurements of Section 4.5 benefitted from this process.

4.4 CHOICE OF MEASUREMENT METHOD FOR SOLIDS

We first set up in Table 15 a list of 'specimen types' to simplify the discussion that follows. The choices described here are independent of whether the specimen is single-layer two-layer or multilayer in structure, since the theory of Section 2 can be applied to all such cases. The specimen *hardness* and *dielectric loss* are more relevant to the issue of deciding which measurement method to adopt. The magnitude of the *real* part of the specimen permittivity, ε', proves to be somewhat less critical for choice of technique, than does the magnitude of ε'' - though ε' should influence the choice of the diameter of the coaxial sensor whenever optimum (low) measurement uncertainties are required [10]. Available specimen size and shape are also of relevance and may force one to use a 'probe' technique (geometry G1 of Scetion 2.3), when a cell method might otherwise be preferred. In order to improve calculability by the programs of Table 3 when the 'probe' method is in use, the largest possible flange should be employed.

Table 15. Measurement method for various specimen types. Geometries G1, G2, etc were defined in Section 2.3. Thus, 'G1' refers to an 'Infinite-Half-Space' geometry (Figure 1 (a)). 'G2' refers to 'Infinite Lamina' geometry, (Figure 1 (b)). 'G3' and 'G4' are cell geometries.

Specimen Type	**Low Loss** $\tan\delta < 0.1$	**High Loss** $\tan\delta \geq 0.1$
liquid	filled cell	filled cell, G1 or G2 with 'probe'
malleable solid	sensor/specimen contact, G3 or G4 measurement in cavity	sensor/specimen contact measurement, G1 or G2 geometry
hard impervious solid	liquid immersion gap before specimen in cell	liquid immersion gap before specimen
hard soluble or porous solid	air/powder (?) immersion, G3 or G4 gap before specimen in cell	air/powder (?) immersion gap before specimen

The rationale behind these recommendations follows from the following discussions (Subsections 4.4.1 – 4.4.5). The important method of liquid immersion will first be described.

4.4.1 Liquid immersion

The following examples illustrate the advantages of using a liquid immersion method. The first example is purely hypothetical. It concerns the measurement of a 2.0-mm thick specimen of polymer having $\varepsilon^* = 2.54 - 0.0j$. Using 'TEH2/3', both in its 'forward' and 'inverted' forms, the measurement error caused by a small gap between the specimen and sensor flange can be computed. This gap is arbitrarily set at 10 μm, just to illustrate the principle. If the presence

of the gap is not known to the metrologist, or (more likely) if he does not know exactly what its thickness, t_1, is, smaller errors will be obtained if the specimen is immersed in cyclohexane, than if it is immersed in air. The figures are gathered together in Table 16.

Table 16 The effect of a 10-μm sensor-to-specimen gap in a measurement upon a 2.00-mm thick polymer specimen for different dielectric fillings in the gap. ε' for the polymer is assumed to be 2.54, for cyclohexane 2.018, for air 1.00. The diameter of the cell is 70 mm and the frequency is 1 GHz.

Gap material	θ ('TEH2')	$\varepsilon'_{2.00mm}$	$\Delta\varepsilon'_{2.00mm}$	$\varepsilon'_{2.01mm}$	$\Delta\varepsilon'_{2.01mm}$
(a). No gap	-14.150°	2.540	0.000	2.548	+0.008
(b). polymer	-14.110°	2.532	-0.008	2.540	0.000
(c). air	-13.937°	2.497	-0.043	2.505	-0.035
(d). cyclohexane	-14.075°	2.525	-0.015	2.533	-0.007

In Table 16, the computed permittivities in the column headed $\varepsilon'_{2.00mm}$ will be obtained from a measurement if the metrologist ignores the gap completely. In running the inverse version of 'TEH2', he has assumed that there is only one dielectric layer present and that its thickness, h is 2.00 mm. The column $\Delta\varepsilon'_{2.00mm}$ gives the error he will obtain in ε'. The last two columns give similar information for a metrologist who knows that his cell is actually 2.01 mm thick but who still performs the inverse computation for a single layer. Geometries (a) and (b) illustrate that if there is no gap (t_1 = 0.0 mm), or if it is actually filled with the same material as the specimen, then only small errors will be obtained. It is the contrast between (c), air, and (d), cyclohexane, which illustrates the benefits of liquid immersion. On the erroneous computational assumption that the cell thickness is the same as that of the sample, an actual 10μm gap gives errors of –0.043 and only –0.015, respectively, in ε', precisely because cyclohexane is much better matched in permittivity to the polymer than is air. The liquid immersion result in this case is approximately three times better than the direct measurement in air. If the metrologist also knows that the actual thickness of the cell is 2.01 mm, the liquid immersion error is even further reduced, as shown by the very last entry in the Table. Clearly it is always best to try to ascertain the thickness of any gaps. It should finally be noted from Table 16 that if ±2% is taken as the uncertainty one is aiming for in this measurement (which is better than our original ±3% target for a single layer), *all* of the above computations actually meet the target. Thus a 10μm gap is not critical in the measurement of this particular low-loss specimen.

Tables such as Table 16 can be created for any specimen/cell combination and if an intelligent estimate of the size of the gap is made, its effects can be compensated for. At least this is seen to be the case for low permittivity specimens. Much larger discrepancies must be expected for high permittivities, ($\varepsilon' \geq 10$). Table 17 (a) is similar to Table 16 but for the barium strontium zirconate specimen described in Table 12, which has a permittivity of 34.2. It can be seen that for such a specimen immersion in cyclohexane does improve upon an air measurement, when no account is taken of the gap, but not by nearly enough. Immersion in methanol, which is better matched to the zirconate, however, gives a much better measurement.

Table 17 (a) As Table 16, but for barium strontium zirconate, $\varepsilon' = 34.2$. Specimen thickness 1.415 mm, gap 10μm. 1 GHz measurements in a 50-mm diameter cell. The permittivity of methanol at 20°C and 1 GHz is $(30.31 - 9.06j)$. As in Table 16, the subscript to ε' are the assumed cell thicknesses, h.

Gap material	θ ('TEH2')	$\varepsilon'_{1.415mm}$	$\Delta\varepsilon'_{1.415mm}$	$\varepsilon'_{1.425mm}$	$\Delta\varepsilon'_{1.425mm}$
(a). No gap	-107.96°	34.20	0.00	34.28	0.08
(b). zirconate	-107.73°	34.11	-0.09	34.20	0.00
(c). air	-41.83°	7.24	-26.96	7.04	-27.16
(d). cyclohexane	-90.44°	29.91	-4.29	29.93	-4.27
(e). methanol	-107.64°	34.08	-0.12	34.16	-0.04

Table 17 (b) As Table 17 (a), but for a gap of 0.1μm. 1 GHz measurements in a 50-mm cell. Only the air and cyclohexane values for $\varepsilon'_{1.415mm}$, (c) and (d), are significantly different from $\varepsilon' = 34.20$.

Gap material	θ ('TEH2')	$\varepsilon'_{1.415mm}$	$\Delta\varepsilon'_{1.415mm}$
(a). No gap	-107.96°	34.20	0.00
(b). zirconate	-107.96°	34.20	0.00
(c). air	-107.60°	34.06	-0.14
(d). cyclohexane	-107.78°	34.13	-0.07
(e). methanol	-107.96°	34.20	-0.00

It can be seen from Table 17 (a) that when measurements are made on a high permittivity material like zirconate ceramic, very large errors occur if no account is made of a gap which is actually there (this is common knowledge). The practical measurement situation is generally that the metrologist knows that there *is* a gap (caused by lack of flatness, for example) but it will not be too clear to him what value for 'equivalent thickness' should be entered into a two-layer computation to compensate for it. However, from measurements with *two-different fluids* filling the gap, the size of the 'equivalent gap' may be estimated. This technique, which has been much used in low frequency dielectric metrology, is referred to as a **'two-fluid' immersion method**. ('Fluid', in this case, rather than 'Liquid', because one of these gap dielectrics may be air). The technique is illustrated by a comparison of Tables 17 (a) and (b), inspecting the results for air and cyclohexane immersion. If the gap is large, as in Table 17(a) a significant difference in Γ (or θ in this case) is obtained between air and liquid. If it is small (Table 17(b)) very little difference is obtained. So from an actual measured difference in θ for the above two fluids, the size of the 'equivalent gap', t_1, can be estimated. The measurement should ideally proceed as follows: (1) A measurement with the specimen in air is taken; (2) without otherwise disturbing the geometry, the liquid is allowed to suffuse the cavity and a second measurement is taken. (3) The value of t_1 in the two-layer computer program is varied until consistent results for ε_2 are obtained – thus both t_1 and ε_2, the permittivity of the specimen, can be obtained simultaneously. Another feature which should be noted from Tables 17 (a) and (b) is that the variation of the apparent ε' with gap depth is far from linear - resonances have an influence here in making the effects of gaps difficult to quantify without the aid of the computer programs. A feature like the very poor agreement for the air-gap measurement (c) in Table 17(a), for example, would be very difficult to predict.

This two-fluid immersion procedure has actually been performed for the measurements in Figure 15. It shows direct contact measurements upon the cordierite specimen of Table 12, using air and cyclohexane immersion. These are compared with a computed curve which takes no account of any possible gap. Compared with the measurements in air, cyclohexane immersion makes a significant improvement ($|\theta|$ is larger) and from the difference, at 1.5 GHz, for example, an 'equivalent gap', t_1 of approximately 0.054 mm can be derived. Feeding this value into the inverse 'TEH2' program gives ε' (cordierite) = 6.00 for the air-immersion case and 5.97 for the cyclohexane case. The same value for t_1 also gave best theory/measurement agreement for the zirconate specimen, which was measured by the same procedure. It is clear from this limited exercise, however, that if the technique is to be used with confidence for such high permittivities, we should ensure that other sources of discrepancy can be accounted for. For example, both the cordierite and zirconate specimens are actually smaller than 25 mm in radius (the figure used in the computation) and the effects of the gap between piston and cylinder are also such as to reduce θ, see item (9) of the uncertainty budget, Section 5.1. Some evidence that the discrepancy is not only caused by the equivalent contact gap comes from the fact that the optimum 'equivalent gap' changes with frequency. Further investigation is required to resolve this for the general case. The whole question of accounting for 'equivalent gaps' and other geometric imperfections will be dealt with in Sections 5 and 6. We should note here, however, that neither air nor cyclohexane are the optimum liquids to use with cordierite or zirconate specimens. Methanol, as shown in Table 17 is much better. However, from the experience gained here, we can say that these two liquids would form the basis for reliable two-fluid measurements upon specimens with permittivity up to about 4.0.

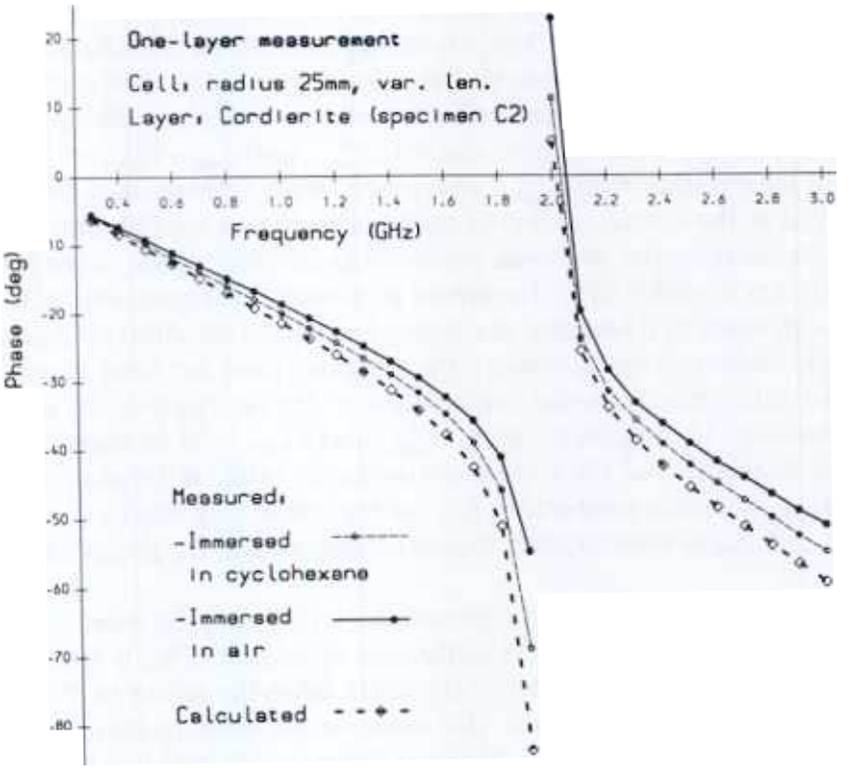


Figure 15 Sensor/specimen 'contact' measurement upon the cordierite specimen of Table 12 for air immersion and cyclohexane immersion. The 'calculated' trace is obtained on the assumption that there is no gap between specimen and sensor (i.e. $t_1 = 0.0$).

Choice of method for porous or soluble specimens

Liquid immersion cannot be used for porous or soluble specimens and so other approaches need to be used to reduce measurement uncertainties. It has nevertheless been seen in 4.4.1 that tolerable results from a non-immersion measurement can be obtained, even for a very-high permittivity specimen, provided gap sizes are known.Failing this possibilty. One recommended technique is liquid *substitution* (rather than immersion), as described in the next section. Another approach that might be tried, though we have not investigated it, is *powder* immersion where a fine dry powder of known permittivity, and of known impacted thickness, surrounds the specimen. Care would have to be taken over packing of the powder so that density-changes could be taken into account, though.

Liquid substitution

In all cases where it is known that significant errors in absolute measurements are unavoidable, it is recognised good practice to use a *substitution* technique. Here, we compare reflection coefficients obtained from the specimen, with those from a known reference liquid. The liquid should have a permittivity as closely matched as possible to that of the specimen. With a multilayer specimen, the liquid permittivity should be made as close as possible to that of layer 1. (If ε_1 is not known, a process of successive approximation can always be used). The procedure is as follows. Fill the cell with the match-liquid. The cell should have the same overall thickness, h, as it will do when the solid specimen is inserted. Record the measured reflection coefficient, $\Gamma^l_{meas.}$, at all frequencies. Compute (using 'RCAV3' or 'TEH3', etc., as appropriate) the corresponding reflection coefficient that should, theoretically, have been measured. Call this $\Gamma^l_{theor.}$. Place the specimen in the cell and measure *its* reflection coefficient, $\Gamma^s_{meas.}$. Provided $|\Gamma^s_{meas.} - \Gamma^l_{meas.}| \leq 0.1$, compute the complex quantity $\Gamma^s_{theor.}$ as $(\Gamma^s_{meas.} - \Gamma^l_{meas.} + \Gamma^l_{theor.})$, and use it in the computation for $\varepsilon*$ rather than $\Gamma^s_{meas.}$. This procedure is nothing more than a 'substitution technique' applied to the special context of computer-centered coaxial sensor measurements. It is equivalent to referring the specimen permittivity directly to that of the reference liquid, which may be known to within ±1%. The sensor then becomes responsible, as it were, only for detecting *small differences* in Γ between the specimen and the standard reference liquid. Note that, unlike liquid *immersion* measurement, the specimen does not need to come into contact with the match-liquid. However, the combination of the two techniques is to be preferred wherever it is possible. The requirement that $\Gamma^s_{meas.}$ and $\Gamma^l_{meas.}$ lie close together on the Γ-plane is the best check to ensure that the applied correction is valid. If the absolute difference between the two $\Gamma_{meas.}$ values is greater than 0.1, the technique may still be used, but with some circumspection, and larger uncertainties should be allocated to the procedure.

A recommended variation of the above procedure, which may be more efficient, is to use the match-liquid once only as one of the calibration standards. This is strictly equivalent to the above procedure only if the calibration algorithm takes the values of ε^* provided for the reference liquid as being exactly correct. This does not generally happen in a 'least-squares' calibration algorithm, but the latter may be better if *two* closely matched liquids are available for calibration. Whether, such 'calibration substitution' or a second independent substitution measurement (as in the last paragraph) should be used will depend on circumstances and specimens. In some cases, it may not be advisable to use the match-liquid as a calibration standard.

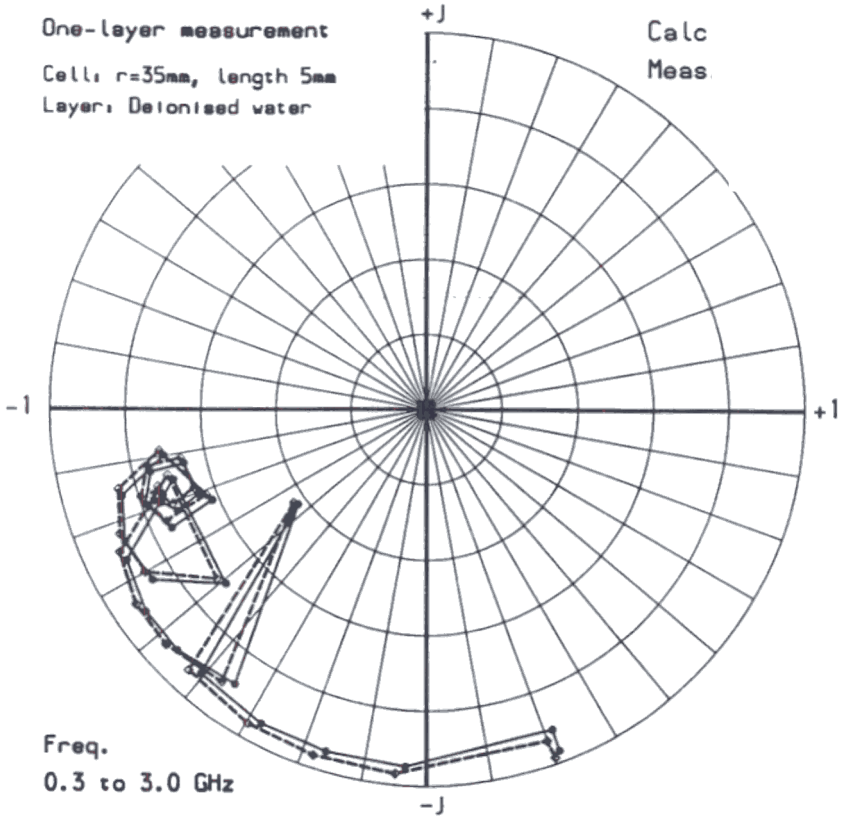


Figure 16 Deionised water in a cylindrical cell. Radius, r = 35 mm, thickness, h = 5.0 mm. The discrepancy between the calculated and measured traces can be attributed to residual calibration errors. It varies systematically only slowly with frequency, and the computed trace otherwise reproduces faithfully all of the resonances in the body of water.

Figure 16 shows an example in which a liquid- (in this case water-) substitution measurement could be advisable. It illustrates the measurement problem in a very high permittivity range which is extremely testing for the 14-mm sensor ($\varepsilon' \approx 78$). The software is clearly predicting the measured response from the body of water, but there is a small displacement between the two traces which is thought to be caused by calibration or geometric errors. This error is, however, systematic in a well-behaved way. If the measurements of Figure 17 were to have been a preliminary for a measurement upon a high permittivity ceramic specimen, for example, applying a substitution correction to the data would much improve the measurement. This would be equal to the vector difference between the two traces in Figure 16.

In some cases there may be a practical difficulty in cleaning the match-liquid out of the cell prior to the introduction of the solid specimen. This is not usually a problem with volatile organic liquids, though it may be with water. If a non-volatile liquid cannot be avoided, it may be better to measure the liquid *after* the specimen. Most of the results presented in this report have *not* been compensated by substitution, because it is essential to assess the intrinsic measurement methods *without compensation* at the initial testing stage of a new technique, in order to come up with a realistic uncertainty budget. However, one example of its use follows. The cyclohexane measurement of Figure 12 showed a discrepancy between the two traces rising to 0.84° at 3 GHz. That measurement was a preliminary to a measurement upon

a two layer system consisting of: layer 1: polystyrene, $\varepsilon_1 \approx 2.57, t_1 = 2.012$mm; and layer 2: cyclohexane, $\varepsilon_2 = 2.018$, $t_2 = 3.038$. Total cell depth, $h = 5.00$ mm in both measurements, and radius $r = 35.0$ mm. Table 18 shows the results of treating layer 1 as an 'unknown' dielectric and using the inverse 'TEH3' program to compute its permittivity. The second column corresponds to the result without compensation, and the third column to the result obtained with cyclohexane liquid-substitution compensation. The computations assume a small contact 'equivalent' gap of 0.03 mm between the polystyrene specimen and the sensor.

Table 18 Application of liquid substitution to a permittivity measurement. Measurement upon a polystyrene specimen, configured as layer 1 in a two layer polystyrene/cyclohexane composite. Computations were by means of the inverse version of 'TEH3'. Figures in italics were influenced by the TM_{010}-mode resonance, see text for details.

Frequency (GHz)	ε_1 Direct Computation	ε_1 Liquid Substitution
0.3	2.747 –0.041*j*	2.600 –0.012*j*
0.5	2.725 –0.062*j*	2.587 –0.027*j*
1.0	2.708 –0.076*j*	2.601 –0.034*j*
1.5	2.670 –0.075*j*	2.584 –0.039*j*
2.0	*	*2.510 – 0.082j*
2.5	*2.665 – 0.046j*	*2.459 – 0.018j*
3.0	2.655 –0.046*j*	2.544 –0.037*j*

* The TM_{01}-mode resonance gives rise to an erroneous value in the 2-GHz 'direct' measurement

The results of the final column of Table 18 are well within the required uncertainties, apart from the 2.0 and 2.5-GHz figures (in italics), which are affected by the resonance, as clearly shown in Figure 12. One should associate a larger uncertainty with these two measurements and, in practice, it would be better to interpolate ε^* for these two frequencies between 1.5 and 3.0 GHz. The measured loss figure is also clearly better after substitution. It was never expected that the sensor technique would measure low losses, below $\tan\delta = 0.05$, and the figures in the table may therefore be taken as indicative of the magnitudes of the resolution to be expected at present. They are consistent with a best estimated resolution (away from resonances) of 0.05 for $\tan\delta$ (see Section 5). From other measurements, it is estimated that ε' for the polystyrene specimen is rising gradually with falling frequency and it probably possesses a permittivity of 2.59 at 300 MHz. The compensated measurements do seem to reflect this real trend, but since the measurement uncertainties are estimated at ±2%, after substitution compensation, the agreement is probably fortuitous – an uncertainty of at least ±0.02 in ε' is expected.

4.4.4 Choice of spacing between sensor flange and specimen

A major decision to be made before measuring a solid specimen is whether or not to introduce a space between the specimen and sensor. This is clearly not necessary in the case of a malleable solid, powder or liquid, where good sensor contact (zero gap width) can be guaranteed. However, for hard solids the uncertainty in thickness of the 'effective gap' between specimen and sensor in a 'contact' measurement is one of the most critical uncertainty contributions. For example, the recession or protrusion of the bead and inner-conductor of the sensor may be

of the order 1-10 μm, and we should wish to minimise the effects of the ensuing measurement uncertainty (see Item 5, Section 5.1). Lack of specimen flatness may increase the uncertainty to as high as $\pm 50\,\mu$m. Before measurement of any specimen, computations should therefore be performed to discover the optimum spacing, t_1, to be used, given that t_1 itself may be uncertain to as much as ± 0.05 mm. There are so many degrees of freedom involved in multilayer measurements (specimen ε', ε'', thickness, flatness, diameter, etc.) that we believe it is best not to try to produce tables of estimated uncertainties for all cases (which would produce a substantial document), but rather to perform the computation on an as-and-when basis for each individual specimen. Table 19 (a) demonstrates such a procedure for a 2.00-mm thick, 25-mm radius specimen of $\varepsilon* = 30.0 - 0.0j$, immersed in cyclohexane.

Table 19 (a) Effect of uncertainty in specimen/sensor spacing, for a specimen with $\varepsilon' = 30.0$. The Table gives the error in measured permittivity, ε'_m, as a function of specimen/sensor spacing, t_1, when t_1 is in error by $\Delta t_1 = 0.01$ mm. The gap is filled with cyclohexane.

Error in $\varepsilon' = 30$

t_1 (mm)	1 GHz	2 GHz	3 GHz
0.05	0.70	0.32	0.36
0.10	0.36	0.25	0.22
0.20	0.34	0.27	0.63
0.40	0.35	0.45	0.53
0.60	0.37	0.62	0.54

Table 19 (b) Change in measured phase, θ, when the specimen permittivity changes from 30.0 to 31.0. The conditions are otherwise as in Table 19 (a)

Change in phase, $\Delta\theta$

t_1 (mm)	1 GHz	2 GHz	3 GHz
0.05	12.65°	4.73°	7.12°
0.10	3.10°	4.36°	68.52°
0.20	1.22°	2.62°	3.75°
0.40	0.46°	1.05°	1.33°
0.60	0.24°	1.22°	0.77°

Table 19 (a) clearly shows that best uncertainties for ε' across the frequency band, *for this particular specimen*, will be obtained if a known gap of approximately 0.1 mm can be set up accurately between the specimen and sensor. The figures in the table, which are effectively proportional to $d\varepsilon'/dt_1$, clearly will not have only one minimum, because of resonances. For example, there is a second minimum at 3 GHz for $t_1 = 0.4$ mm, but the first minimum gives the lowest discrepancies, and therefore will give the lowest uncertainties when Δt_1 is unknown. There is another reason for using the smallest gap consistent with a minimum in $d\varepsilon'/dt_1$, and this has to do with the resolution of the measurement of phase, θ. Table 19 (b) gives, for the same hypothetical specimen, the change in measured phase ($\theta = \arg(\Gamma)$) for a change in ε' from 30.0 to 31.0 (ie. approx. 3.3%). Bearing in mind that the uncertainty for θ is of the order 0.1° or worse, this table provides another reason for measuring with a small value of t_1, since the sensitivity clearly falls with increasing t_1. Thus, a better measurement can be obtained if a *small* gap is introduced between the specimen and sensor than if an attempt is made to

reduce the gap to zero in a 'contact' measurement. The whole procedure requires a good deal of experimental care, however, to ensure that the uncertainty in t_1, Δt_1, is not greater when a gap is present than when a 'contact' measurement is performed.

Miscellaneous techniques

A single sensor measurement (at a given frequency) delivers one complex number (Γ) from which information about the specimen properties is to be deduced. In general, one has to know the complex permittivity of all but one layer of a composite, and all of the thicknesses ($t_1 ... t_n$, for an n-layer composite) in order to compute the permittivity of a single layer. Alternatively, if one knew all permittivities, it might be possible to compute the position of at most one boundary between two layers. There follows a list of techniques which might be used to derive further information, although measurement uncertainties may render the techniques unusable for many specimens.

(1) Measure the specimen from both sides. This delivers twice as much information. One could, for example use this method to estimate both permittivity and thickness of an inaccessible central layer of a three-layer laminate. This method has been tried and examples are given in Section 4.5.

(2) Measure the specimen in different geometries. One could, for example, measure the specimen in contact with the sensor, or with a space in front. Likewise for the gap behind the specimen. This approach has not, so far, been attempted comprehensively.

(3) Use two- (or multiple-)liquid immersion. Section 4.4.1 described one application of the two-liquid immersion technique. It could alternatively be used to provide information on more than one layer of a composite, though this again has not been tried.

(4) Use an open-circuited cell. At present, all measurements on laminas have been performed with a 'back-short' behind the specimen (whether in a cell or not). An alternative, again not yet tested, is to have an 'infinite' air or liquid backing for the specimen. This would produce a very different terminating condition for the measurement. In the case of a cell measurement, it may be necessary to have some centimetres of air behind the specimen (and possibly to restrict the technique to frequencies below the TM_{01}-mode cut-off). One difficulty that might arise is to keep a high pressure contact between specimen and sensor when pressure cannot be applied through a back short.

MEASUREMENTS UPON LAYERED SOLIDS

To summarise what has been covered so far. We have shown that measurements on single-layer laminas and liquids can deliver good agreement between measurement and computation. We have shown that liquid/solid composite measurements are equally successful and, in the light of experience, have developed measurement strategies (Section 4.4.4) which should minimise uncertainties. It is finally necessary to demonstrate that measurements upon true multi-layer specimens are possible, ie. measurements upon n-layers, where $n \geq 3$. One example has already been provided in Section 4.3 of the successful measurement of the permittivity of the third layer of a three-layer composite, where the first layer was a liquid. Here we give two examples of measurements upon three-layer *solid* composites. In both cases, method (1)

of Section 4.4.5 has been used. ie. the same composite specimen has been measured from both sides in order to obtain more information about it.

The first example is of a (PTFE / plate glass / polystyrene) composite (see Table 11 for the properties of each layer). The respective thicknesses were t_1 (t_3) = 2.903 mm, t_2 = 2.078 mm, t_3 (t_1) = 1.007 mm; (the symbols in parentheses give the correct nomenclature for the case when the specimen is reversed). The measurements were both performed by cyclohexane liquid immersion and the results are shown in Figures 17 (a) and (b). As is to be expected (see Section 4.3), close agreement of the traces is not obtained on the resonance because the 'TEH3' computation has been performed on the assumption that there is zero loss in the system. Table 20 shows the results of the measurements when they are interpreted as a measurement of the permittivity of the inaccessible middle (glass) layer of the laminate.

In Table 20, we should first note the difference in the scatter of the results between geometry (a) in the second column and geometry (b) in the last column. We would not expect sensitive measurements of the glass layer to be possible in geometry (a) simply because the first layer, PTFE, is too thick – t_1 is almost 3.0 mm. We discount the 2.0-GHz measurement, which falls on the TM_{01}-mode resonance, but the figures that remain give only a tolerable indication of the permittivity of the glass. The measured loss is too high, though liquid substitution (Section 4.4.3) could have corrected for that, but then it is known that in this particular computation there are unaccounted-for losses elsewhere in the system. The inverse version of the program 'TEH3' can only attribute these losses to the 'unknown' second layer. The values of ε' for the glass are scattered, but we know from all of our other measurements that its loss tangent, tan δ, is certainly less than 0.05 and so its permittivity will hardly be changing over this frequency range [24]. We should therefore be justified in taking an average figure for ε', which is 6.4. The correct value is about 6.8. The lowness of the estimated figure is to some extent caused by ignoring the specimen/sensor gap, which is thought to be 0.03 mm ±0.02 mm. More than this cannot be said about the specimen as measured in geometry (a). The measurement geometry is outside of our specification because the thickness of the first layer reduces the sensitivity of the measurement of the second layer by over an order of magnitude.

Turning to column (b) of Table 20 where only a 1-mm thickness of polystyrene separates the glass from the sensor, we find that we obtain results which are well within specification. All of the figures in the column – apart from the 2 GHz figure which, as already noted, falls on a resonance – are well within 10% of the expected figure ($\approx 6.76 - 0.01j$) which was our target for a *second* layer in a composite. Note again that no corrections for liquid gaps or additional losses in the cell have been applied in the Table, so we are looking at the basic sensitivity of the technique. The loss of the glass again appears to be higher than it should be but it is still within acceptable uncertainty limits for a second layer of a composite. Computations which have been carried out in order to estimate uncertainty show just how sensitive the computed permittivity, ε_2, of the second layer is to the value assumed for the permittivity of the first layer (ε_1). For example, if ε_1 is set at 2.62, instead of 2.58, the computed permittivity for glass at 300 MHz is 6.42, rather than 7.02. This critical dependency of $\varepsilon_{2\text{—estimated}}$ upon $\varepsilon_{1\text{—assumed}}$ tends to fall with frequency and this very phenomenon can be used to gain more information about permittivity of the top layer in a specimen. It is known, for example, that neither the permittivity nor loss of the second layer can vary very quickly with frequency. If an inverse computation gives results for ε_2 which *are* varying rapidly, it is a reasonable to make the assumption that ε_1 has been quantified wrongly.

Table 20 Measurements upon a three-layer composite specimen: PTFE/glass/polystyrene. See text for details. Computations of $\varepsilon^* = \varepsilon_2$ for the inaccessible central glass layer were performed by the inverse version of 'TEH3'. The specimen was measured from both sides: (a) PTFE in contact with sensor (b) polystyrene in contact with sensor.

Frequency (GHz)	ε_2, geometry (a)	ε_2, geometry (b)
0.3	7.02 –0.03*j*	7.02 –0.03*j*
0.5	6.83 –1.5*j*	6.96 –0.41*j*
1.0	5.90 –1.1*j*	6.66 –0.30j
1.5	6.53 –0.85*j*	6.62 –0.33*j*
2.0	*4.44 – 3.77j*	*7.04 – 8.28j*
2.5	5.91 –0.56*j*	6.44 –0.30*j*
3.0	6.08 –0.21*j*	6.43 –0.17*j*

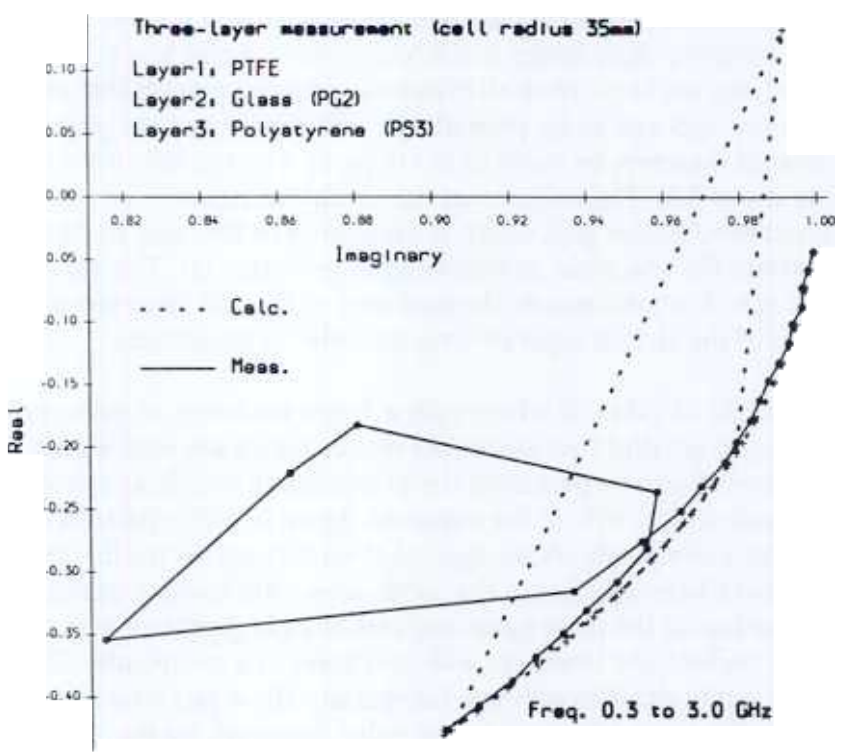


Figure 17 (a) Measurements upon a PTFE/glass/polystyrene composite with PTFE in contact with the sensor (see text for details). The measurement employed cyclohexane immersion. The resonance is not faithfully reproduced because the computation by 'TEH3' assumes very low loss in the cell.

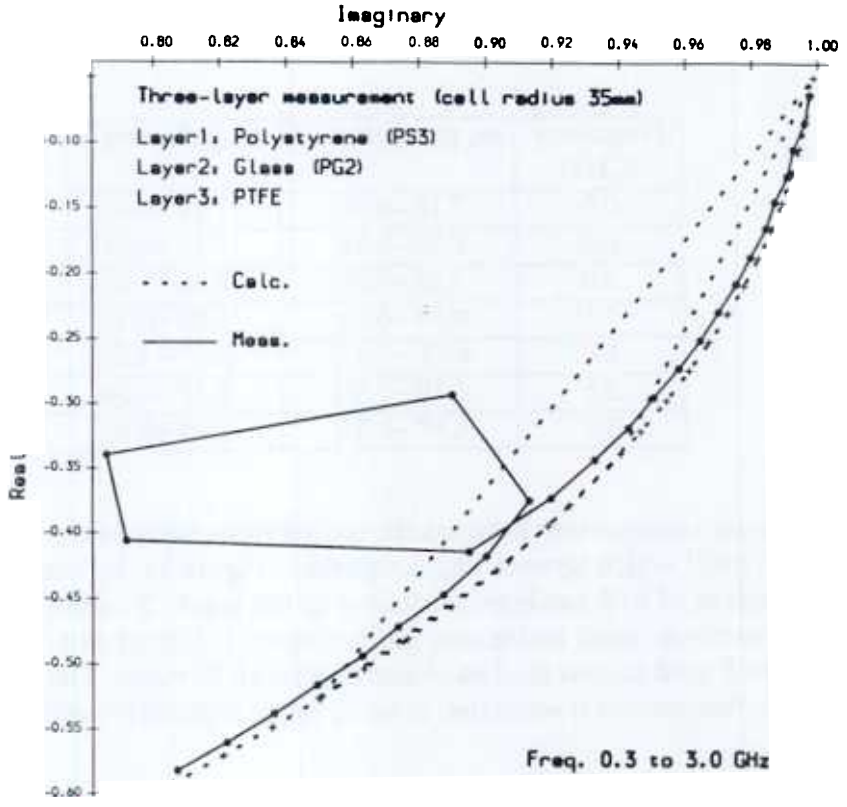


Figure 17 (b) As Figure 17 (a), but with the specimen reversed so that the polystyrene contacts the sensor.

The (PTFE/glass/polystyrene)-specimen, then, demonstrates one reason for inspecting specimens from both sides. We now turn to a (Delrin/glass/polystyrene) specimen, Table 21, which is within geometric specification on both sides. The respective thicknesses were t_1 (t_3) = 1.003, t_2 = 2.078, t_3 (t_1) = 1.007. The measurements were again performed by cyclohexane liquid immersion and the results are shown in Figure 18 and Table 21. We should again discount the 2.0 GHz figure, which lies on the TM_{01} mode resonance, though we can note in passing that the value for ε' is approximately correct in both cases; ε'' is too high, but it is precisely at resonance that unaccounted-for losses will have most effect. At all other frequencies the measurements are well within specification. The negative losses attributed to the glass at 0.3 and 0.5 GHz are caused in this case by attributing excessive losses to the polystyrene first layer at these frequencies. Until full and more flexible account of losses can be taken in the software, anomalies like this will continue to arise. In the meantime, we note that even this discrepancy is compatible with the specified uncertainty limits. The results, as discussed above, are consistent with the polystyrene permittivity having risen to about 2.59 at 300 MHz and so are compatible with the results of Table 18. The loss angle associated with such a rise from ε_∞ (cf. equation 4 and Reference 24) is consistent with a tan δ of about 0.02 which would reduce the measured losses at 0.3 and 0.5 GHz to about zero. The glass specimen, too, is sufficiently lossy to vary in permittivity across the band. Its equivalent static-permittivity ε_s is estimated to be 7.02 and so some rise in ε' with falling frequency is to be expected. Since the tabulated rise is about double that expected, much of it must be attributed to systematic effects, they are nevertheless well within specification.

Table 21 Measurements upon a three-layer composite specimen: Delrin/glass/polystyrene. See text and caption to Table 20 for details. The specimen was measured from both sides: (a) Delrin in contact with sensor (b) polystyrene in contact with sensor.

Frequency (GHz)	ε_2, geometry (a)	ε_2, geometry (b)
0.3	7.12 –0.38*j*	7.11 +0.61*j*
0.5	7.29 –0.13*j*	7.15 +0.24*j*
1.0	7.10 –0.25*j*	7.06 –0.03*j*
1.5	6.74 –0.45*j*	6.83 –0.53*j*
2.0	*6.93 – 1.12j*	*6.77 – 1.58j*
2.5	6.78 –0.37*j*	6.77 –0.24*j*
3.0	6.67 –0.35*j*	6.73 –0.26*j*

Figure 18 (b) shows a comparison between the (polystyrene-layer-1) measurement and a computation with 'TEH3' which ignores loss completely. Figure 19, by contrast, shows the case where a loss tangent of 0.05 has been attributed to the glass. It can be seen that agreement away from resonance is much better, and ±0.05 is again indicated as a suitable value for the resolution for tan δ until further studies of loss effects can be made. The actual loss tangent of the glass at these frequencies is estimated to be no larger than 0.01 – well below the resolution of the method.

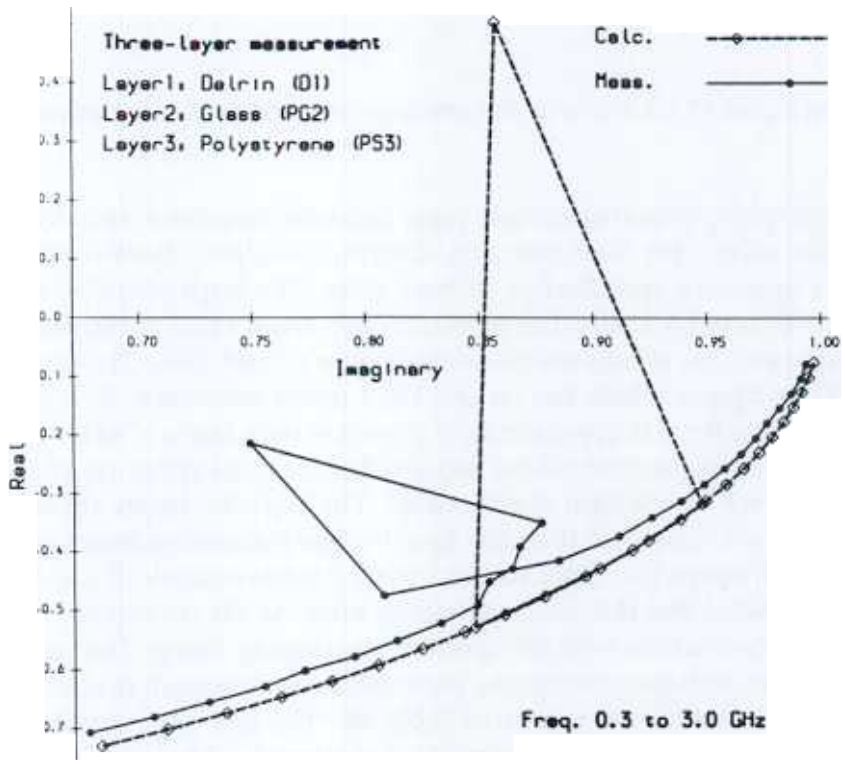


Figure 18 (a) Measurements upon a Delrin/glass/polystyrene composite with Delrin in contact with the sensor (see text for details). The measurement employed cyclohexane immersion.

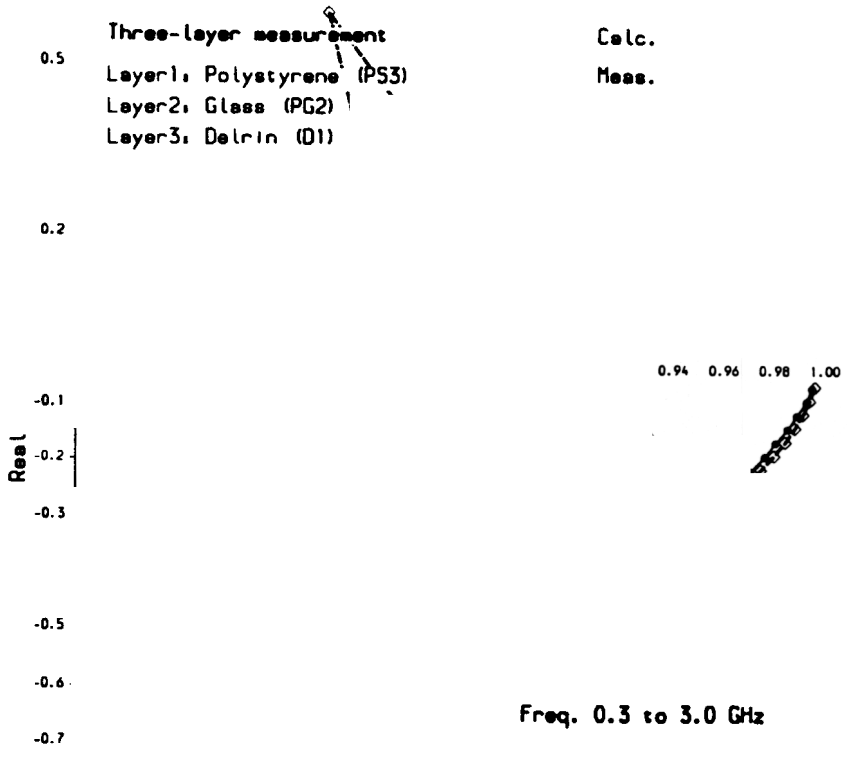


Figure 18 (b) As Figure 18 (a), but with the specimen reversed so that the polystyrene contacts the sensor.

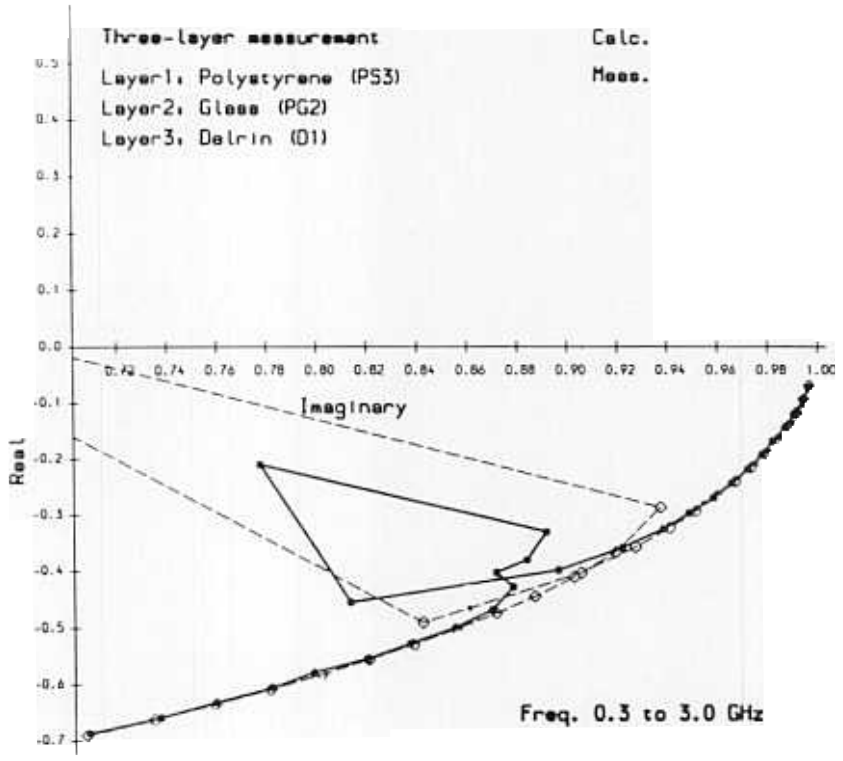


Figure 19 As Figure 18 (b), but with the assumption that tan δ for plate-glass is 0.05.

We have shown with these examples that useful three-layer measurements are possible, that we can meet our desired specifications for such measurements and that further improvements can be expected from a comprehensive modelling of loss processes. We will return to these points in the final section of this report, but it is first necessary to quantify the uncertainties associated with these measurements.

5 UNCERTAINTIES

In this report, it is fortunately not necessary to describe in great depth the procedures that we have followed to estimate uncertainties: previous and forthcoming reports do this in some detail. Thus, considering different classes of error sources:

1. The original critical study of coaxial sensors included discussion of numerical analysis errors [10], as did a subsequent *Electronics Letter* [20] and Section 2 of this report.
2. Errors caused by geometric imperfections in the cell/specimen geometry were discussed previously in References 10 and 21. Spurious resonances in supposed 'infinite half-space' geometries were also described in Reference 10. More generally, a discussion of geometric uncertainty analysis in a variety of liquid cells demonstrates our approach to these issues [19].
3. Errors caused by lack of knowledge of the properties of reference materials have been considered both at NPL [4,18,19] and (as noted in Section 1.4.1) by other workers [33]. While it is now possible to make an educated estimate of their magnitude, we do not regard this issue of reference liquids as being closed and believe that further work is necessary to reduce errors from this source.
4. Intrinsic uncertainties in the network analyser (ANA) have been discussed in depth by Ridler and Medley [35] whose report is particularly apposite because they have used an HP8753B ANA as we have here.
5. Calibration errors are considered by Ridler and Medley [35], insofar as they are intrinsic to all impedance reflectometry, and by Gregory and Clarke [13] for the more specific case of ANA coaxial-sensor dielectric-measurements and for calibration by the means described in Section 3.4.
6. Of most critical importance is the question of imperfections in the geometry of the interface between the specimen and sensor face. As argued in Sections 3.2.2, 4.4.1 and 4.4.3, they can cause the largest errors of measurement that one encounters in coaxial sensor work and if not properly treated can be the weak point of the whole coaxial sensor scheme. These are considered By Gregory and Clarke [13], but, because of their importance, are also treated at some length below.

Based upon the published analyses listed above an uncertainty budget has been prepared which is detailed in Reference [13]. Its conclusions are only summarised here. Uncertainties in RF and microwave metrology are usually dominated by systematic contributions and these often require years of experience to be quantified to everybody's satisfaction. When one is starting with new or extended techniques, as here, one can at best only estimate some of these uncertainties. In the circumstances we at least believe that we have adequately estimated *the majority* of the significant uncertainties - metal and contact losses perhaps being the chief outstanding sources of uncertainty that require further work.

5.1 UNCERTAINTY BUDGET

The uncertainty figures offered below should be taken as being valid only up to 3 GHz using the equipment described in Section 3 in the normal laboratory environment. It is important

to emphasise that, as has been found with all of our sensor work, considerable care and experience is required to work at the uncertainty levels described here. It is not uncommon to have to reject sets of measurements as being invalid in retrospect, the problems typically being caused by the practical difficulties of achieving the geometry assumed by the theory. This issue is discussed further in Section 6.3.1 below.

Major contributions to the uncertainty of measurement are as follows. They are given in a similar order to Reference 13, but in summary form only.

1. **Non-linearity of the ANA** is taken to be negligible [35].
2. **ANA instabilities, noise, drift, cable flexure.** No change in $|\Gamma|$ from these combined causes was found to exceed 0.0005 in the normal working environment. θ can change by up to 0.05° through drift and typically up to 0.1° via significant cable flexure, though this, of course is kept to a minimum in actual measurements. In some measurements using reference liquid calibration, no cable flexure is necessary at all.
3. **Calibration errors.** Typical residual uncertainties using reference liquid (methanol or ethanol) calibration are estimated to be ±0.003 in either Cartesian component of Γ at 95% confidence level (this figure can be converted to an equivalent phase for $|\Gamma| \approx 1.0$).
4. **Numerical Analysis Uncertainties.** It was the purpose of Section 2 of this report and of previous work [20] to demonstrate that the uncertainties of the numerical analysis were considerably smaller than typical measurement uncertainties. It is estimated that uncertainties of no more than ±0.001 in $|\Gamma|$ and ±0.05° are to be expected at frequencies which are separated by more than two resonance-widths from any high Q-factor resonances. This is not to say that larger discrepancies are not in evidence in some tables and figures of Section 2. It should be remembered that the numerical intercomparisons in that Section were deliberately performed for extreme or limiting cases, as well as the more typical cases encountered in practice. It is in the former cases, and in resonance situations, that the largest discrepancies arise. These quoted figures rely upon the assumption that the actual measurement geometry corresponds to the perfect geometry of the numerical model. Uncertainties caused by imperfections in geometry are, however, unavoidable and are significantly larger. They are covered by (5) to (9), as follows.
5. **Non-planarity of the sensor face.** The program 'COAX' was used to model this uncertainty contribution. The findings can be summarised as follows:

   - A recession of l mm of both bead and inner conductor gives a phase error, $\Delta\theta$, $\approx -0.16 l\varepsilon' f$, where f is the frequency in GHz and ε' ($= \varepsilon_1$) is the real permittivity of the first layer.
   - Protrusion of the inner conductor only by l mm gives a phase error, $\Delta\theta$, $\approx -1.3 l\varepsilon' f$. This is also taken (as a safe upper limit) to apply to recession of the inner conductor within the bead (we have no direct means of computing this case at present).

   A commensurate change in $|\Gamma|$ may be assumed if the dielectric is lossy, as computed by substituting ε^* for ε' above.
6. **Radii of inner and outer conductors.** Again 'COAX' was used to estimate errors caused by departure from the correct nominal radii of inner and outer conductors, a and b, respectively. It was found that in both cases, an overestimation of the radius by Δr mm gives a phase error, $\Delta\theta$, $\approx 0.2\Delta r\varepsilon' f$. It may be found surprising that both these effects are similar in magnitude and have the same sign, because the effects upon the actual

fringing capacitance will be in opposing directions for like changes, Δr, in a and b and will be much larger in the former case. However, it should be remembered that we are here computing Γ normalised to the *characteristic impedance of the line* which will also change with a and b so that the change in capacitance will be somewhat compensated, giving only the residual correction described above.

7. **Permittivity of the bead.** The bead permittivity, ε'_b, has been measured using an open resonator to be 2.358 ±0.005 at 95% confidence level. By further modelling with 'COAX', it is found that the phase error, $\Delta\theta$, introduced by a faulty value of ε_b is $\approx 0.3 f \varepsilon' \Delta\varepsilon'_b$.

8. **Error in the thickness of liquid gaps.** With this contribution, we come to three causes of error which are not as yet fully quantified - they require further study for derivation of a comprehensive uncertainty budget. Nevertheless, sufficient information has been obtained about them to give us a feeling for upper limits of uncertainty. The effects of liquid gaps have been dealt with at some length in Sections 4.4.1 and 4.4.2. At present, an uncertainty in the size of the gap between the specimen and the sensor of the order of ±0.02 mm is probably realistic. This should be interpreted as an uncertainty in an 'equivalent' gap. Unlike most of the other uncertainties considered here, it has been arrived at entirely empirically. The figure therefore inevitably includes the effects of the sort considered in (4) above, and probably also includes contributions from other geometric imperfections (see next item). The figure therefore combines at least three sources of error.

9. **Other geometric imperfections in the cell.** These have been discussed at a number of points above and evidence of their effects has been pointed out in Figures 10 (a) onwards. It is inappropriate to quote a figure here for the estimated uncertainty contribution because it will vary enormously from specimen to specimen and with the measurement technique used. Orders of magnitude can be appreciated from the discussions in Section 4.4. The effects can be minimised by means of liquid substitution and immersion, and we are satisfied that for *any reasonable case* a tolerable estimate of uncertainty can be computed. One contribution of this sort is the effect of signal leakage down the side of the piston used in the Geometry (2) cell of Section 3.3 . Although the piston has been machined with a tight sliding fit into the cylindrical cell, it also has a slightly chamferred face (to ease its introduction into the cell). This could have the effect of guiding signals into what is effectively a very-low-characteristic-impedance, lossy, coaxial transmission line between the piston and cylinder. The effects of a gap here can be computed by program 'COAX'. Apart from resonance conditions, they become significant at frequencies above 2 GHz. For example, if the zirconate specimen of Table 12 is inserted into the cell in a 'contact' measurement, the predicted reflection phase magnitude, $|\theta|$, at 3 GHz is reduced by 0.18° (where $\theta \approx -171°$) by a gap of 0.025 mm all the way around the piston. Further investigation is required to relate this type of computed figure to the practical situation.

10. **Cell losses.** The effects of cell metal loss will only be formally quantifiable with the introduction of software which takes explicit account of such loss. The losses which are experienced are, however, thought to be greater than can be accounted for purely by absorption in cell walls. Contact impedances should also be investigated. One effect which can be theoretically quantified, as discussed in the last item, is the loss through the 'coaxial transmission line' formed by the piston and cylindrical specimen cell wall. For the same specimen and geometry discussed there, the effect of a 0.025-mm annular gap around the piston is such as to reduce the value of $|\Gamma|$ from effectively 1.0, down to 0.979 at 3 GHz. This order of loss contribution would be enough to account for the effects generally observed, but, again, it needs to be related to conditions in the actual

cell, where the annular gap would certainly be no greater than 5μm. By inspection of all of the measurements performed so far, we are currently estimating a minimum resolution of ± 0.05 in tan δ for this method *as it stands*. If the further work on loss which is proposed could be followed up, this figure would almost certainly be improved upon for 'well behaved' specimens.

11. **Finite flange diameter for probe-type sensors.** Items 9 and 10 of the uncertainty budget applied specifically to sensor measurements with a cell. There is an analogue to Item 9 for probe-type sensors (Figure 1(a), Geometry G1 in Section 2.3) which arises from the generation of reflections at the edge of the flange. The theory embedded in the computer programs assumes that no such reflections exist. This source of error has been discussed in Sections 2.5.5 and 3.1. One way of looking at these effects is to consider the flange as a resonant element in an antenna. Considered as a circularly-symmetrical resonant 'dipole', it can be seen that flange resonance effects will be likely to occur. Recent measurements of reference liquids [13] have compared the normal 'open' probe geometry with one in which a 50-mm-diameter metal sleeve was placed co-axially immediately around the flange. In methanol, changes of up to 0.03 in $|\Gamma|$ were observed at the frequency corresponding to the TM_{010}-mode resonance for that diameter(approx. 1 GHz). Similar discrepancies at the higher TM-resonant frequencies are reduced by the increase in loss of the liquid, typical discrepancies being of the order 0.005. The maximum discrepancies are only of the order 0.005 for ethanol, which is hence considered to be a better liquid for calibration. As discussed in Section 2.5.5, it is unlikely that the magnitude of these effects during normal probe usage would be as large as this in the absence of the gross mismatch presented by the sleeve. The normal 'open' condition and the shorting 'sleeve' condition will tend to produce effects in antiphase, so the overall discrepancy arising from 'infinite-flange' approximations may be no more than 0.01 at TM-resonant frequencies and about a quarter of this at other frequencies. However, the above findings place a useful upper limit on the uncertainties.

5.2 UNCERTAINTIES FOR MEASURING THE *N*TH LAYER, WHERE $N \geq 3$

It was one of the aims of the project to be able to quantify such uncertainties. It has clearly been demonstrated, as in Section 4.3, above, that discrepancies less than 10% can be obtained, in special circumstances, for even the *third* layer of a composite, but it must not be expected that this will always be the case. Except in special circumstances, we would recommend that, say, the *N*th layer in an *N*-layer composite should be measured directly, if possible, by reversing the specimen, thereby turning it into the *first* layer. Nevertheless, Figure 14 demonstrates that where the permittivity of initial *thin* layers is significantly less than that of the deepest layer, changes in the permittivity of the latter can be detected. This may have some application in a quality control situation, for example, in which liquid flow is being monitored *through* a dielectric window. The program 'COAX ' can be used to estimate uncertainties for measuring ε^* for fourth or deeper layers. In many cases they would be too large to make the measurement worthwhile, but we consider here a hypothetical example in which a useful measurement might be achieved by substitution. We consider a *four*-layer system: (cyclohexane ($\varepsilon_1 = 2.018$, $t_1 = 0.00$ or 0.01) / polymer ($\varepsilon_2 = 2.54$, $t_2 = 0.3$ mm) / cordierite ($\varepsilon_3 = 5.97$, $t_3 = 0.3$ mm) / 'ceramic' (eg. alumina, $\varepsilon_4 = 10.0$, $t_4 = 2.00$ mm)). What change to the estimated value of ε_4 will result from a change of t_1 (the cyclohexane layer) from 0.00 mm to 0.01 mm? The effects are tabulated in Table 22.

Table 22 Effects of the uncertainty in the thickness of the first layer upon the measurement of the fourth layer of a four-layer composite specimen. $\Delta\theta$ and $\Delta\varepsilon_4$ are the changes, respectively, in the measured phase and the attributed permittivity of the fourth layer, caused by a change of 0.01 mm in t_1. Details of the modelled specimen are given in the text. Computations by 'COAX'.

Frequency	$\arg(\Gamma) = \theta$	$\Delta\theta$	$\Delta\varepsilon_4$
1.0	-26.52°	0.35°	0.37
2.0	-49.84°	0.64°	0.36
3.0	-115.03°	2.95°	0.07

The predicted errors in the ε_4 value (10.0) given in Table 22 are quite small – less than 4% at 1 and 2 GHz, and seemingly even smaller at 3 GHz. However, the latter is affected by the TM_{01}-mode resonance and the magnified measurement errors in this condition would more than compensate for the apparent improvement in sensitivity. In general, it must be expected that other measurement errors could swamp small changes such as these and, except in a direct 4th-layer *substitution* measurement where nothing else is disturbed, little benefit could be gained from such measurements unless specimen reversal were used. The program 'COAX' allows similar computations to these to be performed for composites with 5 or more layers. It must again be expected that only when the initial layers are thin (ie. not taking up more than 1.0-mm thickness together) and when there is no gross mismatch from one layer to the next, can realistic substitution measurements be made for the deepest layer.

6 DISCUSSION AND CONCLUSIONS

The major aim of this project was to demonstrate that useful quantitative information on stratified dielectric specimens can be obtained through coaxial sensor measurements. This has clearly been shown in Sections 4 and 5 of this report. A good proportion of this report has not been concerned with direct measurements upon multilayered structures, but rather with auxiliary measurements and demonstrations. This was a necessary feature of this programme of work. It has been our major goal to show, not just that multilayer measurements are *possible*, but also that they can be *traceable*. It is a matter of common experience in metrology that the latter task always requires several times more effort than the former. A good deal of work must go into background investigations which deliver figures for uncertainties and which form an essential role in providing confidence. The research that has been described in Sections 2 and 4.1 to 4.4 is largely auxiliary work of this nature. The work carried out has been sufficient to demonstrate the feasibility of using this technique as part of the National Measurements System and there is no reason why the present system, even without the suggested improvements of Section 6.3, below, cannot be so used. It should be pointed out, however, that, as is *always* the case in dielectrics measurements, further auxiliary measurements and computations should be performed for each specimen individually if confidence is to be retained. This is particularly the case here where each 'multilayer' measurement has at least 12 degrees of freedom associated with it: specimen diameter, surface structure (flatness, hardness, malleability), frequency of measurement, and ε', ε'' and thickness for each of at least three layers.

The following subsections summarise what has been achieved and also make proposals for further improvements.

6.1 SUMMARY OF WHAT HAS BEEN ACHIEVED IN THIS PROJECT

6.1.1 Immediate aims

In the required frequency range up to 3 GHz it has been shown that:

1. Multilayer specimens of diameter less than 50 mm can be measured.
2. Low loss specimens can be measured.
3. Hard surface specimens can be measured.
4. Uncertainties in the permittivity of the first layer of a multilayer specimen can be better than ±3% (95% confidence level) for suitable specimens.
5. Similar uncertainties for the second layer of ±10% or better can be achieved with suitable specimens.
6. Uncertainties for measurement of deeper layers can be estimated.
7. Computer programs have been written, as required, to make all of these measurements and uncertainty estimates possible.
8. The system is already in a state where it can be used for traceable measurements as part of the National Measurement System.

6.1.2 How this work contributes to coaxial sensor metrology

Of equal importance to the achievement of the immediate aims of the project, is the fact that the work advances coaxial sensor metrology in other ways. The attraction to the metrological community of the 'probe' technique has been evident for some years but the problem of achieving adequate contact onto hard specimens has only recently become theoretically accessible. The progress of other workers [27,32,43] is of relevance here, but it is always important to be able to estimate uncertainties [33] when measurements are undertaken, and we believe that this is best done through a comprehensive programme of *traceable measurements* such as has been presented here. Not only has the critical problem of specimen contact been studied, but so has that of specimen resonances and edge reflections. Their magnitudes can now be realistically estimated, and with this capability comes that of measuring low-permittivity, low-loss specimens in a traceable way. The liquid immersion techniques developed here, while they are by no means new to dielectric metrology in general, appear not to have been addressed in depth elsewhere in relation to coaxial sensor measurements. They offer improved uncertainties in many cases. Finally, though our work was limited to the frequency range up to 3 GHz, it has direct application at much higher frequencies. Frequency and sensor diameter scale directly, so that what we have discovered about a 14-mm sensor at 1 GHz would apply equally to a 3.5-mm sensor at 4 GHz, for example. The computer programs which are used to predict uncertainties are capable of handling a very wide variety of sensor/specimen coaxial geometries, not just those used at NPL.

6.2 POTENTIAL APPLICATIONS OF THE WORK

Section 1.1.2 considered the importance of work on multilayer structures. Here we further consider the specific applications of this work in dielectric metrology. The most direct applications as far as NPL is concerned are likely to be to single layer and 'natural' (or 'natural'-phantom) multilayer specimens. It has always been our contention that the coaxial sensor has a role to play in accurate, but convenient, metrology of dielectric laminas. The present project has enabled us to demonstrate this because precisely the same techniques are required to measure a single layer lamina well (and traceably) as are required to make multilayer measurements possible *at all*. For example, a two or three layer analysis is demanded by a measurement upon a hard solid, because of the known presence of gaps [32].

In dielectric metrology there is no overall 'industry-standard' dielectric specimen shape. There cannot be because there are too many degrees of freedom associated with dielectric measurements. However, a circular disc 30 - 100 mm in diameter and 1 - 10 mm thick is as close as one comes to such a standard. Many metrological techniques used at NPL and elsewhere use specimens of this general shape, and it precisely for such specimens that our sensor measurements are most appropriate. The enhancements to the sensor technique broaden our options of measuring one and the same specimen by a number of independent methods at a number of different frequencies. This provides the best basis for traceable dielectric measurements and so will make an important contribution to the services we can offer as part of the National Measurement System.

The original development of coaxial sensors at NPL was associated with biomedical (and allied food technology) applications. The importance of the present work in these areas is immediate because virtually all of the tissues of interest (eg. muscles, skin, etc.) are inhomogeneous, but in a way that makes a multilayer assumption a very useful approximation to the natural distribution of permittivities. It is known from our earlier work [9] that assumption of homogeneity (as made, for example, in the 'infinite half-space' model) can give spurious results for stratified media, because of the omission of interlayer reflection effects from the analysis. The related area of safety testing of electromagnetic fields at RF and Microwave frequencies requires the development of phantoms (human body models) or tissue equivalent materials which are structured dielectrically in a layered fashion like the human body. A final area of importance for NPL is measurements upon Radio Absorbing Materials (RAM) which often have layered structure (whether by design or not) and, in fact, measurements of this type have already been performed.

Outside NPL, the more general relevance of this work perhaps lies in two areas. The first has already been mentioned: uncertainties for the generality of coaxial sensor measurements can be estimated for all types of sensors and at all frequencies by the techniques employed here. This kind of information can be of value in experimental design. Secondly, we observe that, outside the immediate area of precision metrology, coaxial sensors are widely used but with set-ups in which uncertainties of 5 - 10% for *one layer* of dielectric are to be expected. Not only is it possible to tighten up on these figures, as just described, but similar uncertainties can now be expected for the *second or deeper* layer of a composite, which opens up the possibility of measuring materials through a 'window' material, provided the window is suitably thin, see Section 5.2.

Finally, of course, the capability for measuring truly stratified laminas has been provided and applications in this area were discussed in Section 1.1.2.

PROBLEMS AND SUGGESTIONS FOR FURTHER WORK

The report, as summarised in Section 6.1 demonstrates that the aims of this programme of work have been more than achieved. However, the project encompassed only one year's work and, as is usually the case in metrology, it has shown up areas in which further advances could be made. Some of these, the more cost-effective, are listed below. Some proposals represent a natural next step from the state-of-the-art which has been achieved. Others recognise that there are practical and theoretical difficulties which restrict the range of application at present. We therefore include suggestions as to how they might be overcome.

Reliability of measurements

There is no doubt that the Type C cylindrical cell fulfilled its purpose of allowing us to measure low loss laminas and stratified media whilst reducing uncertainty from edge reflections to a less significant level. However it is possible that the particular design chosen may not be the best to ensure repeatability of measurement. Where solid specimens are intended to be in full contact with the sensor face, considerable pressure has to be applied to them to ensure this contact is repeatable. It is possible that a lever-clamp system might be a better way of achieving this than the screw-thread clamp actually used. Again, part of an initial repeatability problem was traced to changes in the geometry of the specimen within the cell after its assembly. For example, nylon wire spacers did not always stay in the place that was intended. The incidence of these problems was reduced as experience was gained. It is impossible to inspect the inside of the cell after it has been assembled and it is difficult to think of any design that could allow for this, but a lever clamp system could make it easier to dismantle and reassemble the cell to ensure that all was well. It is likely that, for spacing specimens away from the flange face, purpose-built machined annuli made from a suitably matched polymer would be better and more repeatable than nylon wire. It should be noted that measurements would normally require the placing of just one (perhaps stratified) specimen in the cell. During the testing phase, up to three specimens were placed in the cell simultaneously and some lack of repeatability must be associated with the process of clamping them all together *with no gaps in between.* This would be absent in normal measurements.

As experience was gained, repeatability and reliability of even the most awkward measurements improved to the extent that the sort of agreement shown in Figures 10 (a) to 19 could reliably be achieved. Such measurements require the care of an experienced metrologist to ensure that sensible results are being obtained, but this is normal in microwave dielectric metrology.

Cavity resonances

Cavity resonances are a natural consequence of using the cylindrical cell in this work. It has been our policy during this project to discount measurements at frequencies close to a high Q-factor resonance because they are most prone to errors from geometric imperfections and because our programs ignore metal-loss. This may appear to be a limitation of the method, but it is important to point out that it is only a temporary one - one which can be avoided even now and which, in the longer term may prove to be an *asset* of the method, rather than a liability. Thus:

Inspection of Figure 13, for example, illustrates why, at present, we might wish to exclude measurements at frequencies between 2.1 and 2.5 GHz from the list of those at which precise measurements can be performed. The reasons have been spelt out above - there are reactive errors caused by geometric imperfections and resistive errors caused by the absence of metal loss in the numerical model. These errors are amplified close to a resonance. Perfectly acceptable measurements are clearly possible above and below the resonance. However, these considerations do not mean that a sample of this composite (ethanol/cordierite) specimen cannot be measured at these frequencies at present. All that is required for this is that a specimen of *another diameter* be measured in a suitable cell. If the cell-diameter were halved, for example, the first resonance would not occur until 4.7 GHz, so that our whole frequency range to 3 GHz could be covered. If a 70-mm specimen and the 70-mm cell were used, the resonant frequency would be reduced to 1.7 GHz and 2.1 to 2.5 GHz would again be sufficiently far from a resonance to be measured.

2. The discounting of measurements over part of our measurement frequency range, even if it were necessary in the long-term, would not generally represent a critical limitation for this technique. Complex permittivity over the whole of the RF and microwave frequency range changes very slowly and for homogeneous materials it is invariably possible to interpolate permittivities between frequencies on either side of a gap. Only if the *structure* of stratification of the multilayer material were such that high-Q resonances could be set up in the material - eg. if the specimen were acting as a dielectric resonator of itself - would rapid evolution of its intrinsic properties with frequency be expected, but then change of specimen diameter would again overcome the problem.

3. It is to be noted from Figure 14 that the permittivity of layer 3 of the specimen affects not only the off-resonance phase, θ, from which ε' is largely computed, but also the *frequency of the first, TM_{010}, resonance, f_1*. The model has correctly predicted the change in f_1 with the permittivity of layer 3. This feature provides another approach to measuring the specimen. Indeed, it corresponds to what one might call the 'standard' (longstanding) method of using TM_{0n} cavities for dielectric measurements: namely to use the frequency of resonance to compute ε', and the Q-factor of the resonance to compute ε'' and $\tan\delta$. Our technique here differs from the 'standard' one in having a much greater coupling coefficient into the cavity and by dealing with high losses. Q-factors of the order 200 - 5000 would normally be expected in this frequency range for the 'standard' resonance technique, as opposed to no more than about 10 here. Further effort is required to investigate this approach, but we see no reason why this should not be brought to fruition.

Consideration of (1) and (2) again points to ways in which cell design might be changed in order to improve the situation. One obvious suggestion is to apply the technique to *much smaller* diameter specimens - down even to the diameter, b, of the coaxial line outer conductor (see, eg. [1]). This would move the first resonance to a frequency well outside our standard measurement range.

6.3.3 Suitability of specimens

Prolonged experience teaches one that there is no *panacea* for dielectric measurements: no one technique will serve to characterise all specimens, even if one restricts oneself to a limited region of the electromagnetic spectrum. In this respect, measurements upon dielectrics are dissimilar to measurements upon artefact impedance standards. The latter are invariably

selected from a limited range of possible components, while dielectric specimens are characterised by a much wider range of degrees of freedom. In practice, the coaxial sensor technique for dielectrics probably has a wider range of application in this respect than most others, but the method is not without its difficulties. The strong-points of this particular technique have been listed above, but even if one takes what at first appears to be an ideal specimen, problems can arise which restrict its utility.

One example that has actually been encountered is of a material whose outer layer was so conductive that it effectively shorted out the sensor, thereby rendering measurement of internal layers effectively impossible. Lack of flatness or an unsuitable surface structure are other contributions that can effectively make measurements impossible, as with other measurement techniques, and generally a visual and mechnical inspection of a specimen is required before it is possible to say whether it can be measured.

Knowledge of the properties of the reference liquids

As mentioned elsewhere in our work [13,18,19], one of the limiting factors in coaxial sensor measurements is lack of precise knowledge of the dielectric properties of the reference liquids employed for calibration and liquid immersion and substitution. An international intercomparison is being organised to improve knowledge of the properties of the liquids commonly used and to promote a consensus upon the parameters that should be adopted to characterise the liquids (see Table 13 and equation 4 for the figures we use at present). Even though permittivities can sometimes be computed to 1% or better, this is not always the case, and improvement in measurement of multilayer uncertainties can be anticipated as a result of the proposed intercomparison. One respect in which present data are inadequate, for example, is that there are no really well known liquids in the permittivity range 4.0 - 15.0 which can be used for liquid substitution or immersion. Even in the range 15.0 - 20.0 covered by propanol - pentanol, their properties are not well enough known above 1 GHz. Liquids such as methylene chloride and chloroform are used in this role elsewhere to provide permittivities in the range 4.0 - 6.0, but they carry other problems with them, such as health risks.

Metal and contact loss in cells

The one major problem that has been identified that can be handled by software enhancements is the absence of metal and leakage loss from the computer models and programs. It is known that versions of 'COAX' and 'TEH2' can be produced that can analyse metal loss along the direction of the axis of the coaxial system. It is not clear, as yet, what can be done about losses in flanges and back-shorts, although modelling them by adding a thin ($< 1\mu$m) lossy dielectric layer may be possible. It is in any case believed at present that a significant portion of the loss arises from contacts, whether between flanges or between cylinder and piston in the coaxial cell. Our present capability for loss meets our originally desired specification, but there is every indication that this could be improved upon if program enhancements were carried out.

7 ACKNOWLEDGEMENTS

We wish to acknowledge the valuable exchange of ideas we have had with Dr Soe Min Tun of SMT Consultants Ltd and thank him for permission to include his own data in Table 7. One of the established computer programs employed for checking new software, 'AGPW', was originally conceived by A G P Warham, then at NPL, now at MoD Fort Halstead, Sevenoaks. We are indebted to him also for suggesting the use of quadratic extrapolation and the improvements which have accrued from it. We thank Dr S. Etzel (formerly S Jenkins) whose work as a research associate at NPL placed us in a position to carry out the present project and we acknowledge the re-use of her measurement data in Tables 6 and 7. We thank Dr A.C. Lynch for the open resonator measurements in Table 11. Finally, we wish to thank the NPL workshop for their careful machining and manufacture of the new sensors and measurement cell.

8 REFERENCES

[1] BELHADJ-TAHAR, N.-E., FOURRIER-LAMER, A. and DE CHANTERAC, H., Broad-band simultaneous measurement of complex permittivity and permeability using a coaxial discontinuity, *Trans. IEEE Microwave Theory Tech.*, **MTT-38**, 1990, 1 - 7.

[2] BELHADJ-TAHAR, N.-E., and FOURRIER-LAMER, A., Broad-band simultaneous measurement of complex permittivity and permeability for uniaxial or isotropic materials using a coaxial discontinuity, *J. Electromagn. Waves and Appl.*, **6**, 1992, 1225 - 1245.

[3] BLACKHAM, D., Use of network analyzer and coaxial probe to determine complex permittivity. *Proceedings of the MRS Symposium, Microwave Processing of Materials II, (Materials Research Society, USA)*, **189**, 123 - 128, 1991.

[4] CLARKE, R.N. and JENKINS, S., Measurements of the static permittivity of polar organic dielectric reference liquids in a micrometer-driven parallel-electrode admittance cell, *NPL Report in preparation*

[5] DAYWITT, W.C., Complex admittance of a lossy coaxial open circuit with a hollow center conductor, *Metrologia*, **24**, 1987, 13 -22.

[6] ENGELDER, D.S. and BUFFLER, C.R., Measuring the dielectric properties of food products at microwave frequencies, *Microwave World*, **12**, No. 2, Summer 1991.

[7] FAN, S. and MISRA, D., A study on the metal-flanged open-ended coaxial line terminating in a conductor-backed dielectric layer, *Proceedings of the Conference on Microwave Theory and Techniques, IEEE Proceedings CH2735-9/90*, 1990, 43 - 46.

[8] GRANT, J.P., CLARKE, R.N., SYMM, G.T. and SPYROU, N.M., A critical study of the open-ended coaxial line sensor for medical and industrial dielectric measurements, *Proceedings of the IEE colloquium on Industrial and medical applications of microwaves, London, IEE Digest No. 1986/73*, 1986

[9] GRANT, J.P., CLARKE, R.N., SYMM, G.T. and SPYROU, N.M., *In vivo* dielectric properties of human skin from 50 MHz to 2.0 GHz, *Phys. Med. Biol.*, *33*, 1988, 607 - 612.

[10] GRANT, J.P., CLARKE, R.N., SYMM, G.T. and SPYROU, N.M., A critical study of the open-ended coaxial line sensor technique for RF and microwave complex permittivity measurement, *J. Phys. E: Sci. Instrum.*, **22**, 1989, 757 - 770.

[11] GRANT, J.P. and SPYROU, N., Complex permittivity differences between normal and pathological tissues: mechanisms and medical significance., *J. Bioelectricity*, **4**, 1985, 419 - 458.

[12] GREGORY A.P. A new design of coaxial sensor with a beadless adaptor for the attachment of calibration standards, *in preparation.*

[13] GREGORY, A.P. and CLARKE, R.N., On the design, calibration and accuracy of a coaxial sensor for permittivity measurement, *in preparation.*

[14] HODGETTS, T.E., The calculation of the equivalent circuits of coaxial-line step discontinuities, *Royal Signals and Radar Establishment Memorandum No. 3422*, 1981.

[15] HODGETTS, T.E., The open-ended coaxial line: a rigorous variational treatment, *Royal Signals and Radar Establishment Memorandum No. 4331*, 1989.

[16] JENKINS, S. Measurement of the complex permittivity of dielectric reference liquids and human tissues, *PhD. Thesis*, (Bristol University, Faculty of Medicine), 1991.

[17] JENKINS, S., CLARKE R.N., HORROCKS, M. and PREECE, A.W., Dielectric measurements on human tissues between 100 MHz and 3 GHz, *Proceedings of The European Association of Thermology Microwave Group meeting on Advances in medical microwave imaging, Lille, France*, November 1989.

[18] JENKINS, S. and CLARKE R.N., Measured values and uncertainties for the complex permittivity of selected organic reference liquids at 20° to 30° and frequencies up to 3 GHz, *NPL Report in preparation.*

[19] JENKINS, S., HODGETTS, T.E., CLARKE , R.N. and PREECE, A.W., Dielectric measurements on reference liquids using automatic network analysers and calculable geometries, *Measure. Sci. Technol.*, **1**, 1990, 691 - 702.

[20] JENKINS, S., HODGETTS, T.E., SYMM, G.T., WARHAM, A.G.P., CLARKE , R.N. and PREECE, A.W., Comparison of three numerical treatments for the open-ended coaxial line sensor, *Electron. Lett.*, **26**, No. 4, 1990, 234 - 236.

[21] JENKINS, S., WARHAM, A.G.P. and CLARKE, R.N., Use of an open-ended coaxial line sensor with a laminar or liquid dielectric backed by a conducting plane, *Proc. IEE, Pt. H*, **139**, 1992, 179-182.

[22] JOHNSON, R.H., GREEN, J.L., ROBINSON, M.P., PREECE, A.W. and CLARKE, R.N., A resonant open-ended coaxial line sensor for measuring complex permittivity, *Proc. IEE, Pt. A, 139*, 1992, 261 - 264.

[23] LI, L.L., ISMAIL, N.H., TAYLOR, L.S. and DAVIS, C.C., Flanged coaxial probes for measuring thin moisture layers, *Trans. IEEE, Biomed. Eng.*, **39**, 49 - 57, 1992.

[24] LYNCH, A.C., Relationship between permittivity and loss tangent, *Proc. IEE*, **118**, 244 - 246, 1971.

[25] MACPHIE, R.H., OPIE, M. and RIES, C.R., Input impedance of a coaxial line probe feeding a circular waveguide in the TM_{01} mode, *IEEE Trans. Microwave Theory Tech.*, **MTT-38**, 1990, 334 - 337.

[26] MISRA, D., CHABBRA, M., EPSTEIN, B.R., MIROTZNIK, M and FOSTER, K.R., Noninvasive electrical characterization of materials at microwave frequencies using an open-ended coaxial line: test of an improved calibration technique, *Trans. IEEE Microwave Theory Tech.*, **MTT-38**, 1990, 8 - 14.

[27] MOSCHURING, H. and WOLFF, I. The measurement of inhomogeneities and of the permittivity distribution in MIC-substrates, *IEEE Conference on Instrumentation and Measurement, Boston, IEEE conference proceedings IMtc/87, Cat. no. 87CH2405-9*, 1987.

[28] MOSIG, J.R., BESSON, J.C.E., GEX-FABRY, M. and GARDIOL, F.E., Reflection of an open-ended coxial line and application to non-destructive measurement of materials, *IEEE Trans. Instrum. Meas.*, **IM-30**, 1981, 46 - 51.

[29] NEVELS, R.D., BUTLER, C.M. and YABLON, W., The annular slot antenna in a lossy biological medium, *Trans IEEE Microwave Theory Tech.*, **MTT-30**, 1985 314 - 319.

[30] NEVELS, R.D. and WHEELER, J.E., Near field radiation from four coaxial line fed structures, *Microw. and Optical Technol. Lett.*, **3**, 1990, 90 - 95.

[31] NISHIKATA, A. and SHIMIZU, Y., Analysis for reflection from coaxial end attached to lossy sheet and its application to nondestructive measurement, *Electron. Commun. Jpn. 2*, **71**, 1988, 95 - 101.

[32] NISHIKATA, A. and SHIMIZU, Y., Effectiveness of gaps for lossy dielectric sheet measurements by coaxial electrode, *Electron. Commun. Jpn. 2*, **73**, 1990, 14 - 22.

[33] NYSHADHAM, A., SIBBALD, C.L. and STUCHLY, S.S., Permittivity measurements using open-ended sensors and reference liquid calibration - an uncertainty analysis, *Trans. IEEE Microwave Theory Tech.*, **40**, 1992, 305 - 314.

[34] OTTO, G.P. and CHEW, W.C., Improved calibration of a large open-ended coaxial probe for dielectric measurements, *Trans. IEEE, Instrum. Measure.*, **IM-40**, 742 - 746, 1991.

[35] RIDLER, N M and MEDLEY, C J, An uncertainty budget for VHF and UHF reflectometers, *NPL Report DES 120*, May 1992.

[36] SAED, M.A., A method of moments solution of a cylindrical cavity placed between two coaxial transmission lines, *Trans. IEEE, Microwave Theory Tech.*, **39**, 1991, 1712 - 1717.

[37] SAED, M.A., RIAD, S.M. and DAVIS, W.A., Wide-band dielectric characterization using a dielectric filled cavity adapted to the end of a transmission line. *Trans IEEE, Instrum. Measure.*, **39**, 1990, 485 - 491.

[38] TUN, S M, Manual for 'COAX', Version 1.01, January 1992, (Antenna Software Ltd., Gt. Malvern).

[39] WARHAM, A.G.P. Annular slot antenna radiating into lossy material. *NPL Report DITC 152/89*, November 1989.

[40] WHEELER, J.E. and NEVELS, R.D., Reflection and transmission properties of annular slot covered by dielectric hemisphere, *Proc. IEE Part H*, **136**, 1989, 59 - 63.

[41] XU., Y, and BOSISIO, R.G., Calculations on the increased sensitivity of dielectric constant measurements using open-end coaxial line with a hemispherical center conductor extension, *Microw. and Optical Technol. Lett.*, **3**, 1990, 74 - 78.

[42] XU, Y., BOSISIO, R.G., and BOSE, T.K., Some calculation methods and universal diagrams for measurement of dielectric constants using open-ended coaxial probes, *Proc. IEE Pt. H*, **138**, 1991, 356 - 360.

[43] XU., Y, and BOSISIO, R.G., On the measurement of resistive thin films and dielectric slabs using an open-ended coaxial line, *J. Electromagn. Waves and Appl.*, **6**, 1992, 1247 - 1258.